


9-2017

STUDY OF REGULATED CELL DEATH IN TWO SYSTEMS: PD-1 IN NATURAL KILLER CELLS AND RIP3 IN NEURONS

YU HUANG

Follow this and additional works at: https://digitalcommons.library.tmc.edu/utgsbs_dissertations

 Part of the [Cell Biology Commons](#), [Immunology and Infectious Disease Commons](#), and the [Molecular and Cellular Neuroscience Commons](#)

Recommended Citation

HUANG, YU, "STUDY OF REGULATED CELL DEATH IN TWO SYSTEMS: PD-1 IN NATURAL KILLER CELLS AND RIP3 IN NEURONS" (2017). *The University of Texas MD Anderson Cancer Center UTHealth Graduate School of Biomedical Sciences Dissertations and Theses (Open Access)*. 811.
https://digitalcommons.library.tmc.edu/utgsbs_dissertations/811

This Dissertation (PhD) is brought to you for free and open access by the The University of Texas MD Anderson Cancer Center UTHealth Graduate School of Biomedical Sciences at DigitalCommons@TMC. It has been accepted for inclusion in The University of Texas MD Anderson Cancer Center UTHealth Graduate School of Biomedical Sciences Dissertations and Theses (Open Access) by an authorized administrator of DigitalCommons@TMC. For more information, please contact digitalcommons@library.tmc.edu.

STUDY OF REGULATED CELL DEATH IN TWO SYSTEMS:

PD-1 IN NATURAL KILLER CELLS AND RIP3 IN NEURONS

by

Yu Huang, B.S.

APPROVED:

Michael Xi Zhu, Ph.D.
Advisory Professor

Jeffrey A. Frost, Ph.D.

Kartik Venkatachalam, Ph.D.

Guangwei Du, Ph.D.

Zhizhong Pan, Ph.D.

APPROVED:

Dean, The University of Texas
MD Anderson Cancer Center UTHealth Graduate School of Biomedical
Sciences

STUDY OF REGULATED CELL DEATH IN TWO SYSTEMS:
PD-1 IN NATURAL KILLER CELLS AND RIP3 IN NEURONS

A

DISSERTATION

Presented to the Faculty of

The University of Texas

MD Anderson Cancer Center UTHealth

Graduate School of Biomedical Sciences

in Partial Fulfillment

of the Requirements

for the Degree of

DOCTOR OF PHILOSOPHY

by

Yu Huang, B.S.
Houston, Texas

December, 2017

DEDICATION

To my parents and my wife,
for their unconditional love and support.

ACKNOWLEDGEMENTS

First and foremost, I would like to acknowledge my mentor, Dr. Michael Xi Zhu, for his support and guidance during these six years. He is very patient in training student: Mike's door is always opened for us, no matter how busy he is; the writing draft I sent to him for comments always returned with labels on almost every sentence; he always discussed with me about every details of my projects including clearly defined negative and positive controls for all tests. Dr. Zhu always has great ideas and deeper thought in the data I got. I am very fortunate to have Mike as my mentor, his thoughts for science inspires me during my PhD study and will continue inspiring me in my future career.

I would like to thank Dr. Dongfang Liu for his support of 2 years in his lab at Baylor College of Medicine. He offered me a great opportunity to pursue something totally new and expand my fields of scientific interests a lot.

I'd like to thank my excellent advisory and candidacy examination committees: Dr. Guangwei Du, Dr. Kartik Venkatachalam, Dr. Jeffery Frost, Dr. Zhizhong Pan, Dr. Roger O'Neil, Dr. David Loose, and Dr. Yong Li, for their helpful suggestions and critiques.

I would also like to thank all current and past lab members in Dr. Zhu's lab: Dr. Jinbin Tian, Dr. Jaepyo Jeon, Dr. Qiaochu Wang, Jian Xiong, Dr. Dhananjay Thakur, Dr. Yingmin Zhu, Dr. Pu Yang, and Dr. Xinhua Feng. The people in Dr. Dongfang Liu's lab helped me a lot in that two years: Dr. Peilin Zheng, Dr. Joon Hee Jang, Dr. Xi Kang, Dr. Shengjian Huang, Dr. Yuhui Chen, Grant Bertolet, and Qian Hu. My collaborators

from Dr. Tianle Xu's lab in China helped me a lot for the data of the second project: Dr. Yizhi Wang, Dr. Qin Hu, and Junlong Huang.

I also wish to express my sincere acknowledgement to the Department of Integrative Biology and Pharmacology, The University of Texas McGovern Medical School, the Cell and Regulatory Biology Graduate Program and The University of Texas Graduate School of Biomedical Sciences at Houston.

Lastly, I would like to thank my family again for their endless love and support. Their patience and understanding is critical for my life.

STUDY OF REGULATED CELL DEATH IN TWO SYSTEMS:

PD-1 IN NATURAL KILLER CELLS AND RIP3 IN NEURONS

Yu Huang, B.S.

Advisory Professor: Dr. Michael Xi Zhu, Ph.D

Cell death is not only an essential phenomenon in normal development and homeostasis, but also crucial in various pathologies. It is now clear that many types of cell death can be regulated by pharmacological or genetic interventions. These were largely achieved by identifying the molecular mechanisms underlying the regulated cell death (RCD). While in the immune system, RCD needs to be facilitated to help the clearance of pathogens and tumors, in healthy cells, especially the terminally differentiated neurons in the nervous system, it is more desirable to protect cells from dying due to stress under pathological conditions. Thus, understating the inhibitory and the activating signals for RCD in different systems is important. In this thesis, I will discuss the study of two key molecules involved in RCD: programmed death 1 (PD-1, as inhibitor for RCD) and receptor-interacting serine/threonine-protein kinase 3 (RIP3, as promoter for RCD) in two different systems.

First, I studied the role of PD-1 signaling in the cytotoxicity of natural killer (NK) cells. In recent years, PD-1 has become a hot target of immunotherapy. However, because most studies on PD-1 have focused on T cells, the precise mechanism by which PD-1 mediates its effects on NK cells remains poorly characterized. Using NK cell lines that express PD-1, I found that PD-1 activation blocked NK cell cytotoxicity. However, PD-1 signaling did not inhibit cell-cell conjugation between NK and target

cells as NK cells that expressed PD-1 formed stable immunological synapse (IS) with target cells that expressed the PD-1 ligand, PD-L1. Instead, the PD-1 engagement by PD-L1 blocked lytic granule (LG) polarization *via* disruption of the integrin 'outside-in' signaling pathway and abolished the calcium signaling for degranulation. Similar to T cells, the immunoreceptor tyrosine-based switch motif (ITSM) but not immunoreceptor tyrosine-based inhibitory motif (ITIM) of PD-1 was crucial for its inhibitory effect on cytotoxicity.

In the second part, I examined the involvement of RIP3 in acidosis-induced cell death, which critically contributes to ischemic brain injury and was recently shown to occur through necroptosis, a new form of programmed necrosis. Although RIP3 has been proven to be an important mediator of necroptosis, whether acidosis-induced neuronal death requires RIP3 is not clear. Here, I show that RIP3 is required for acidosis-induced cell death, in which serum starvation is another critical contributing factor. There are at least two key downstream molecules of RIP3 for acidosis/starvation-induced cell death: mixed lineage kinase domain-like pseudokinase (MLKL) and mitochondrial apoptosis-inducing factor (AIF). Inhibiting RIP3 by an FDA approved anti-cancer drug, dabrafenib, reduced both acid-induced death of mouse cortical neurons *in vitro* and brain infarction in mice subjected to middle cerebral artery occlusion (MCAO) *in vivo*.

Depending on the specific scenarios and the physiological systems involved, the goals for pharmacological and/or genetic modification of RCD can be quite different. Thus, a better understanding of both the positive (e.g., RIP3) and negative (e.g., PD-

1) regulators of RCD is of significant values for both basic sciences and therapeutic development in treating different diseases in the future.

Table of Contents

Approval page	i
Title page.....	ii
Dedication	iii
Acknowledgements.....	iv
Abstract	vi
Table of Contents	ix
List of Figures	xii
List of Tables.....	xiv
Abbreviations	xv
Chapter 1 Introduction.....	- 1 -
Chapter 2 PD-1 Blocks Lytic Granule Polarization and Calcium signaling in Natural Killer Cell.....	- 4 -
2.1 Background.....	- 4 -
2.1.1 NK cells in immune system.....	- 4 -
2.1.2 PD-1.....	- 5 -
2.1.3 Integrin signaling in NK cells.....	- 6 -
2.1.4 Calcium signaling in NK cells	- 8 -
2.2 Materials and methods:	- 10 -
2.2.1 Cell Culture.....	- 10 -
2.2.2 cDNA expression constructs and transduction of CD16-KHYG-1, K562, and Daudi cell lines.....	- 10 -
2.2.3 Chromium ⁵¹ release assay.....	- 12 -
2.2.4 Conjugation assays	- 12 -
2.2.5 Immunofluorescence staining.....	- 13 -
2.2.6 Laser scanning fluorescence confocal microscopy.....	- 14 -
2.2.7 Intracellular Ca ²⁺ measurement	- 14 -
2.2.8 Statistical analysis.....	- 15 -
2.3 Results	- 16 -
2.3.1 PD-1 signaling attenuates NK cell cytotoxicity	- 16 -
2.3.2 Stable immunological synapse formation in NK cells in the presence of PD-1 signaling..	- 21 -
2.3.3 PD-1 signaling does not affect NK-target cell conjugation	- 26 -
2.3.4 PD-1/PD-L1 engagement blocks lytic granule polarization at immunological synapse of	

the NK cell	- 28 -
2.3.5 PD-1 signaling inhibits integrin signaling.....	- 31 -
2.3.6 PD-1 signaling blocks receptor-activated calcium response in NK cells.....	- 34 -
2.3.7 ITSM domain is required for the inhibitory function of PD-1.....	- 41 -
2.4 Summary, discussion and future directions	- 44 -
2.4.1 PD-1 and IS stability.....	- 45 -
2.4.2 PD-1 and integrin 'outside-in' signaling induced LG polarization in NK cells	- 47 -
2.4.3 Calcium and LG polarization.....	- 49 -
2.4.4 Exchange of PD-1 and PD-L1 in NK and target cells	- 50 -
Chapter 3 RIP3 dependent necroptosis is involved in acidosis induced cell death <i>via</i> MLKL & AIF...-	
54 -	
3.1 Background.....	- 54 -
3.1.1 Ischemic stroke.....	- 54 -
3.1.2 Acidosis and acidotoxicity	- 55 -
3.1.3 Acid-sensing ion channel.....	- 56 -
3.1.4 Necroptosis and Parthanatos	- 58 -
3.2 Materials and methods	- 61 -
3.2.1 Cell lines and mouse cortical neuron culture.....	- 61 -
3.2.2 Cell death assay.....	- 61 -
3.2.3 Knocking down of mouse MLKL	- 64 -
3.2.4 Patch clamp electrophysiology.....	- 64 -
3.2.5 Co-immunoprecipitation	- 64 -
3.2.6 Immunoblotting (Western blotting).....	- 65 -
3.2.7 Immunocytochemistry	- 66 -
3.2.8 Focal ischemia	- 67 -
3.2.9 Statistical analysis.....	- 68 -
3.3 Results	- 68 -
3.3.1 RIP3 is involved in acidosis-induced neuronal cell death.....	- 68 -
3.3.2 Re-introduction of RIP3 increases cell death in response to acidosis	- 71 -
3.3.3 MLKL is involved in acidosis-induced cell death in N2a-RIP3 cells.....	- 79 -
3.3.4 pH 6.0 ECS down regulates RIP1 and I κ B α in N2a cells independently of RIP3	- 83 -
3.3.5 Starvation plays a critical role in acidosis-induced cell death	- 87 -
3.3.6 Acidosis induces AIF nuclear translocation	- 92 -
3.3.7 ROS and MPTP are involved in AIF nuclear translocation in response to acidosis/	

starvation	- 95 -
3.3.8 RIP3 inhibitor dabrafenib attenuated ischemic brain damage <i>in vivo</i>	- 97 -
3.4 Summary and discussion	- 99 -
3.4.1 Starvation is a critical contributing factor for acidosis induced cell death.....	- 100 -
3.4.2 RIP3 and MLKL are involved in acidosis/starvation-induced cell death	- 101 -
3.4.3 AIF translocation in acidosis/starvation induced cell death.....	- 102 -
3.4.4 Contribution of mitochondria in acidosis/starvation-induced necroptosis	- 104 -
3.4.5 Acidosis/starvation-induced necroptosis and stress adaption.....	- 104 -
Chapter 4 Discussion	- 107 -
References.....	- 110 -
Vita	- 131 -

List of Figures

Figure 1. Cell death classification recommended by NCCD.....	- 2 -
Figure 2. Schematic model of cell death inhibition by PD-1.....	- 3 -
Figure 3. Schematic model of acidotoxic cell death mediated by RIP3.	- 3 -
Figure 4. Verification of PD-1 and PD-L1 protein expression in NK and target cells, respectively, by flow cytometry.....	- 17 -
Figure 5. Fluorescence protein-tagged PD-1 and PD-L1 are expressed on the plasma membrane of NK and target cells, respectively.....	- 18 -
Figure 6. PD-L1-positive target cells inhibit the cytotoxicity of PD-1-positive NK cells....	- 20 -
Figure 7. NK cells cannot perform ADCC without rituximab.	- 21 -
Figure 8. GFP or PD-1-GFP expression does not affect the surface expression of activating receptors CD16 and NKG2D in NK cells.	- 23 -
Figure 9. PD-1 and PD-L1 molecules accumulate at immunological synapse (IS) in NK cells.....	- 24 -
Figure 10. PD-1 and PD-L1 molecules accumulate at immunological synapse (IS) in NK cells.-	- 25 -
Figure 11. PD-1 signaling does not affect the conjugation between NK and target cells. ...	- 27 -
Figure 12. PD-1 engagement blocks lytic granule (LG) polarization.....	- 29 -
Figure 13. PD-1 engagement constantly blocks lytic granule polarization.	- 30 -
Figure 14. PD-1 signaling blocks the accumulation of ILK to IS in NK cells.	- 32 -
Figure 15. PD-1-GFP expression does not affect the overall expression of LFA-1 in NK cells.....	- 33 -
Figure 16. BAPTA blocks LG polarization.....	- 37 -
Figure 17. PD-1 signaling blocks Ca ²⁺ -response in NK cells.	- 38 -
Figure 18. PD-1 signaling blocks both ER calcium release and receptor activation-dependent Ca ²⁺ influx in NK cells.....	- 39 -
Figure 19. PD-1 signaling does not block pharmacological store-operated calcium entry.-	- 40 -
Figure 20. PD-1 mutants accumulate at IS normally with PD-L1.	- 42 -
Figure 21. Y248 of PD-1 is crucial for its inhibition of NK cell cytotoxicity.....	- 43 -
Figure 22. Schematic working model.....	- 45 -
Figure 23. Exchange of PD-1 and PD-L1 between NK and target cells after long-time conjugation.....	- 51 -
Figure 24. RIP3 is involved in acidosis-induced neuronal cell death.	- 70 -
Figure 25. Verification of RIP3 expression in HEK293 cells.	- 73 -
Figure 26. hRIP3 expression confers TSZ-induced cell death and differential responses to	

pH 7.4 and pH 6.0 ECS, as determined by CTB assay.	- 74 -
Figure 27. hRIP3 expression confers TSZ-induced cell death and differential responses to pH 7.4 and pH 6.0 ECS, as determined by LDH assay.	- 75 -
Figure 28. Re-introduction of RIP3 increases acidosis-induced death of mouse neuroblastoma N2a cells.	- 78 -
Figure 29. MLKL is involved in acidosis-induced cell death.	- 81 -
Figure 30. MLKL knocking down suppresses acidosis-induced cell death.	- 82 -
Figure 31. Acidosis down regulates RIP1 independently of RIP3.	- 85 -
Figure 32. Acidosis down regulates I κ B α in an ASIC1-dependent manner but independently of RIP3.	- 86 -
Figure 33. Treatment with ECS triggers a decrease in LC3-II levels in WT N2a cells independent of pH.	- 89 -
Figure 34. Starvation is required for acidosis induced cell death.	- 90 -
Figure 35. The lack of effect of pH 6.0 medium on RIP1 and I κ B α levels in the absence of starvation.	- 91 -
Figure 36. Acidosis induces AIF and RIP3 nuclear translocation.	- 94 -
Figure 37. VDAC inhibitors and antioxidants attenuated acidosis induced cell death. ...	- 96 -
Figure 38. Neuroprotection by RIP3 inhibitor dabrafenib and ASIC1a gene knock out. .	- 98 -
Figure 39. Schematic working model.	- 100 -

List of Tables

Table 1. Reagents used for cell death assay	- 63 -
Table 2. Different acid sensitivity of various cells.....	- 71 -

Abbreviations

ACD: accidental cell death

aCSF: artificial cerebrospinal fluid

ADCC: antibody dependent cellular cytotoxicity

AD: Alzheimer's disease

AIF: mitochondrial apoptosis-inducing factor

ASICs: acid-sensing ion channels

BASIC: bile acid-sensitive ion channel

BSA: bovine serum albumin

CHO: Chinese hamster ovary

CsA: cyclosporine A

CTB: cell titer blue

CTLs: cytotoxic T lymphocytes

DC: dendritic cell

DR: death receptor

ECS: extracellular solution

ENaC/Deg: epithelial sodium channels/ degenerin

ER: endoplasmic reticulum

FACS: fluorescence-activated cell sorting

FBS: fetal bovine serum

HBSS: Hank's Balanced Salt Solution

hBECs: human brain endothelial cells

HEK293T: human embryonic kidney 293T

HIF-1: hypoxia-inducible factor-1

HD: Huntington's disease

ICD: immunogenic cell death

i.c.v.: intracerebroventricularly

ITSM: immunoreceptor tyrosine-based switch motif

ITIM: immunoreceptor tyrosine-based inhibitory motif

ICAM-1: intercellular adhesion molecule 1

ILK: integrin-linked kinase

IS: immunological synapse

KIR: killer cell immunoglobulin-like receptor

LAD-I: leukocyte adhesion deficiency syndrome type I

LCMV: lymphocytic choriomeningitis virus

LDH: lactate dehydrogenase

LFA-1: leukocyte function-associated antigen 1

LG: lytic granules

MCAO: middle cerebral artery occlusion

MLKL: mixed lineage kinase domain-like pseudokinase

MPTP: mitochondrial permeability transition pore

MTOC: microtubule-organizing center

NCCD: Nomenclature Committee on Cell Death

N2a: Neuro-2a

Nec1: necrostatin-1

NK cell: natural killer cell

NC: natural cytotoxicity

NKG2D: NK group 2 member D

PAR polymers: poly(ADP-ribose) polymers

PARP: poly(ADP-ribose) polymerase

PCR: polymerase chain reaction

PcTX1: psalmotoxin 1

PD: Parkinson's disease

PD1: programmed death 1

PMA: phorbol 12-myristate 13-acetate

P/I: PMA/ionomycin RCD: regulated cell death

PVDF: polyvinylidene fluoride

RGC: retinal ganglion cells

RIP1: receptor-interacting serine/threonine-protein kinase 1

RIP3: receptor-interacting serine/threonine-protein kinase 3

ROS: reactive oxygen species

SOCE: store-operated Ca^{2+} entry

STIM1: stromal interaction molecule 1

TCR: T cell receptor

T_{reg}: regulatory T cell

TG: Thapsigargin

TNFR1: tumor necrosis factor receptor 1

tPA: tissue plasminogen activator

TTC: 2,3,5-triphenyltetrazolium hydrochloride

VDAC: voltage-dependent anion channels

VCP: vertical cell pairing

Chapter 1

Introduction

Cell death is the event when a cell ceases to carry out its function. It occurs naturally as old cells are replaced by new ones, or it may result from stress due to disease or injury. Due to technical limitations, the early classifications of cell death were purely based on morphological changes. For a long time, apoptosis, necrosis and autophagic cell death were considered to be the three main kinds of cell death. However, with recent improvements in knowledge and research tools, more forms of cell death have been uncovered, for example, necroptosis parthanatos, anoikis, entosis and so on. Cells die by a variety of mechanisms; a cell death nomenclature will be considered useful only if it predicts the possibilities to modulate (induce or inhibit) cell death. Thus, the Nomenclature Committee on Cell Death (NCCD) recently suggested a new way to classify cell death based on two major categories (**Figure 1**). In the first kind, cells exposed to extreme physicochemical or mechanical stimuli can die in an uncontrollable manner; such an unavoidable cellular demise is referred to as “accidental cell death” (ACD). In the second kind, which applies to most settings, cell death is initiated by a genetically encoded apparatus and its course can be altered by pharmacological or genetic interventions; this is now referred to as “regulated cell death” (RCD) (1).

For RCD, on one hand, it is necessary for the body to replace or destroy the old, malfunctioning or sick cells. This is achieved by promoting them to undergo

programmed death or recruiting other cells such as phagocytes and lymphocytes to kill them. On the other hand, it is desirable to prevent the loss of healthy or functional cells such as neurons. For this purpose, the body has developed multiple adaptive mechanisms to detect and respond to environmental danger and whereby protect the cells from being damaged.

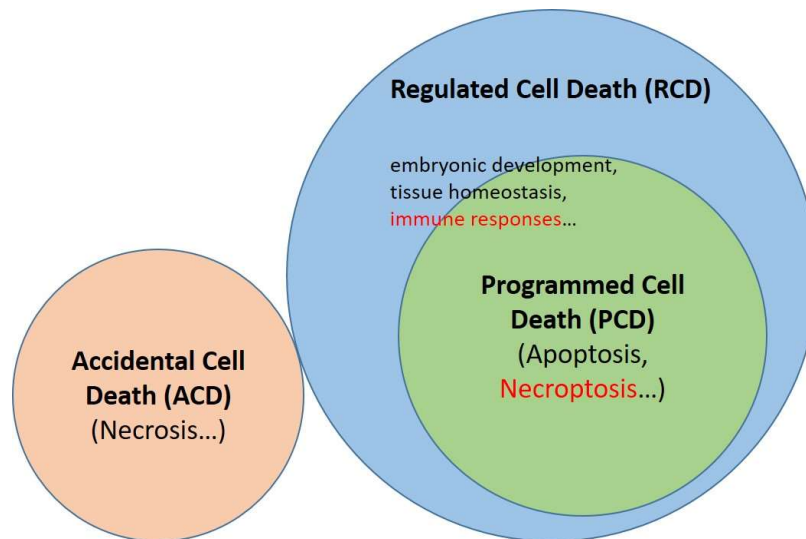


Figure 1. Cell death classification recommended by NCCD. Cell death can be classified to ACD and RCD based on whether or not it can be altered by pharmacological or genetic interventions. The “immune responses” and “necroptosis” labeled in red are the subjects studied and reported in this thesis.

Cancer cells develop many ways to avoid death by either upregulating proteins that inhibit death or downregulating those that play important roles in mediating cell death. The two excellent examples are pathways that involve PD-1 and RIP3. While PD-1 is an inhibitor of RCD (**Figure 2**), RIP3 directly mediates RCD (**Figure 3**). In studies described in this thesis, I have examined the role and mechanism of PD-1 in

cytotoxic killing by natural killer (NK) cells and the function and signaling pathways by which RIP3 contributes to acidosis-induced cell death.

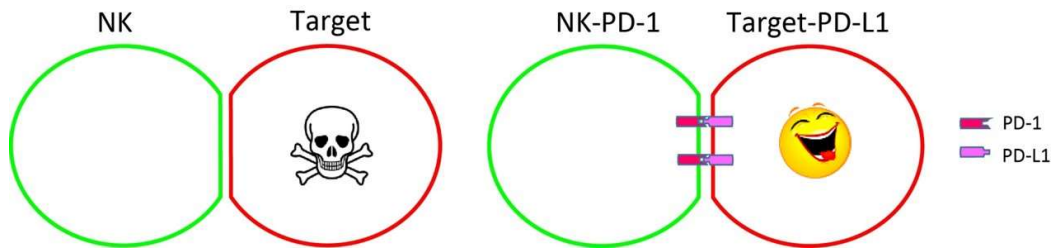


Figure 2. Schematic model of cell death inhibition by PD-1. In the absence of PD-1/PD-L1 engagement (*left*), NK cell destroys an encountered target cell. However, in the presence of PD-1/PD-L1 engagement (*right*), which triggers inhibitory signaling, the cytotoxicity of NK cell is suppressed, resulting in the survival of the target cell.

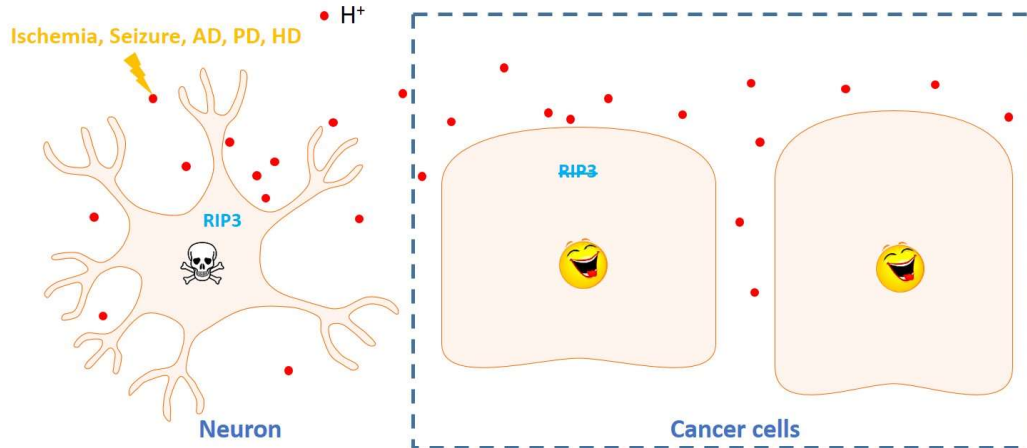


Figure 3. Schematic model of acidotoxic cell death mediated by RIP3. Tissue acidosis occurs in both cancers and nervous system diseases, such as brain ischemia, trauma, seizure, Alzheimer's disease (AD), Parkinson's disease (PD), and Huntington's disease (HD). In neurons, RIP3 mediates cell death in response to acidosis, whereas in many cancer cells, the expression of RIP3 is suppressed, allowing them to thrive in acidic environment.

Chapter 2

PD-1 Blocks Lytic Granule Polarization and Calcium signaling

in Natural Killer Cell

This chapter is based upon “Huang Y, Jang JH, Bertolet G, Kang X, Huang SJ, Hu Q, Qin LD, Zhu MX, Liu DF. PD-1 blocks lytic granule polarization in natural killer cell immunological synapse via impairing integrin ‘outside-in’ signaling”, *currently under revision for the Journal of Allergy and Clinical Immunology*.

2.1 Background

2.1.1 NK cells in immune system

NK cells provide the first line of defense to cancer and virus infection (2, 3). These cells can migrate into almost any tissue triggered by inflammation and other factors (4). Traditionally, NK cells are considered to be innate immune cells since they do not rearrange genes to acquire antigen-specific receptors like B and T lymphocytes. Instead, they attack targets *via* an array of germ line encoded cell surface receptors (5).

Like cytotoxic T lymphocytes (CTLs), NK cells mostly defend against threats by targeting the affected cells for destruction through delivery of lytic granules (LG). This pathway is triggered by signals from activating receptors such as NK group 2 member D (NKG2D), which induces natural cytotoxicity (NC), or Fc receptors CD16, which mediates antibody dependent cellular cytotoxicity (ADCC). For effective elimination of

virus-infected cells or tumor cells, NK cells have to integrate both activation receptor signaling and inhibitory receptor signaling (3, 6). One of the most important inhibitory signals with which NK cells must contend is that generated by PD-1.

2.1.2 PD-1

Since its discovery in 1992 by the Honjo group (7), PD-1 has emerged as a crucial regulator of the immune system. PD-1 is expressed on the surface of a variety of immune cells, including activated/exhausted T cells, activated/exhausted B cells, activated monocytes, dendritic cells, regulatory T cell (T_{reg}) (8) and NK cells (9-11).

PD-1, when bound by either of its ligands, PD-L1 (12) and PD-L2 (13), delivers an inhibitory signal via recruitment and activation of the phosphatases SHP-1 and SHP-2, which dephosphorylate critical signaling molecules (e.g., ZAP-70) involved in the activation cascade downstream of activating immunoreceptors (14). Of the two, SHP-2 appears to be the primary player, as it is the only molecule that directly interacts with the immunoreceptor tyrosine-based switch motif (ITSM) domain of PD-1 (14). PD-1 signaling can protect against tissue damage and autoimmune diseases by inducing and maintaining T cell tolerance (11) and inhibiting self-reactive T cells (15), respectively. However, PD-1 signaling can be maladaptive, as it is the major cause of effector cell exhaustion during long-term, chronic antigen stimulation (11). Specifically, PD-1 signaling blocks T, B, and NK cell functions, including proliferation (16), development (8), cytokine (e.g., IL-2) production (17), adhesion (18), and cytotoxicity (19).

Due to its important role in suppression of the immune response, therapeutic approaches targeting the PD-1 pathway have garnered heavy attention from both academic researchers and pharmaceutical companies. Of particular focus has been antibody-mediated blockade of either PD-1 itself or its ligands, with the rationale being that suppression of PD-1 signaling allows activation of tumor-specific CTLs or other effector cells (e.g., NK cells) by removing the cytotoxic lymphocyte activation 'brake' and modifying the tumor microenvironment (20, 21). Currently, a search for 'PD-1 blockade' in the clinicaltrial.gov database yields 96 hits, indicating extensive clinical research and applications focusing on blockade of PD-1 pathways.

PD-1 pathway blockade can be effective for both hematological cancer (e.g., leukemia) and solid cancers (e.g., myeloma, metastatic bladder cancer, and non-small cell lung cancer) with durable clinical responses and tolerable side effects (22-24). Additionally, PD-1 pathway blockade has the potential to restore the function of exhausted T cells in chronic viral infection, such as HIV (25, 26), HCV (27, 28), and HBV (29, 30). However, despite the great promise seen in these successful studies and trials, the importance of NK cells in combating diseases, and the known effects of PD-1 on NK cells, the precise mechanism whereby PD-1 mediates its effects in NK cells remains poorly characterized.

2.1.3 Integrin signaling in NK cells

Integrins are heterodimeric proteins consisting of α and β subunits that bind to the extracellular matrix and other proteins to regulate interactions among cells or matrix.

Integrins play an essential role in many processes, including cell cycle, cell adhesion and migration (31). In mammals, there are 18 α and 8 β integrin subunits. Lymphocyte function-associated antigen 1, also known as LFA-1, consists of a family of leukocyte integrins that are made of α L (CD11a) and β 2 (CD18) subunits. They bind to intercellular adhesion molecule 1 (ICAM-1) expressed on other cells and function as adhesion molecules.

The high-affinity conformation of integrins β 1 and β 2 families is dependent on “inside-out” signals delivered by receptors that stimulate extension of the $\alpha\beta$ heterodimer and exposure of the ligand-binding site (32). In turn, the binding of integrin to its ligand transduces “outside-in” signals, which regulate lymphocyte motility, polarity, and adhesion. The loss of β 2 integrin results in leukocyte adhesion deficiency syndrome type I (LAD-I), which is characterized by severe abnormalities in the adhesion-dependent functions of leukocytes (33).

No single molecule alone can be used to define ‘outside-in’ or ‘inside-out’ signaling of integrins in either NK or T cells (34, 35). In T cells, T cell receptors (TCR) signaling alone can induce granule polarization. TCR signaling also provides strong ‘inside-out’ signals to LFA-1, and the co-engagement of LFA-1 and TCR enhances the extent of granule polarization induced by the TCR alone (36). However, in NK cells, the ligation of LFA-1 with ICAM-1 alone is sufficient to trigger LG polarization. Other NK receptors are thought to be only responsible for degranulation but not LG polarization. Thus, NK cells have proven useful in the analysis of ‘outside-in’ signaling by LFA-1 independently of other signals (37). A recent study by Zhang et al. revealed

a signaling network centered on an integrin-linked kinase (ILK)-Pyk2-paxillin pathway that becomes active after the binding of the integrin to its ligand (outside-in) and is required for LG polarization in NK cells (38). ILK is recruited to immunological synapse (IS) as shown by proximity ligation assays and its silencing impairs the polarization of LGs in NK cells (38). In the current study, I tested whether PD-1 signaling affects this integrin 'outside-in' signaling in NK cells.

2.1.4 Calcium signaling in NK cells

Uptake of extracellular calcium ions (Ca^{2+}) is required for lymphocyte cytotoxicity (39, 40). ORAI1 and stromal interaction molecule 1 (STIM1) were identified as the main molecular mediators for Ca^{2+} entry into T cells and NK cells following the activation of TCR and NK cell receptors, respectively. Upon receptor activation, Ca^{2+} is released from the endoplasmic reticulum (ER) *via* the activation of IP_3 receptors. STIM1, localized on the ER membrane, acts as the sensor of the ER contents and becomes aggregated upon ER Ca^{2+} depletion. It then approaches the plasma membrane and forms a physical interaction with ORAI1 to trigger extracellular Ca^{2+} influx. This process is termed store-operated Ca^{2+} entry (SOCE) (41). Significantly, patients with mutations of ORAI1 or STIM1 have severe immunodeficiency due to impaired SOCE (42, 43).

It has been demonstrated that SOCE *via* ORAI1 is critical for target cell-induced LG exocytosis in NK cells and CTLs (39, 44). However, the involvement of Ca^{2+} influx in signaling processes that mediate target cell adhesion, LFA-1 activation and LG

polarization is not clear. Although it has been shown that LG polarization is not affected in NK cells from patients with ORAI1 mutation (44), I found a defect of LG polarization when using BAPTA-AM to strongly block the rise in intracellular Ca^{2+} concentration in NK cells. Furthermore, I also tested the effect of PD-1 engagement on Ca^{2+} flux in NK cells.

In this study, I investigated the role of PD-1 in human NK cell cytotoxicity. I found that PD-1 activation by PD-L1 blocked NK cell cytotoxicity. However, PD-1 signaling did not inhibit cell-cell conjugation between NK and target cells, an initial step for NK-mediated immune responses. Instead, NK cells that expressed PD-1 formed stable inhibitory IS with target cells that expressed PD-L1. However, LG polarization was blocked by PD-1 engagement *via* disruption of the integrin 'outside-in' signaling pathway. NK cell receptor activation-induced intracellular Ca^{2+} concentration rise was also abolished by PD-1 engagement. Similar to T cells, the ITSM but not ITIM domain of PD-1 is crucial for its inhibition effect on NK cells.

2.2 Materials and methods:

2.2.1 Cell Culture

Human Embryonic Kidney 293T (HEK293T) cells were maintained in DMEM (Gibco, USA) with 10% fetal bovine serum (FBS, Gibco), 2 mM L-Glutamine (Gibco), and 10 mM HEPES (Gibco). K562 and Daudi cell lines (American Type Culture Collection, ATCC) were cultured in R10 medium, which contains RPMI 1640 medium (Gibco) supplemented with 10% FBS, 2 mM L-Glutamine, 10 mM HEPES, 1 mM sodium pyruvate (Cellgro, USA), and 1% MEM non-essential amino acids solution (Gibco). CD16-KHYG-1, a human NK cell line capable of both ADCC and natural cytotoxicity (45), was a gift from Dr. David Evans (University of Wisconsin, Madison, WI) and cultured in R10 medium supplemented with 1 µg/ml cyclosporine A (CsA, Sigma-Aldrich, USA), 50 µg/ml Primocin (Invivogene, USA) and 10 U/ml interleukin-2 (IL-2, Roche, USA). All cells were cultured at 37°C in a humidified atmosphere with 5% CO₂. For all experiments, the culture medium of CD16-KHYG-1 cells was replaced to remove CsA one day before the experiments.

2.2.2 cDNA expression constructs and transduction of CD16-KHYG-1, K562, and Daudi cell lines

The GFP, PD-1-GFP, mCherry, PD-L1-mCherry lentiviral plasmids were generated as previously described (46). Briefly, to generate the PD-1-GFP construct, the full length of PD-1-GFP (OriGene, USA) was subcloned into the lentiviral expression vector, pCDH (System Biosciences, USA), using EcoRI and BamHI

(Thermo Scientific, USA) insertion sites. To make the C-terminal mCherry-tagged PD-L1 construct, the PD-L1 cDNA (OriGene) was subcloned into EcoRI and BamHI digested pmCherry-N1 vector (Clontech, USA) first. The sequence of PD-L1-mCherry was amplified by polymerase chain reaction (PCR) and inserted into EcoRI digested pCDH using the In-fusion cloning system (Clontech, USA). The sequence of turboGFP or mCherry was inserted into pCDH to create the construct for GFP or mCherry, respectively, for lentiviral production, and for serving as experimental control.

QuikChange II Site-Directed Mutagenesis Kit (Agilent Technologies, USA) was used to make PD-1 mutations on the generated PD-1-GFP lenti-plasmid. The primers for Y223F are 5'-cagctccccaagtcacagagaacacagg-3' and 5'-cctgtgtctctgtggactttgggagctg-3', for Y248F are 5'-aatggtggcaaactccgtctgctcaggac-3' and 5'-gtccctgagcagacggagtttgccaccatt-3'. The PD-1-GFP double mutation was made by introducing Y223F mutation on the plasmid that already contained Y248F. All plasmids were verified by sequencing.

To generate polyclonal stable cell lines, the lentivirus was generated by co-transfecting HEK293T cells with the desired lentiviral vector and 3 packaging plasmids (pMLg/pRRE, pRSV-Rev, and pMD2.g) using Lipofectamine reagent (Invitrogen, USA). Briefly, 4 µl Lipofectamine was mixed with 0.8 µg total DNA (0.128 µg desired pCDH construct, 0.32 µg pMLg/pRRE, 0.16 µg pRSV-Rev, 0.192 µg pMD2.g) and added into one well of HEK293T cells cultured in a 6-well plate at approximately 70% confluence. At 48 hours after transfection, viral particles were harvested by filtering the culture medium via a 0.45 µm filter (GE Healthcare Life Sciences, USA). Then, CD16-KHYG-

1 cells were infected with 4 ml viruses for GFP or PD-1-GFP, and K562 and Daudi cells were infected with 4 ml viruses for mCherry or PD-L1-mCherry, at a density of 5×10^4 cells/ml suspended in 4 ml R10 medium. The transduced cells were cultured for 24 hours in the presence of 8.0 $\mu\text{g/ml}$ polybrene (Santa Cruz Biotechnology, USA) and subsequently sorted by an Aria II cell sorter (BD Biosciences, USA). The expression of green or red fluorescence in these cells was verified by flow cytometry using an LSR Fortessa cell analyzer (BD Biosciences).

2.2.3 Chromium⁵¹ release assay

NK cell cytotoxicity toward K562 or Daudi target cells was examined using a ⁵¹Cr-release assay as described (47). Briefly, the target cells were labeled with ⁵¹Cr at 37°C for 1 hour. After washing 3 times with fresh R10 medium, cells were re-suspended in R10 medium at a density of 1×10^5 cells/ml. An aliquot of the target cells (0.1 ml for 1×10^4 cells) were mixed with a serial dilution of NK cells, and the mixture cultured at 37°C for 4 hours. At the end of the incubation, culture medium was collected and radioactivity measured using a Topcount NXT Scintillation and Luminescence Counter (Perkin Elmer, USA). The mean percentage of specific lysis of triplicate wells was calculated as follows: $[(\text{test counts} - \text{spontaneous counts}) / (\text{maximum counts} - \text{spontaneous counts})] \times 100\%$.

2.2.4 Conjugation assays

NK-target conjugates were measured as described previously (48). NK cells

and target cells (K562 or Daudi) were washed 3 times with phosphate-buffered saline (PBS) and allowed to mix at 37°C with the densities of 1×10^5 NK cells and 2×10^5 target cells per ml in total volume of 200 μ l for 0 to 30 min. At the end of incubation, cells were fixed by freshly prepared 0.5% paraformaldehyde in PBS for 15 min at room temperature. After a gentle vortex, cells were analyzed using the LSR Fortessa flow cytometer. The NK-target conjugates were identified as dual-color positive particles with both green and red signals.

2.2.5 Immunofluorescence staining

An aliquot of the NK-target conjugates, as described above, was added to the poly-lysine- coated slide, prepared as described previously (49) and allowed to settle for 15-30 min. After the conjugates attached, the slide was washed 3 times with PBS, and cells were fixed with 4% paraformaldehyde in PBS for 20 min. The fixed cells were washed 3 times with PBS and permeabilized with a buffer containing 0.1% Triton X-100 and 5% normal donkey serum before incubation with the primary antibodies at 4°C overnight. The primary antibodies were: perforin (δ G9, Pierce Chemical Co.) and ILK (Abcam). The cells were washed and probed with the fluorophore-conjugated secondary antibodies (Invitrogen, USA) at room temperature for 1.5 hours. When needed, Alexa Fluor dye-conjugated phalloidin (Invitrogen, USA) was used to stain F-actin. The slide was mounted with a glass coverslip using the ProLong Gold antifade reagent containing DAPI (Life Technologies, USA).

2.2.6 Laser scanning fluorescence confocal microscopy

For live cell imaging, high-resolution images were captured by a confocal fluorescent microscope (Leica TCS SP8, Leica Microsystem, Germany) equipped with a 63× oil immersion objective lens (NA 1.47, Leica Microsystem) under 37°C. The fluorescence from GFP, mCherry, and the bright field images were detected simultaneously. For imaging fixed cells, images were acquired using the LASAF software (Leica Microsystem). Three-dimensional (3D) images were reconstructed from acquired z-stacks of X-Y scanning of entire cells for perforin, F-actin, and ILK. ImageJ was used for image processing and creating projected images from 3D reconstructions.

To measure the distance between LGs (perforin staining) and IS (F-actin staining), ImageJ and Imaris (Bitplane) software were used. From the 3D image, coordinates for the center of a “dot” (perforin, x_1 , y_1 , z_1) and that of the “surface” (accumulated F-actin, x_2 , y_2 , z_2) were obtained for each conjugate, and entered into the equation: $D = \sqrt{(x_1 - x_2)^2 + (y_1 - y_2)^2 + (z_1 - z_2)^2}$, where D is the average distance of every perforin to the center of the IS for each pair of NK-target conjugate.

2.2.7 Intracellular Ca^{2+} measurement

A ratiometric dye, Indo1-AM (ThermoFisher Scientific, USA), was used for measuring intracellular Ca^{2+} concentrations. For each condition, 5×10^5 NK cells were incubated with 1 μM Indo1-AM in R10 medium for 30 min in the cell culture incubator. The cells were then washed with PBS once and incubated with primary antibodies on

ice for 30 min in 200 μ l extracellular solution (ECS) that contains 140 mM NaCl, 2 mM CaCl_2 , 5 mM KCl, 1 mM MgCl_2 , 10 mM Glucose, 10 mM HEPES, pH 7.4. The primary antibodies were: anti-CD16, anti-NKG2D and anti-PD-1 (Biolegend, USA). The antibody-coated cells were then washed once with cold PBS, resuspended in 500 μ l ECS, and then subject to fluorescence-activated cell sorting (FACS). An ultraviolet (UV) laser (355 nm) was used to excite Indo1, and two filters (DAPI 405/20, Indo1 525/50) were used to collect the emission signals. Before each experiment, cells were warmed in a 37°C water bath for 5 min. To trigger the Ca^{2+} response, a secondary goat $\text{F}_{(\text{ab})2}$ anti-mouse IgG antibody (Jackson ImmunoResearch Laboratories, Inc., USA) was added to each sample and mixed by vortex. To distinguish ER Ca^{2+} release from extracellular Ca^{2+} influx, ECS without added Ca^{2+} was used first and ECS containing 4 mM CaCl_2 was introduced after ER Ca^{2+} mobilization had subsided. For some experiments, BAPTA-AM (ThermoFisher Scientific, USA) was used to chelate the intracellular Ca^{2+} and thus abolish the Ca^{2+} response. Thapsigargin (TG) (Sigma, USA), phorbol 12-myristate 13-acetate (PMA) (Sigma, USA), and ionomycin (Sigma, USA) were used to trigger Ca^{2+} responses as needed. The data were analyzed by FlowJo software. Calcium signal was indicated by the ratio of the fluorescence intensities acquired at 405 and 525 nm emission wavelengths.

2.2.8 Statistical analysis

Unpaired or paired two-tailed t-tests were performed using Prism software (GraphPad Software, Inc.).

2.3 Results

2.3.1 PD-1 signaling attenuates NK cell cytotoxicity

As a first step to understand PD-1 signaling in NK cells, I generated a stable CD16-KHYG-1 cell line expressing PD-1-GFP (NK-PD-1-GFP). CD16-KHYG-1 is a human NK cell line that recognizes and kills target cells, such as K562 and Daudi cell lines, through two distinct mechanisms: natural cytotoxicity (NC) through activating receptors, such as NKG2D (50), and antibody-dependent cellular cytotoxicity (ADCC) through CD16 (3),(51). To test NC and ADCC of NK cells in response to PD-1 signaling blockade, K562 and Daudi cell lines stably expressing the PD-1 ligand, PD-L1-mCherry (named as K562-PD-L1-mCherry and Daudi-PD-L1-mCherry, respectively), were used as target cells. CD16-KHYG-1 and K562 (or Daudi) cell lines stably expressing GFP only or mCherry only (named as NK-GFP, K562-mCherry, and Daudi-mCherry) were used as respective controls. The expression of GFP in the stable CD16-KHYG-1 cell lines and that of mCherry in the stable K562 and Daudi cell lines were verified by flow cytometry (**Figure 4, left panels**). Using PD-1 and PD-L1 antibodies, I showed that more than 95% cells expressed PD-1 and PD-L1 in the NK-PD-1-GFP and K562-PD-L1-mCherry (or Daudi-PD-L1-mCherry) cells, respectively. However, no PD-1 staining was seen in the parental wild-type CD16-KHYG-1 cells or NK-GFP cells, and no PD-L1 was detected in the wild-type or mCherry-expressing K562 or Daudi cells (**Figure 4, right panels**). Thus, I successfully established a PD-1-positive NK cell line and PD-L1-positive target cells and their control groups for testing the effects of PD-1 signaling on NK cell cytotoxicity.

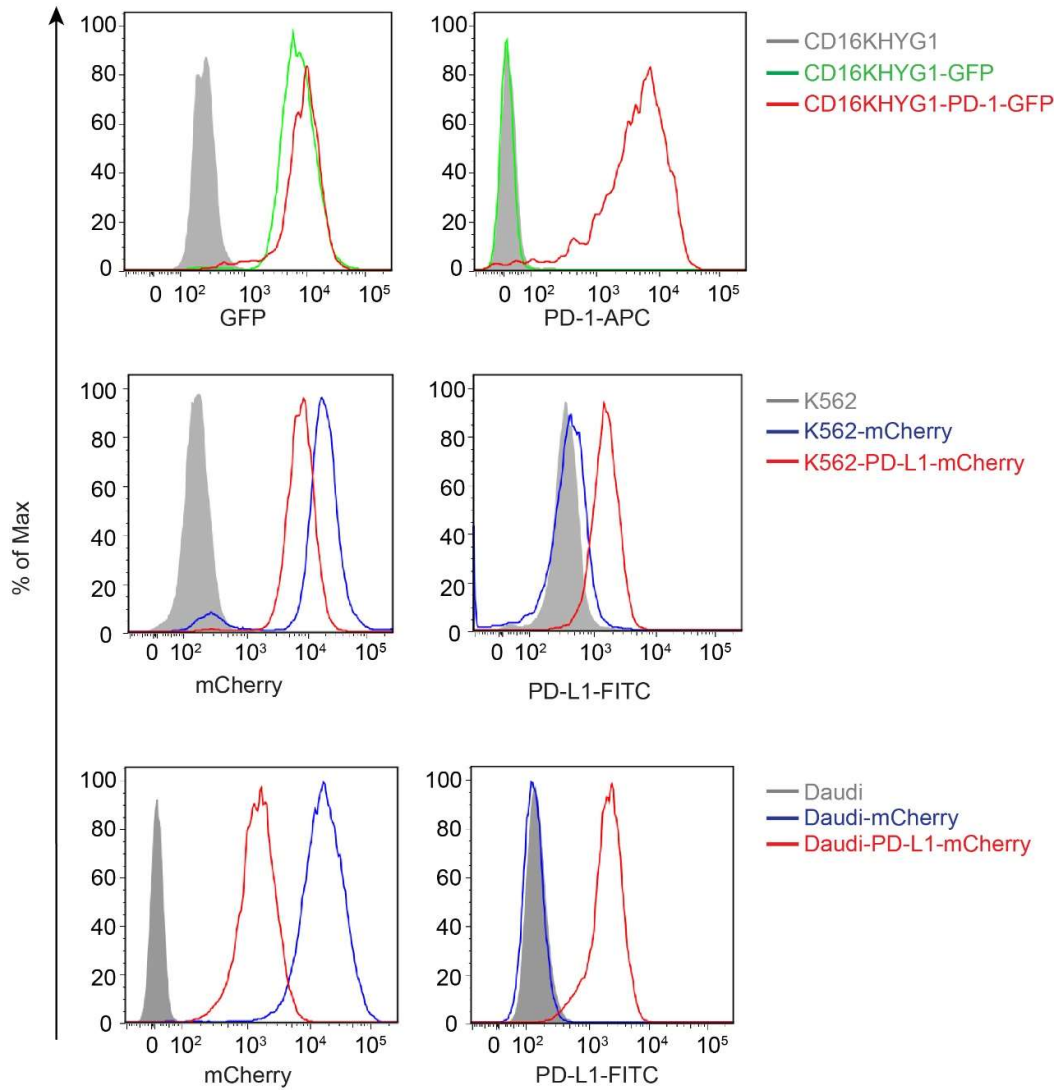


Figure 4. Verification of PD-1 and PD-L1 protein expression in NK and target cells, respectively, by flow cytometry. First row, histograms of wild-type (*gray*), and GFP- (*green*), or PD-1-GFP- (*red*) transduced CD16-KHYG-1 cells tested by flow cytometry for GFP fluorescence (*left*) and APC-tagged PD-1 antibody staining (*right*). Second and third rows, histograms of wild type (*gray*), and mCherry- (*blue*) or PD-L1-mCherry- (*red*) transduced K562 (*second row*) and Daudi (*third row*) cells measured by flow cytometry for mCherry fluorescence (*left*) and FITC-tagged PD-L1 antibody staining (*right*).

First, I examined the subcellular distribution of the expressed PD-1-GFP and PD-L1-mCherry in transduced cells. Prominent plasma membrane localization and intracellular aggregation of PD-1 and PD-L1 was observed in cells expressing PD-1-GFP and PD-L1-mCherry (**Figure 5, left panels**), but not in cells expressing GFP only and mCherry only (**Figure 5, right panels**). Plasma membrane localization and intracellular aggregation have previously been reported for endogenous PD-1 in primary T cells (52). Therefore, the subcellular localization of the expressed PD-1 and PD-L1 in the stable CD16-KHYG-1 and K562 (and Daudi) cells resembled that of endogenous PD-1 in primary T cells.

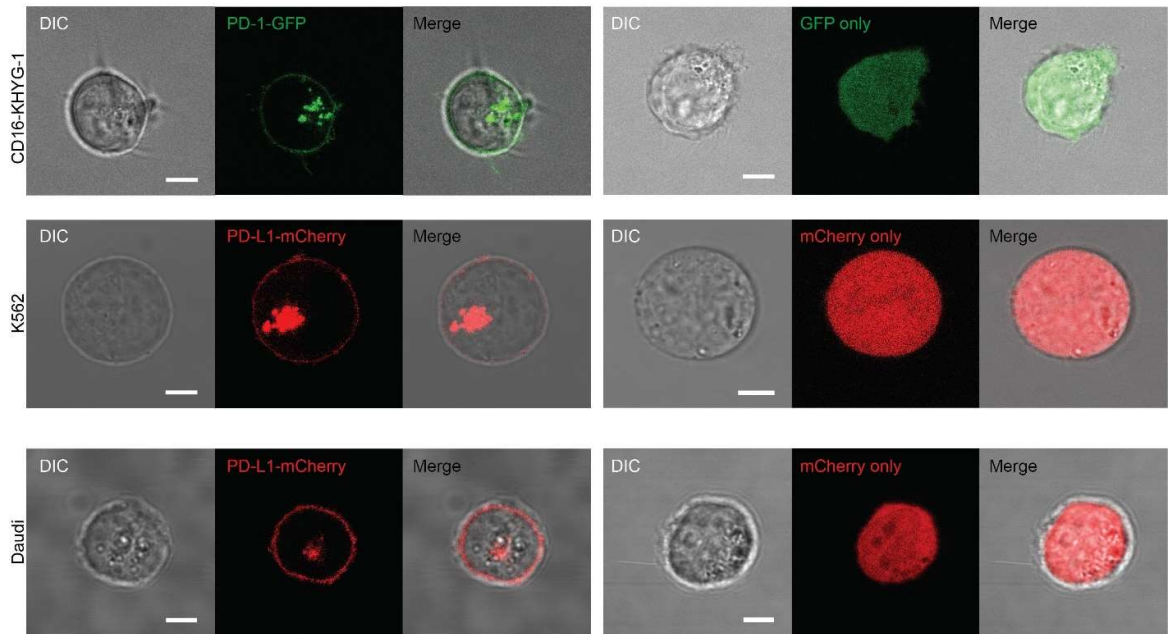


Figure 5. Fluorescence protein-tagged PD-1 and PD-L1 are expressed on the plasma membrane of NK and target cells, respectively. Representative confocal DIC and fluorescence images of GFP and mCherry for single cells that expressed GFP or PD-1-GFP (*green*) in CD16-KHYG-1 and mCherry or PD-L1-mCherry (*red*) in K562 or Daudi cells. Scale bars: 5 μ m.

To test the effect of PD-1 signaling on the cytotoxicity of NK cells, I examined the NC and ADCC ability of NK-PD-1-GFP cells using a chromium-51 (⁵¹Cr) release assay. For NC, NK-GFP and NK-PD-1-GFP cells were co-incubated for 4 hours with ⁵¹Cr-loaded K562-mCherry or K562-PD-L1-mCherry cells, whereupon the amount of ⁵¹Cr in the medium was determined. The results showed that co-incubation of NK-PD-1-GFP cells with K562-PD-L1-mCherry cells inhibited the cytotoxicity of NK cells against K562 (**Figure 6B**), but NC was unaffected without engagement of PD-1 and PD-L1 (**Figure 6A, B**). Similarly, ADCC, as examined using Daudi-mCherry or Daudi-PD-L1-mCherry cells as NK target cells, induced by rituximab (anti-CD20) (pre-incubated with Daudi cells for 30-60 min before mixing with the NK cells) was abolished only when NK-PD-1-GFP cells were co-incubated with Daudi-PD-L1-mCherry cells (**Figure 6D**). Co-incubation of CD16-KHYG-1 cells expressing PD-1 with Daudi cells not expressing PD-L1 or co-incubation of Daudi cells expressing PD-L1 with CD16-KHYG-1 cells not expressing PD-1 did not alter ADCC (**Figure 6C, D**). The NK cells failed to trigger ADCC towards Daudi cells without rituximab (**Figure 7**). Thus, the engagement of PD-1 with its natural ligand is required for inhibition of NC and ADCC. PD-1 signaling attenuates NK cell cytotoxicity.

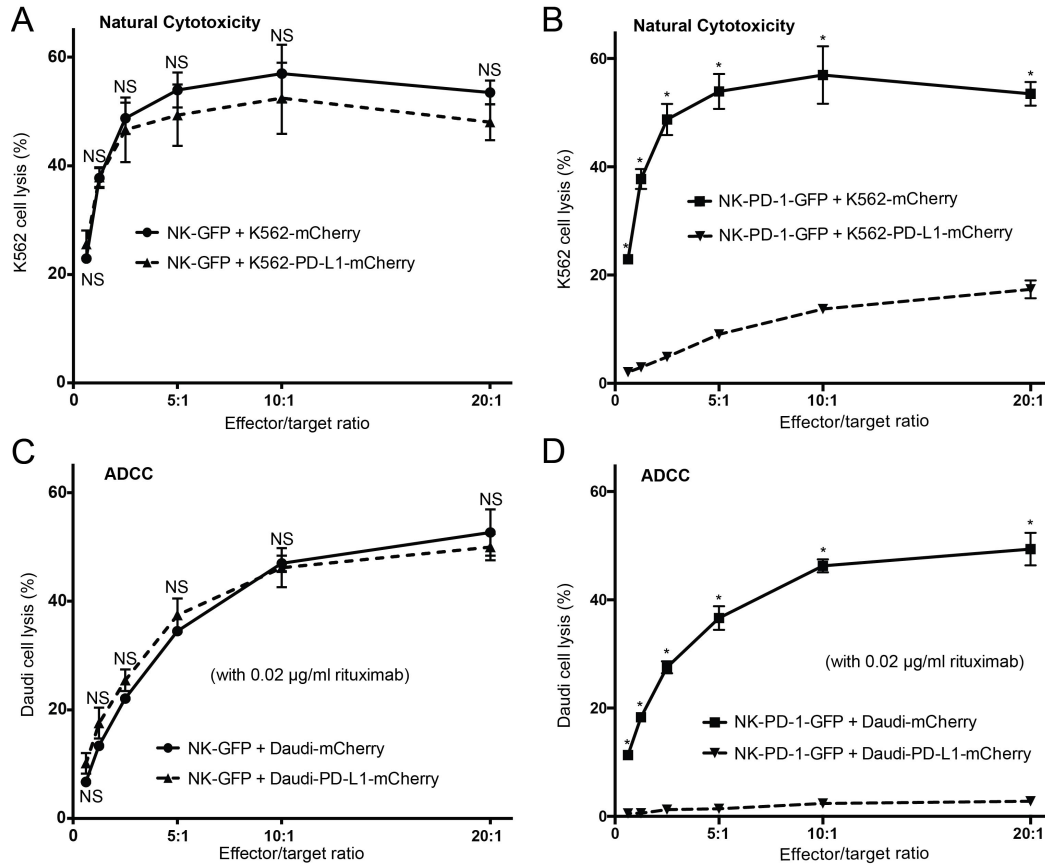


Figure 6. PD-L1-positive target cells inhibit the cytotoxicity of PD-1-positive NK cells. The natural cytotoxicity (NC) of CD16-KHYG-1 cells expressing GFP (NK-GFP) (**A**) or PD-1-GFP (NK-PD-1-GFP) (**B**) towards K562 cells that expressed either mCherry (K562-mCherry) or PD-L1-mCherry (K562-PD-L1-mCherry) was measured by a standard 4-hour ^{51}Cr -release assay with varying NK/K562 (effector/target) ratios. The antibody-dependent cellular cytotoxicity (ADCC) of NK-GFP (**C**) or NK-PD-1-GFP (**D**) towards Daudi cells that expressed mCherry (Daudi-mCherry) or PD-L1-mCherry (Daudi-PD-L1-mCherry) was measured by the ^{51}Cr -release assay in the presence of rituximab, which was pre-incubated with Daudi cells for 30 min and present throughout the 4-hour incubation period. Results are representatives of three independent experiments. Error bars represent SDs. NS, Not significant. *, $p < 0.05$.

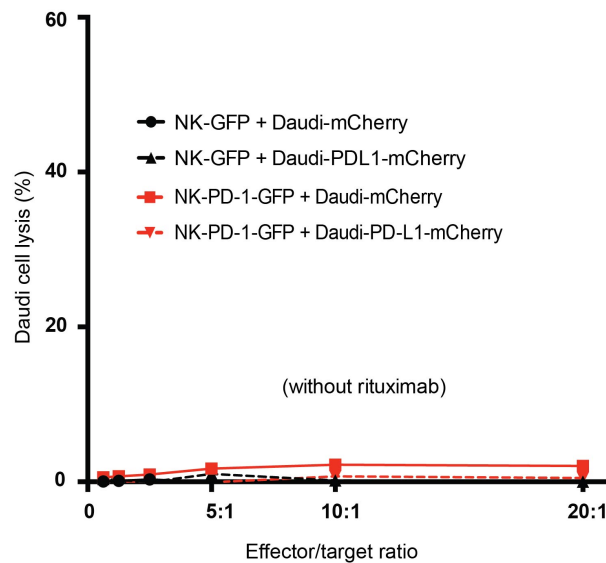


Figure 7. NK cells cannot perform ADCC without rituximab. The ADCC of NK-GFP and NK-PD-1-GFP towards Daudi-mCherry or Daudi-PD-L1-mCherry was measured by the ^{51}Cr -release assay in the absence of rituximab with varying NK/Daudi (effector/target) ratios.

2.3.2 Stable immunological synapse formation in NK cells in the presence of PD-1 signaling

The unaltered killing capability of NK-PD-1-GFP cells on PD-L1-negative target cells indicated that the activating receptors functioned normally in the transduced CD16-KHYG-1 cells in the absence of PD-L1. Indeed, by antibody staining, I showed that neither GFP nor PD-1-GFP affected the surface expression of CD16 or NKG2D (**Figure 8**), the major activating receptors in CD16-KHYG-1 cells that mediate NC and ADCC, respectively, indicating that PD-1 overexpression or lentivirus infection did not change the expression of these two major activating receptors in NK cells. Therefore,

it was likely that the PD-1/PD-L1 ligation directly inhibited the cytotoxicity of NK cells through interference with the function of its activating receptors.

To further understand the underlying molecular basis of PD-1 inhibition of human NK cytotoxicity, I investigated the role of PD-1 in regulating formation of the NK IS, a pivotal platform for mediating an effective immune response in both the adaptive and innate immune systems (46, 53, 54). For cytotoxic killing, an IS forms between the lymphocyte and the target cell, where activating receptors accumulate followed by release of LGs (55). To determine whether PD-1 in NK cells binds to IS with PD-L1 from their susceptible target cells, NK-GFP and NK-PD-1-GFP cells were allowed to form conjugates with K562 or Daudi cells that expressed either mCherry only or PD-L1-mCherry in a 1:1 ratio, and were then inspected by confocal microscopy. As shown in **Figure 9 & 10**, PD-1-GFP accumulated in IS only when the NK-PD-1-GFP cells were conjugated with K562 (for examining NC) or CD20 antibody pretreated Daudi cells (for examining ADCC) that expressed PD-L1-mCherry, which was also concentrated at the IS. The accumulation occurred within minutes and persisted for more than four hours, resembling that reported for T cells (52, 56) and inhibitory IS formation in NK cells (46). By contrast, if the target cells expressed mCherry only instead of PD-L1-mCherry, PD-1-GFP did not accumulate at the IS. *Vice versa*, PD-L1-mCherry failed to concentrate at the IS without the expression of PD-1-GFP in the NK cells (**Figure 9 & 10**). We conclude that stable inhibitory IS is formed in NK cells only in the presence of PD-1 signaling in both NC and ADCC.

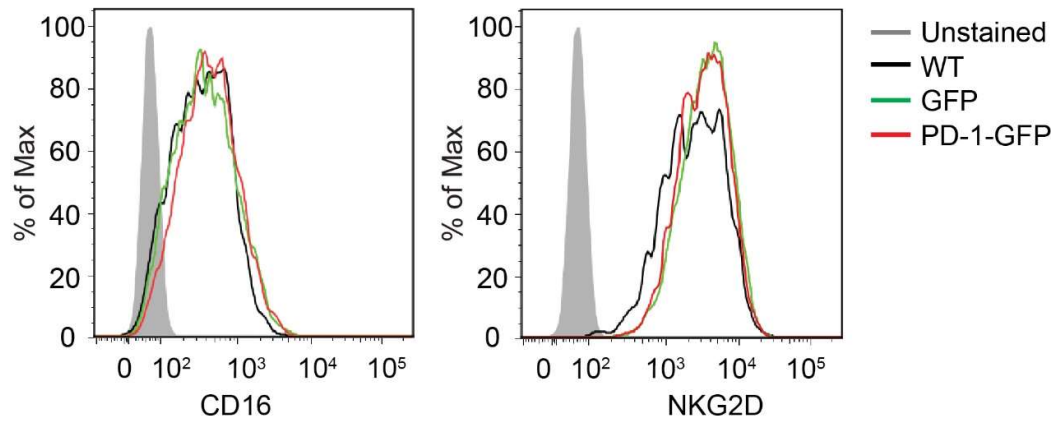


Figure 8. GFP or PD-1-GFP expression does not affect the surface expression of activating receptors CD16 and NKG2D in NK cells. Histograms of flow cytometry analyses of cell surface staining by CD16 (*left*) and NKG2D (*right*) antibodies in wild-type (*black*), and GFP- (*green*) or PD-1-GFP- (*red*) transduced CD16-KHYG-1 cells.

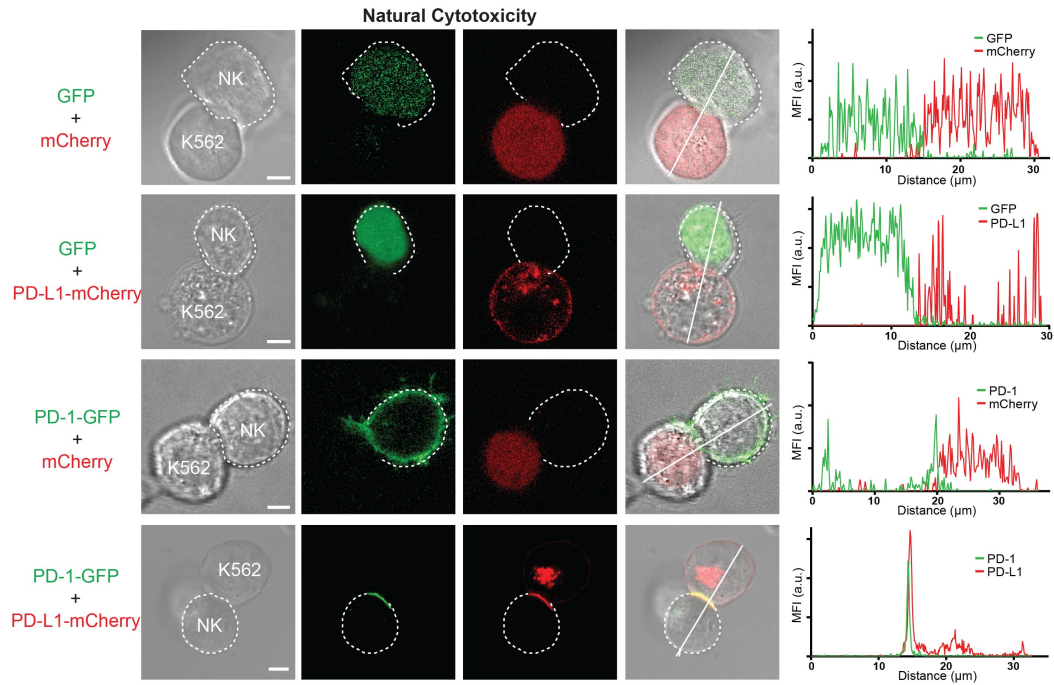


Figure 9. PD-1 and PD-L1 molecules accumulate at immunological synapse (IS) in NK cells. Live-cell imaging of NK-GFP or NK-PD-1-GFP effector cells (*green*) conjugated with target cells (*red*) that expressed mCherry or PD-L1-mCherry. K562 cells were used as CD16-KHYG-1 susceptible target cells for evaluating NC. The effector/target pairs were mixed at a 1:1 ratio. Representative live cell images were taken by confocal microscopy at 15-60 min after conjugation. Scale bars: 5 μm . IS was identified by the colocalized green and red signals (*yellow in the merged images at right*) in the bottom panels. Fluorescence intensity profiles of green and red signals as indicated were measured across the white line in the right panel.

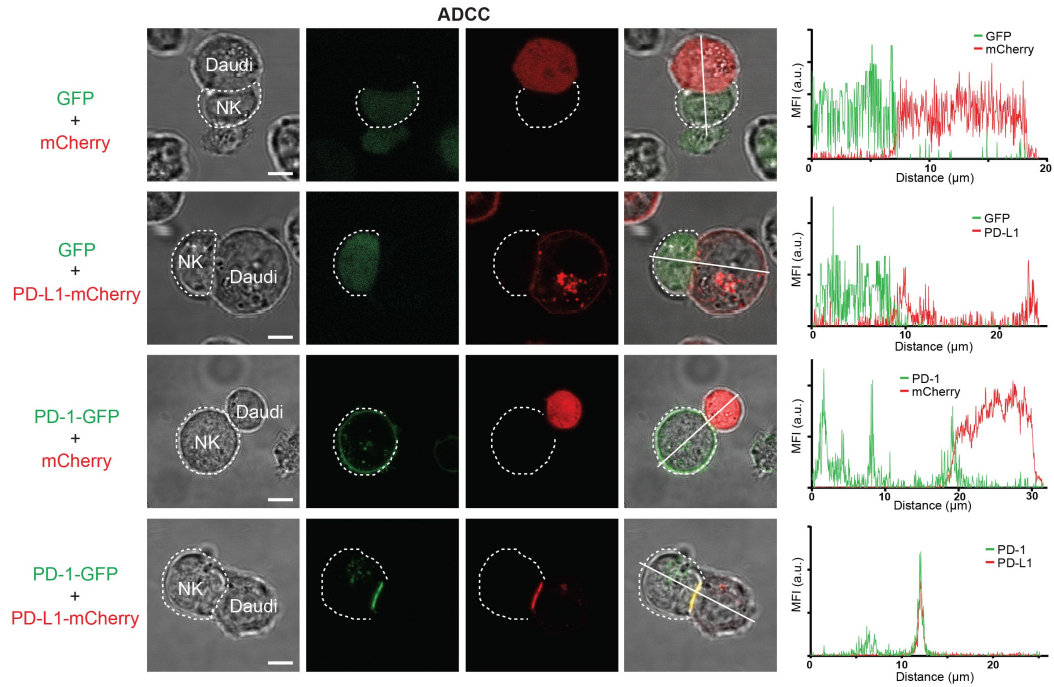


Figure 10. PD-1 and PD-L1 molecules accumulate at immunological synapse (IS) in NK cells. Live-cell imaging of NK-GFP or NK-PD-1-GFP effector cells (*green*) conjugated with target cells (*red*) that expressed mCherry or PD-L1-mCherry. Daudi cells in the presence of rituximab were used as CD16-KHYG-1 susceptible target cells for evaluating ADCC. The effector/target pairs were mixed at a 1:1 ratio. Representative live cell images were taken by confocal microscopy at 15-60 min after conjugation. Scale bars: 5 μm. IS was identified by the colocalized green and red signals (*yellow in the merged images at right*) in the bottom panels. Fluorescence intensity profiles of green and red signals as indicated were measured across the white line in the right panel.

2.3.3 PD-1 signaling does not affect NK-target cell conjugation

NK cytotoxicity involves multiple distinct steps, including conjugation with target cells, LG polarization, degranulation and cytotoxicity (53). The engagement of PD-1 with PD-L1 inhibited cytotoxic killing of target cells by CD16-KHYG-1, suggesting the formation of inhibitory synapses between PD-1 expressed in the NK cells and PD-L1 expressed in the target cells. My live imaging data shown above indeed demonstrated the close apposition between PD-1-GFP and PD-L1-mCherry expressed in NK and target cells, respectively, at the IS, which remained stable for hours (**Figure 9 & 10**). However, whether this represented stable conjugations between NK cells and target cells and how it compared to cells that did not express the inhibitory receptor were unclear.

To address this question, I used flow cytometry to determine the percentage of CD16-KHYG-1 cells that were conjugated with target cells. Interestingly, no difference in the percentage of GFP and mCherry double-positive conjugates was observed over the period of 30 min in either the NC (**Figure 11A**) or the ADCC (**Figure 11B**) assays among the different combinations of NK and target cells, with or without PD-1 and PD-L1 expression. Together, these results indicate that the PD-1/PD-L1 engagement does not affect the conjugation of NK cells with their target cells, which indicates that the PD-1 signaling may affect the downstream steps of NK cytotoxicity.

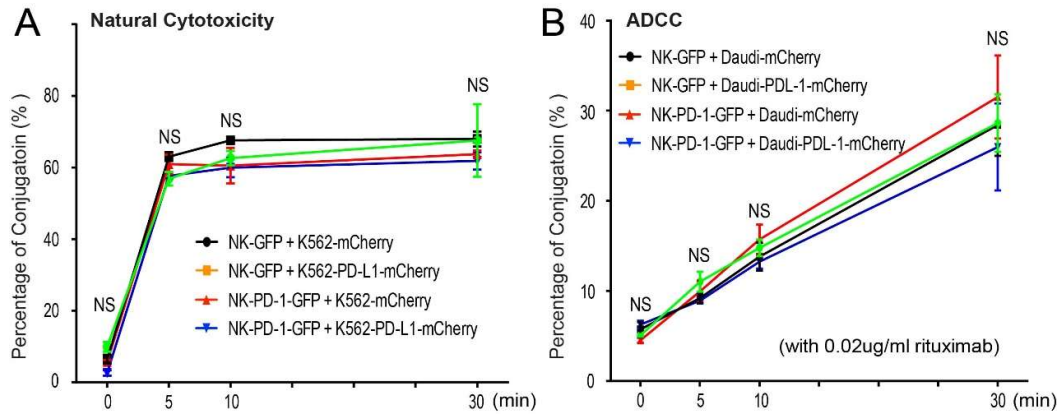


Figure 11. PD-1 signaling does not affect the conjugation between NK and target cells.

NK-GFP or NK-PD-1-GFP cells were mixed with their target cells, as indicated, at a 1:2 ratio for 30 min. Cells were fixed, and then analyzed by flow cytometry. The ratios of GFP and mCherry double-positive events to total GFP-positive NK cells were calculated to determine the percentage of conjugation. K562 cells (**A**) were used for NC and Daudi cells (**B**) were used for ADCC, where rituximab was included throughout the experiment. *Error bars represent SDs.*

Data are from three independent experiments. NS, Not significant.

2.3.4 PD-1/PD-L1 engagement blocks lytic granule polarization at immunological synapse of the NK cell

After conjugation with target cells, LGs in NK cells, which contain perforin, become polarized to the IS (49, 55). This represents another key step of cytotoxic killing (57). To examine if PD-1/PD-L1 engagement affected LG polarization in NK cells, I measured the distance of perforin-labeled LGs to the IS in target-conjugated CD16–KHYG-1 cells that expressed GFP or PD-1-GFP. Cells were co-stained for F-actin and perforin, and 3D fluorescence images of individual cell conjugates were collected by confocal microscopy. In these images, NK cells were identified by positive staining with perforin; the IS was indicated by the accumulated F-actin signal at the boundary between NK and the target cells (55). The distance between perforin, modeled as a “round dot” and the accumulated F-actin, modeled as the “surface”, was determined using Imaris software (Bitplane) and plotted for individual NK cells (**Figure 12**).

In both the NC and ADCC models, the distance between the perforin positive LGs and the IS was significantly increased in conjugates formed between NK-PD-1-GFP cells and the target cells that expressed PD-L1-mCherry, as compared to that between NK-GFP cells and targets that expressed mCherry only at 30 min after conjugation (**Figure 12**). The LG also failed to polarize on IS at later time points (60 min ,120 min) in the presence of PD-1 signaling (**Figure 13**), exclude the possibility that granule polarization could still occur during PD-1 engagement with different kinetics. PD-1/PD-L1 engagement rendered the LGs of the NK cells unable to reach the IS for successful killing of their susceptible target cells. Thus, PD-1/PD-L1

engagement specifically blocks LG polarization at inhibitory NK IS.

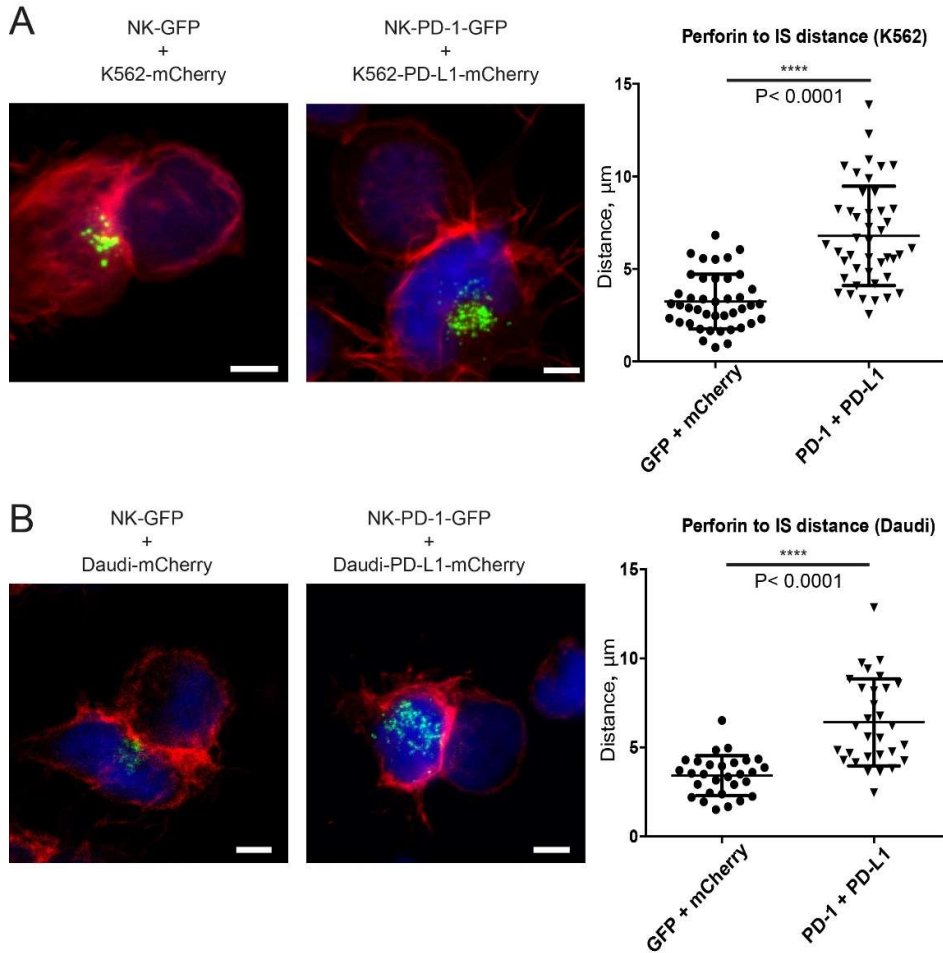


Figure 12. PD-1 engagement blocks lytic granule (LG) polarization. Conjugates were made between NK and target cells as indicated. Cells were fixed and stained with anti-perforin (green, for LGs), phalloidin (red, for F-actin staining), and DAPI (blue, for nuclei staining). Representative images for 3D-reconstruction projections of paired cells are shown for NC (**A**) and ADCC (**B**). NK cells were identified by perforin staining. IS was identified by accumulated F-actin. Scale bars: 5 μm . The mean distance of the perforin cluster to IS in each NK-target conjugate (represented by individual data points) was calculated using Imaris software and summarized in the right panel. The average values and SDs are shown by the horizontal lines (****, $p \leq 0.0001$, by Student's *t* test).

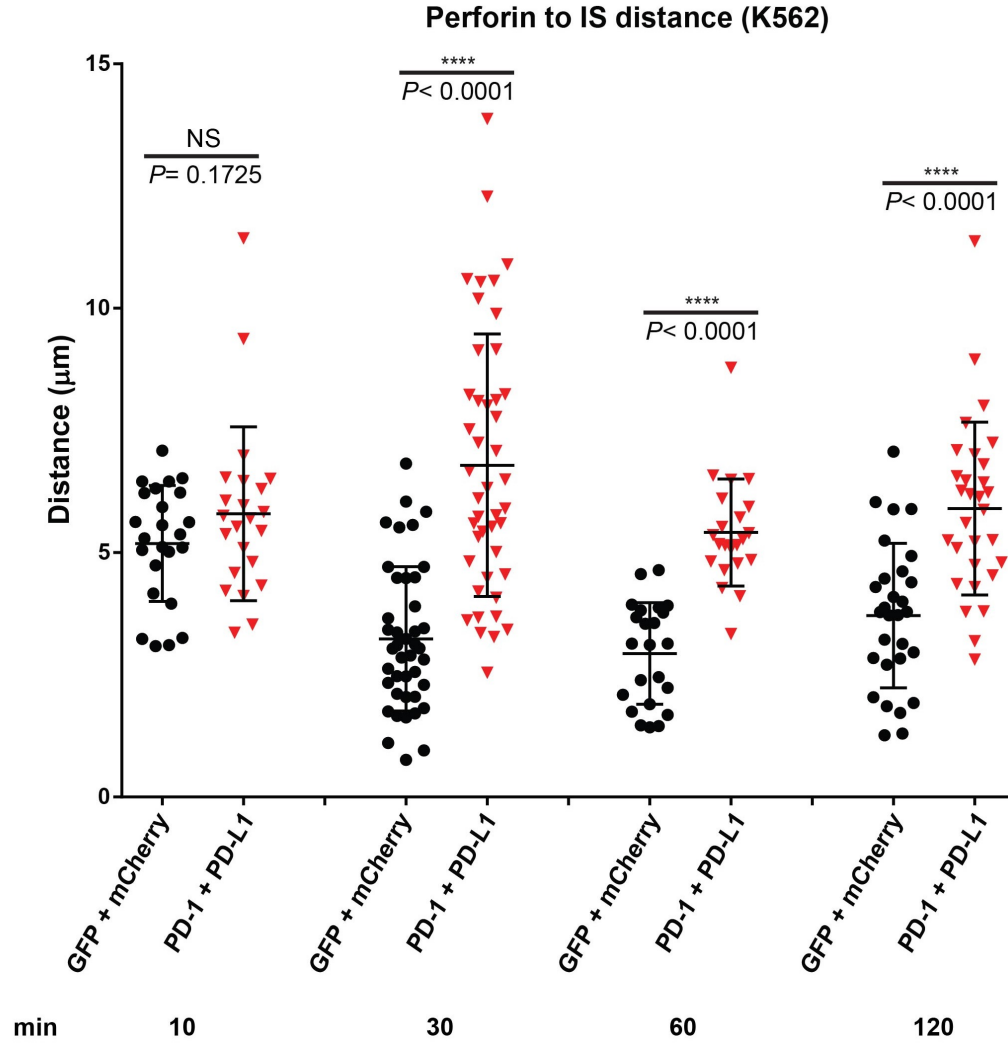


Figure 13. PD-1 engagement constantly blocks lytic granule polarization. The mean distance of the perforin cluster to IS in each NK-target conjugate (*represented by individual data points*) was calculated and summarized for each indicated time point after conjugation. “G+m” represents NK-GFP conjugated with K562-mCherry; “P+L” represents NK-PD-1-GFP conjugated with K562-PD-L1-mCherry. *The average values and SDs are shown by the horizontal lines (NS, Not significant; ****, $p \leq 0.0001$, by Student’s t test).*

2.3.5 PD-1 signaling inhibits integrin signaling

The integrin signaling pathway regulates LG polarization in NK cells (38). In response to either antibody stimulation of the activating receptors or the activation of leukocyte function–associated antigen 1 (LFA-1, also called $\alpha_L\beta_2$ integrin) by its ligand, intercellular adhesion molecule 1 (ICAM-1), the LGs along with the microtubule-organizing center (MTOC) in the NK cell, polarize towards the target cell. This process requires a signaling network consisting of integrin-linked kinase (ILK), Pyk2, paxillin, and several other proteins, among which ILK also accumulates at the IS in response to NK cell activation (38). To gain insights into the functional relationship between PD-1/PD-L1 engagement and integrin-mediated adhesion and consequent LG polarization, I co-stained ILK and perforin in target-conjugated NK-GFP and NK-PD-1-GFP cells. Confocal fluorescence imaging revealed that while both ILK and perforin concentrated in the IS between the majority of conjugated NK-GFP and K562-mCherry cells at 30 min and 60 min after conjugation (**Figure 14B**), indicative of accumulation at the IS. Although the accumulation dropped at 120 min in control groups, ILK appeared as dispersedly distributed puncta in most of the conjugated NK-PD-1-GFP and K562-PD-L1-mCherry cells at all the time points we tested (**Figure 14**). Similar to that shown in **Figure 12**, perforin positive LGs also did not move to the IS between the two cells. To rule out the possibility of decreased overall expression of integrin molecules in NK cells transduced with PD-1, I measured the mean fluorescence intensity (MFI) of LFA-1 using flow cytometry and found comparable overall expression of LFA-1 in NK cells transduced with either GFP only or PD-1-GFP (**Figure 15**). Therefore, we concluded

that PD-1/PD-L1 engagement disrupted integrin signaling, known to be required for LG polarization in NK cells.

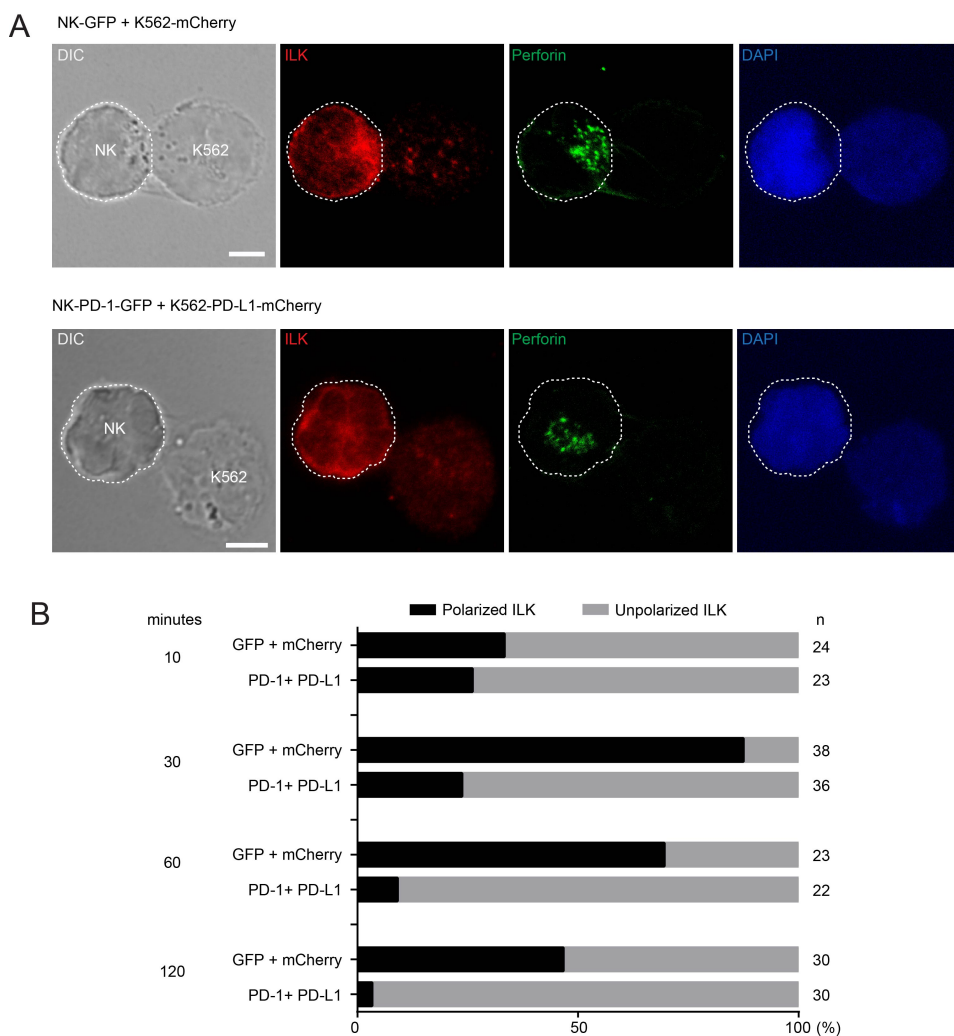


Figure 14. PD-1 signaling blocks the accumulation of ILK to IS in NK cells. Conjugates were made between NK and K562 cells as indicated. Cells were fixed and stained with anti-perforin (*green*), anti-ILK (*red*), and DAPI (*blue, for nuclei*). (**A**) Representative images of 3D-reconstruction projections of paired NK-K562 cells without (*upper panels*) and with (*lower panels*) PD-1/PD-L1 engagement at 30 min after conjugation. Scale bars: 5 μ m. (**B**) Quantification of the percentage of NK-target conjugates showing accumulation of ILK at IS at different time points after conjugation. N indicates the total number of conjugates counted.

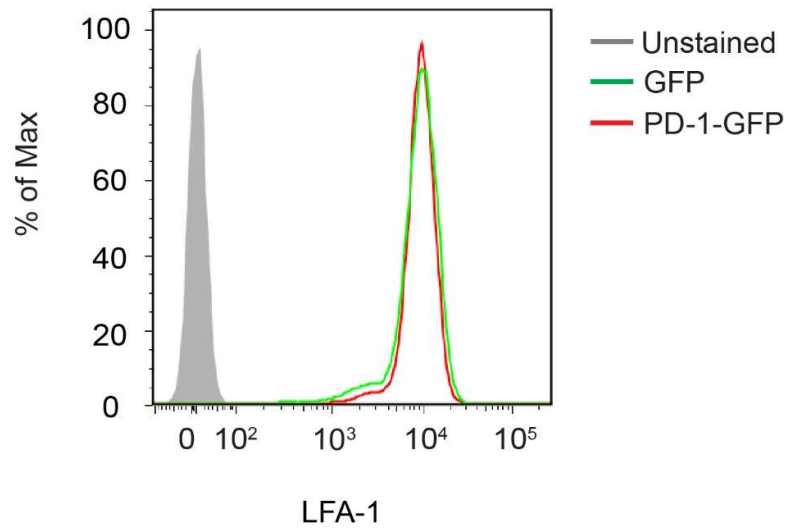


Figure 15. PD-1-GFP expression does not affect the overall expression of LFA-1 in NK cells. Histogram of flow cytometry analysis of the staining by LFA-1 antibody in GFP- (*green*) or PD-1-GFP- (*red*) transduced CD16-KHYG-1 cells.

2.3.6 PD-1 signaling blocks receptor-activated calcium response in NK cells

The increase of intracellular Ca^{2+} level is also an important indicator for the activation of NK cells. It has been showed that activating receptor induced store-operated Ca^{2+} entry (SOCE) through ORAI channels is required for the cytotoxicity of NK cells. Calcium is also important for the exocytosis of cytotoxic granules to release perforin and Granzyme B (44). To test whether calcium is also crucial for LG polarization, I loaded NK cells with the chelator BAPTA to suppress intracellular Ca^{2+} rise. Not only the Ca^{2+} response triggered by PMA/ionomycin was largely abolished in the BAPTA-loaded NK cells (**Figure 16A**), but also LG failed to polarize to the IS (**Figure 16B**).

To investigate the effect of PD-1 on the activation of NK cells, I examined the Ca^{2+} response to different activating receptors in the presence of PD-1 signaling. Since NKG2D is mainly responsible for NC, and CD16 is to mediate ADCC, I first measured the effect of PD-1 signaling on Ca^{2+} response induced by these activating receptors in normal ECS that contains 2 mM CaCl_2 . Cross-linking CD16 or NKG2D through primary and secondary antibodies evoked intracellular Ca^{2+} concentration increase in CD-KHYG1-1 cells that expressed either GFP or PD-1-GFP (**Figure 17**). Cross-linking using the PD-1 antibody alone did not trigger any Ca^{2+} response. When I activated activating receptor and PD-1 together, the Ca^{2+} response was totally abolished in the NK-PD-1-GFP cells but unaffected in NK-GFP cells (**Figure 17**). These results suggest that activation of PD-1 specifically inhibit the Ca^{2+} response elicited by NK cell activating receptors

The receptor-induced Ca^{2+} response has two distinct phases. In the first phase, Ca^{2+} is released from the ER via IP_3 receptors (IP_3R). In the second phase or SOCE, the decrease in ER Ca^{2+} content signals influx of extracellular Ca^{2+} via plasma membrane Ca^{2+} channels such as ORAI (41). To investigate whether PD-1 signaling preferentially affects ER Ca^{2+} store depletion or Ca^{2+} influx, cells were placed in a Ca^{2+} -free ECS first and then Ca^{2+} (2 mM) was added back. Under these conditions, the activation of CD16 alone triggered a transient intracellular Ca^{2+} response in the Ca^{2+} -free ECS (**Figure 18**) representing ER Ca^{2+} release. This response was abolished by cross-linking the cells with the PD-1 antibody, which did not elicit a response on its own. Therefore, the activation of PD-1 signaling blocked the ability of activating receptors to cause ER Ca^{2+} release.

Upon increasing the extracellular Ca^{2+} concentration to 2 mM, the intracellular Ca^{2+} level also went up, indicative of extracellular Ca^{2+} influx (**Figure 18**). Here, a large background “ Ca^{2+} leak” appeared in these cells as seen by the robust increase in the Indo1 ratio in cells treated with the anti-PD-1 antibody. SOCE was shown by the extra peak in the CD16 antibody-treated cells on top of the “ Ca^{2+} leak” (**Figure 18**). Importantly, in the presence of PD-1 activation, the CD16 antibody no longer evoked SOCE (**Figure 18**), suggesting that the activating receptor-induced SOCE is also blocked by PD-1 signaling. This is expected since SOCE is activated as a consequence of ER Ca^{2+} store depletion. As a control, I used thapsigargin (TG) to deplete the ER Ca^{2+} and examined SOCE using the above Ca^{2+} -free/ Ca^{2+} readdition protocol. In this case, the engagement of PD-1 failed to block TG-induced ER Ca^{2+}

release and SOCE (**Figure 19**), suggesting that the inhibitory action of PD-1 signaling is at the level downstream from activating receptor activation but before ER Ca^{2+} release.

I noticed that in some of the PD-1/PD-L1 conjugates, perforin could still reach the IS (**Figure 12&13**). Therefore, the ability of PD-1 signaling to abolish the Ca^{2+} response induced by the activating receptors may further inhibit the exocytosis/degranulation of the LGs. Taken together, my data indicate that PD-1 signaling may use redundant mechanisms, inhibiting granule polarization and Ca^{2+} response, to block the activation of NK cells. This may help ensure the silence of immune response. However, it cannot be ruled out at this point that the Ca^{2+} signal is also involved in granule polarization to the IS, as a part of the 'outside-in' integrin signaling.

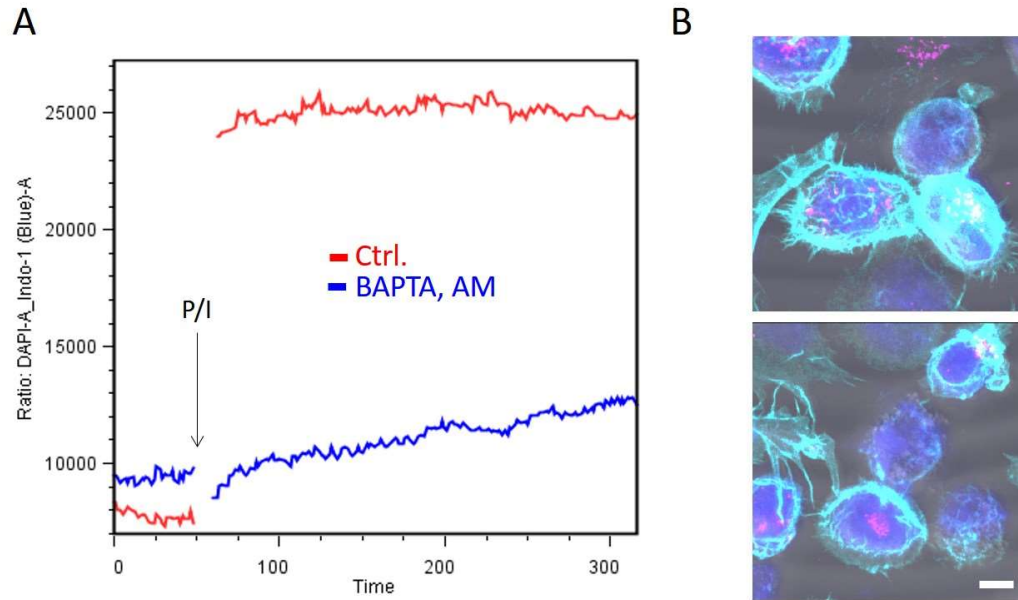


Figure 16. BAPTA blocks LG polarization. NK cells loaded with Indo1-AM dye were treated with PMA/ionomycin (P/I) while fluorescence ratios of Indo1 were recorded by flow cytometry. **A.** Representative time course of Indo1 ratios in control (*red*) NK cells and cells pre-incubated with BAPTA-AM for 30 min (*blue*). **B.** NK cells pre-loaded with BAPTA-AM for 30 min were conjugated to wild type K562 cells, fixed and stained with anti-perforin (*magenta, for LGs*), phalloidin (*cyan, for F-actin staining*), and DAPI (*blue, for nuclei staining*). Representative images for 3D-reconstruction projections of paired cells are shown. Scale bars: 5 μ m.

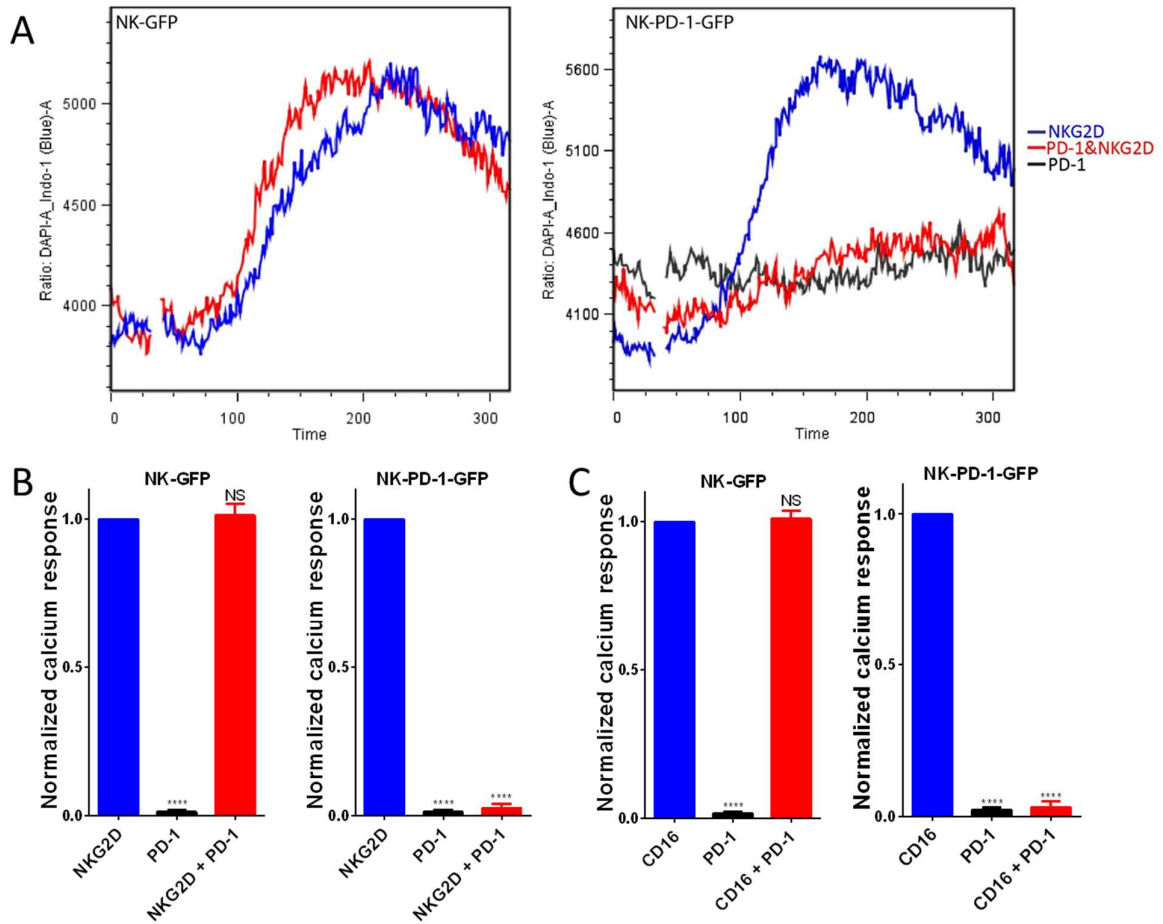


Figure 17. PD-1 signaling blocks Ca^{2+} response in NK cells. **A.** NK-GFP (*left*) and NK-PD-1-GFP (*right*) cells were loaded with Indo1-AM dye. Intracellular calcium rise (*shown by the increase of Indo1 ratio*) was triggered by crosslinking the cells with anti-NKG2D and the secondary antibodies. Representative time courses of Indo1 ratio changes are shown for cells crosslinked by antibodies for NKG2D alone (*blue*), PD-1 alone (*black*), or NKG2D+PD-1 (*red*). **B.** Summary of normalized peak values for treatments as indicated. **C.** Summary of normalized peak values for cells treated with CD16 and PD-1 antibodies as shown in similar fashions as (**A**). Error bars represent SDs. Data are from three independent experiments. NS, Not significant. ****, $p \leq 0.0001$, by Student's *t* test.

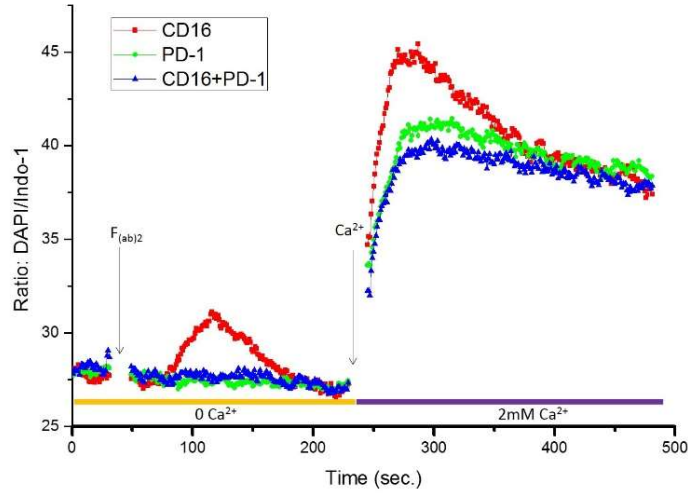


Figure 18. PD-1 signaling blocks both ER calcium release and receptor activation-dependent Ca^{2+} influx in NK cells. NK-PD-1-GFP cells loaded with Indo1-AM dye were coated with antibodies for CD16 alone (*red*), PD-1 alone (*green*), or CD16+PD-1 (*blue*) in a Ca^{2+} -free ECS and Indo1 fluorescence ratios were recorded 30 seconds to establish the baselines. The cells were then treated with $\text{F}_{(\text{ab})2}$ secondary antibody to induce crosslinking in the Ca^{2+} -free ECS, followed by the addition of an equal volume of ECS containing 4 mM CaCl_2 (*final extracellular Ca^{2+} concentration of 2 mM*) as indicated. Shown are representative time courses of three independent experiments.

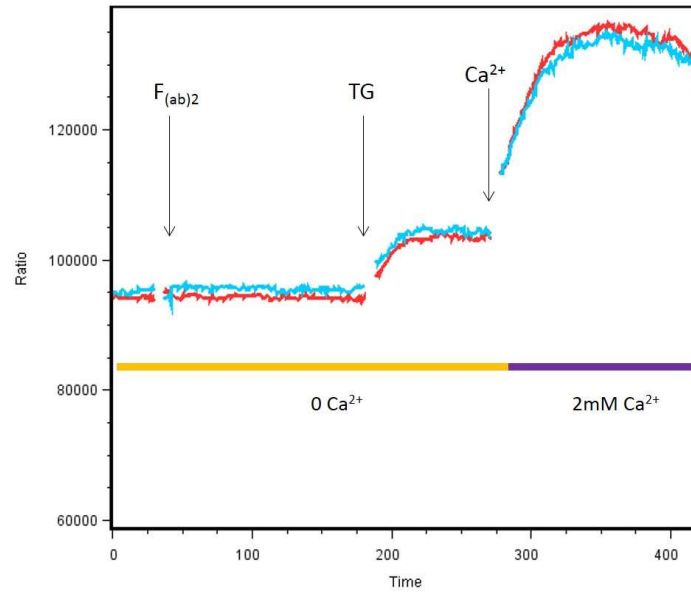


Figure 19. PD-1 signaling does not block pharmacological store-operated calcium entry.

NK-PD-1-GFP cells loaded with Indo1-AM dye were coated (red) or not (cyan) with the antibody for PD-1 in the Ca^{2+} -free ECS and recorded for 30 seconds to establish the baselines. The cells were then treated with $\text{F}_{(\text{ab})2}$ secondary antibody for crosslinking before the application of TG ($2\ \mu\text{M}$) to cause passive ER Ca^{2+} store depletion in the Ca^{2+} -free ECS, independent of activating receptors. Finally, 2 mM CaCl_2 was added back to ECS by mixing the equal volume of ECS that contained 4 mM CaCl_2 .

2.3.7 ITSM domain is required for the inhibitory function of PD-1

Previous data showed that the ITSM instead of ITIM domain of PD-1 is crucial for its function in T cells (14). To investigate whether this is also the case in NK cells, I tested the involvement of these two domains in PD-1 inhibition of NK cell cytotoxicity. I made the Y223F mutation at ITIM or the Y248F mutation at ITSM to disrupt the functions of each domain, as well as the double Y223F/Y248F mutant to interrupt both domains. NK cells that expressed single mutations as well as that with double mutation were established by lentivirus transduction as described above for the wild type PD-1. First, I showed that none of the mutations affected the conjugation of NK and target cells and the mutated PD-1-GFP proteins were still able to accumulate at the IS with PD-L1 (**Figure 20**). Then, I used the ^{51}Cr release assay to test the cytotoxicity of the NK cells that expressed different PD-1 mutations. In both NC and ADCC, the Y248F mutant and double mutant failed to exhibit inhibition of NK cell cytotoxicity to PD-L1 expressing cancer cells, whereas the Y223F mutant exerted a similar level of inhibition as the wild type PD-1 (**Figure 21**). These data indicate that similarly as it does in T cells, the ITSM domain (containing Y248) of PD-1 is also important for its inhibitory action in NK cells for both NC and ADCC. The ITIM domain (containing Y223) of PD-1, however, is not involved in the inhibition effect of PD-1 in NK cells.

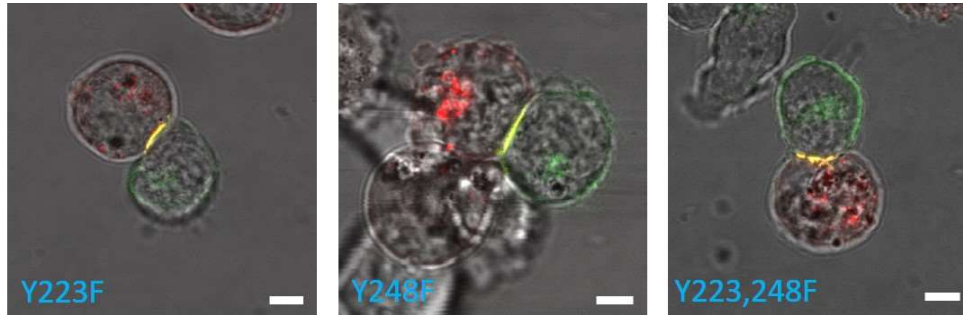


Figure 20. PD-1 mutants accumulate at IS normally with PD-L1. Live-cell imaging of NK effector cells (green) that stably expressed mutant PD-1-GFP as indicated (cyan) and conjugated with target K562-PD-L1-mCherry cells (red). Images were taken by confocal microscopy at 30 min after conjugation. Scale bars: 5 μ m. IS is shown as the co-localized green and red signals (*yellow*).

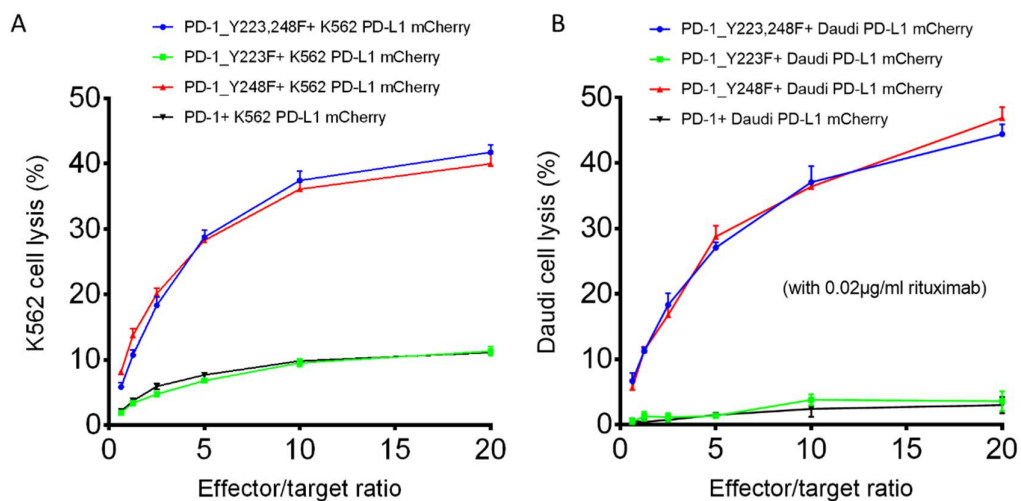


Figure 21. Y248 of PD-1 is crucial for its inhibition of NK cell cytotoxicity. (A) The natural cytotoxicity (NC) of CD16-KHYG-1 cells stably expressing PD-1-GFP (*black*), or PD-1-GFP mutations Y223F (*green*), Y248F (*red*), and Y223,248F (*blue*) towards K562-PD-L1-mCherry was measured by the standard 4-hour ^{51}Cr release assay at varying NK/K562 (effector/target) ratios. (B) The ADCC of the same set of NK cells towards Daudi-PD-L1-mCherry was measured by the ^{51}Cr -release assay in the presence of rituximab. Results are representatives of three independent experiments. *Error bars represent SDs.*

2.4 Summary, discussion and future directions

In this study, I show that PD-1 signaling blocks NK cell-mediated immune responses through impairing LG polarization to the NK cell IS. Neither NK-target cell conjugation nor NK-target cell IS formation was blocked by PD-1 engagement. In NK cells, PD-1 functions as an inhibitory receptor through its ITSM domain, similar that in cytotoxic T cells and other lymphocytes (28, 58). The engagement of PD-1 expressed in NK cells with its ligand PD-L1 expressed on NK-sensitive target cells inhibited both forms of NK-mediated cytotoxicity, NC and ADCC. The engagement of PD-1 blocked ILK-mediated integrin 'outside-in' signaling, which may account for the interference of LG polarization and the consequent inhibition of cytotoxicity. Furthermore, PD-1 signaling blocks activating receptor-induced Ca^{2+} response in NK cells, which may also account for the inhibition of LG polarization and degranulation (**Figure 22**).

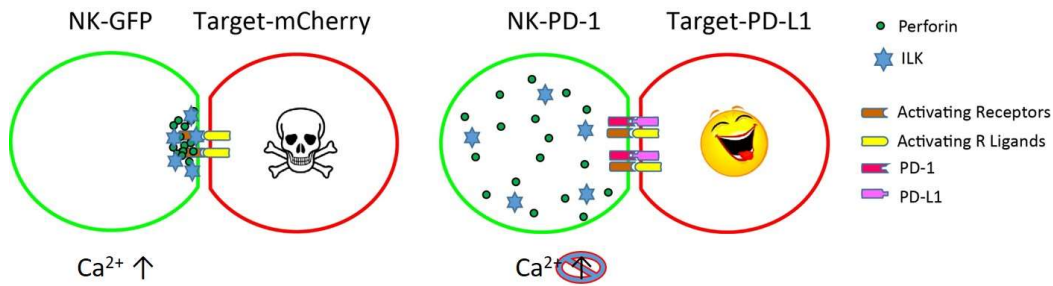


Figure 22. Schematic working model. In the absence of PD-1/PD-L1 engagement (*left*), when the NK cell encounters a target cell, the activation of activating receptors in the NK cell induces the accumulation of ILK and perforin-containing granules to the IS, which is accompanied with elevated intracellular Ca^{2+} concentration. This leads to a consequent degranulation and cytotoxic killing of the target cell. However, in the presence of PD-1/PD-L1 engagement (*right*), which evokes inhibitory signaling, the polarization of perforin and ILK is blocked and the Ca^{2+} response is abolished, resulting in the inhibition of NK cytotoxicity and survival of the target cell.

2.4.1 PD-1 and IS stability

It remains controversial whether inhibitory receptors alter IS stability. Some previous studies have suggested that inhibitory receptors destabilize the NK IS, causing the NK cell to disengage from its target before it can successfully initiate a cytolytic attack (59, 60). This concept also gained support from experiments with mouse CD4^+ T cells, where continued PD-1/PD-L1 interactions destabilized adhesion of self-reactive CD4^+ T cells in the pancreas by inhibiting the TCR-driven ‘stop signals’, blockade of PD-1 or PD-L1 prolonged T cell-dendritic cell (DC) engagement (18), and PD-1/PD-L1 binding blocked stable synapse formation on supported glass-supported

lipid bilayers containing PD-L1 molecules (56). However, this observation is in contrast to that found for long-term (> 40 min) PD-1/PD-L1 interactions in virus-specific CD8⁺ T cells in mice chronically infected with lymphocytic choriomeningitis virus (LCMV) clone 13 (a strain establishes persistent viral infection) (61). Nevertheless, in the current study, we demonstrated that NK cells can form stable IS even when the inhibitory signaling dominates as reported before (49, 62). The discrepancy may be explained by the differential impact of PD-1 signaling on cytotoxic lymphocytes (including NK and CD8⁺ T cells) and CD4⁺ T cells due to different downstream signaling cascades.

Moreover, it has been reported that inhibitory receptor signaling does not block accumulation of activating receptors (49, 62). This has been shown with 2B4 and CD2 both accumulated at inhibitory synapses with target cells (62) and with the minimal combination of activation ligand human IgG1 Fc (a ligand for the low affinity Fc receptor FcγRIIIA, also known as CD16) and HLA-E (a ligand for inhibitory receptor CD94/NKG2A) (49). Recently, using a newly developed vertical cell pairing (VCP) system, my colleagues and I showed the formation of a stable inhibitory IS after engaging PD-1 expressed on NK cells with PD-L1 expressing target cells (46), supporting the idea that stable inhibitory IS formation indeed occurs during inhibitory signaling in NK cells. These results await further validation with a large sample size, but meanwhile bring a question whether inhibitory receptor signaling acts through destabilization of the IS in NK cells or through other unidentified molecular mechanisms. My data strongly support the notion that PD-1 inhibits NK cells through disruption of downstream intracellular signaling following IS formation rather than

disruption of IS formation per se. However, further studies should be done to check whether PD-1 signaling affect the accumulation of activating receptors and the activating synapse.

2.4.2 PD-1 and integrin 'outside-in' signaling induced LG polarization in NK cells

The current study shows that PD-1 signaling does not decrease the percentage of NK-target cell conjugation. Usually, cell-cell adhesion is the initial step in immune responses (53, 63, 64). After effector-target conjugation, immunoreceptors on the NK cell surface then bind to their respective ligands on the target cell surface and initiate immune signaling, which can be either activating or inhibitory, depending on which receptors are engaged. The current dogma is that inhibition of early signaling (e.g., adhesion) is more effective at suppressing NK cell activation than blocking the later phases of signaling. Unexpectedly, however, my data show that PD-1 inhibitory signaling preferentially blocks integrin-mediated LG polarization without affecting NK-target cell adhesion or cell-cell conjugation. Based on the crystal structure, the extracellular region of PD-1 is a short single immunoglobulin variable (IgV) domain (65). Integrins are much longer, so it makes sense that PD-1 could only be engaged after some integrin signaling had already occurred.

It is well appreciated that, for cytotoxic killing, integrin molecules in CTL possess both 'inside-out' signaling and 'outside-in' signaling (32, 66). LFA-1-dependent 'outside-in' signaling in T cells requires 'inside-out' signaling to enhance polarization of LGs (36), but it is not known whether LFA-1 receives TCR-dependent 'inside-out'

signals merely to promote adhesion or to provide essential signals for polarization. In contrast, NK cells have proven useful in the analysis of 'outside-in' signaling by LFA-1 independently of other signals because the binding of LFA-1 on NK cells to ICAM-1 on target cells is sufficient to induce the polarization of LGs to NK IS (37). Therefore, 'outside-in' and 'inside-out' signaling can be generally measured by LG polarization and conjugate formation assays, respectively, in NK cells. My data suggest that PD-1 preferentially impairs LFA-1-dependent 'outside-in' signaling, rather than 'inside-out' signaling pathway. This differs from the recent studies in T cells, in which the engagement of PD-1 with its physiological ligand inhibited T cell adhesion (67, 68). The different LFA-1 signaling pathways between T and NK cells could cause this discrepancy (69).

The fact that PD-1 engagement preferentially blocks LG polarization to the NK cell IS is reminiscent of previous studies showing that inhibitory receptors block signals for LG polarization (by integrin LFA-1) more effectively than signals for degranulation (69). Using a *Drosophila* cell line S2 transfected with various ligands of human NK cell receptors, Das and Long investigated whether inhibitory receptors could block LG polarization and degranulation. They showed that LG polarization was highly sensitive to inhibition mediated by killer cell immunoglobulin-like receptor (KIR) and CD94-NKG2A receptors (69). However, this study did not specifically define the underlying molecular basis of this inhibition. In the current study, I discovered that PD-1 signaling specifically blocked polarization of the common integrin signaling molecule ILK at the NK cell IS. To our knowledge, although PD-1 signaling is well characterized in T cells

and SHP-2 is the only cellular molecule that directly interacts with immunoreceptor tyrosine-based switch motif (ITSM) domain of PD-1 (11), ILK is a newly-identified molecule targeted by PD-1 signaling. The underlying mechanisms of how PD-1 signaling blocks ILK polarization at the NK cell IS requires further investigation.

2.4.3 Calcium and LG polarization

In T cells, the increase in cytosolic free Ca^{2+} concentrations ($[\text{Ca}^{2+}]_i$) plays a major role in the activation of LFA-1. Eliciting cytosolic Ca^{2+} elevation by ionomycin or stimulating CD3 was capable of directly activating LFA-1 (70). It has been reported that both anti-CD11a and anti-CD18 can prolong the Ca^{2+} response induced by anti-CD3 (71). More importantly, aggregation of the intact cytoplasmic domain of integrin $\beta 2$ was sufficient to trigger Ca^{2+} transients in Jurkat cells, which was abrogated in T cells that do not express the T cell receptor (72).

However, it remains controversial whether cytosolic Ca^{2+} rise is involved in LG polarization and NK cell activation. First, although the activation of LFA-1 by antibodies did not trigger any Ca^{2+} response in NK cells, it is sufficient to induce LG polarization to NK IS (69). Second, despite that ORAI1 channels were triggered following stimulation of activating receptors (73), LG polarization is not affected in NK cells from patients with ORAI1 mutation in which SOCE is largely impaired (44). On the other hand, my current data from chelation of intracellular Ca^{2+} with BAPTA indicate that a rise in intracellular Ca^{2+} is essential for LG polarization in NK cells. It is possible that some important proteins in the integrin 'outside-in' signaling pathway require Ca^{2+} for

their normal functions and these may be interrupted by BAPTA.

Therefore, the relations between the integrin 'outside-in' signaling and intracellular Ca^{2+} responses need to be examined more carefully. It would be interesting to test whether co-activation of LFA1 with activating receptors might enhance the Ca^{2+} response in NK cells as compared to that induced by activating receptors alone. Importantly, whether there is actually a Ca^{2+} response in the cellular system of LFA-1 activation (conjugation of NK with S2 cells expressing ICAM1) needs to be tested carefully.

Irrespective to whether the Ca^{2+} signal is required for LG polarization or not, it has long been reported that inhibitory receptors can block the Ca^{2+} response in lymphocytes (74). Here, I also found that PD-1 engagement abolished the Ca^{2+} response triggered by activating receptors NKG2D and CD16, consistent with the finding in T cells where PD-1 signaling blocked the Ca^{2+} response triggered by TCR activation (75). It is quite clear that Ca^{2+} should be crucial for degranulation since LG exocytosis requires Ca^{2+} (76). Thus, the blockade of Ca^{2+} signaling by PD-1 in NK cells would further suppress the cytotoxicity of these cells.

2.4.4 Exchange of PD-1 and PD-L1 in NK and target cells

During the course of this study, I observed an interesting phenomenon that the GFP signal of PD-1 transferred into the target cells while the mCherry signal of PD-L1 translocated to NK cells after long-term (16 hr) conjugation (**Figure 23**), indicating that these cells may exchange their contents in the presence of PD-1 signaling. Receptor

transfer has been studied by other groups in different models (77, 78); however, the underlying mechanisms and the physiological significance of this phenomenon remain largely unexplored. It is possible that the exchange for PD-1 and PD-L1 between effector and target cells is caused by the direct binding between these two proteins. Interestingly, it was found that there are polarized release of TCR-enriched micro-vesicles at the IS recently (79).

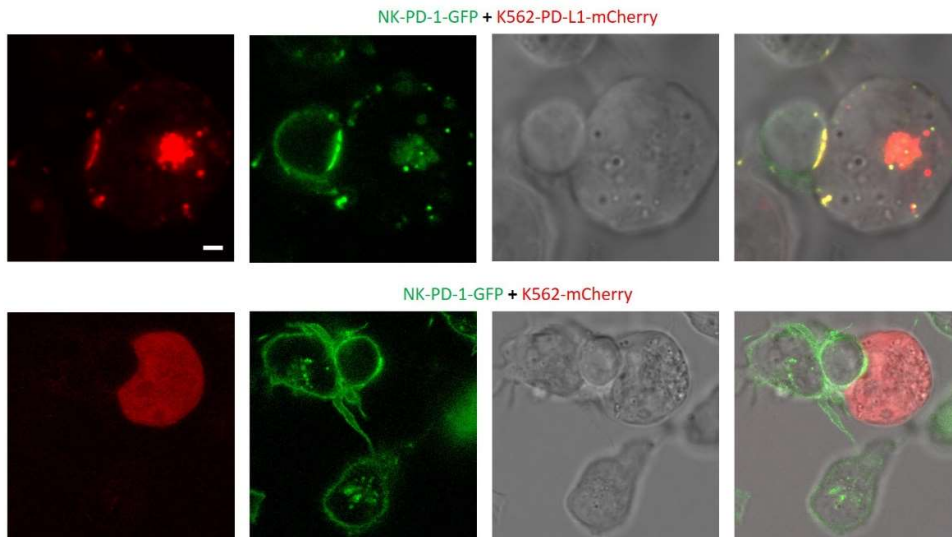


Figure 23. Exchange of PD-1 and PD-L1 between NK and target cells after long-time conjugation. Live-cell imaging of NK-PD-1-GFP cells (*green*) conjugated with the target K562-PD-L1-mCherry cells or K562-mCherry (*red*). Images were taken by confocal microscopy at 16 hr after conjugation. Scale bars: 5 μ m.

Previously, Jewett and Bonavida have reported that the levels of CD16/CD2/CD56 in NK cells were decreased after conjugation with K562 cells. In the sorted NK cells after the conjugation, the cytotoxic activity were also found to be decreased (80). However, after dissociation with K562 or other target cells NK cells still maintain certain degree of cytotoxic activity especially in the presence of IFN α and/or IL2 (80, 81). Indeed, it was shown that a single NK cell could kill up to 10 targets over a 6-hr period (82). Thus, I hypothesize that in addition to inhibiting LG polarization/degranulation and calcium signaling, the PD-1 receptor and its ligand, PD-L1, may be also able to further down regulate the post-conjugation functions of NK cells and thereby inhibit the serial killing by these cells. The above observed transfer may then explain why PD-L1 was found in tumor infiltrating lymphocytes and could serve as a prognostic marker in some cancers (83).

In conclusion, I investigated the role of PD-1 in NK cell-mediated cytotoxicity, which revealed the underlying molecular basis of the inhibitory receptor PD-1 in NK cell immune responses. Although PD-1 expression is limited in NK cells from healthy individuals, it is upregulated in NK cells from patients with a variety of chronic diseases (9, 10, 84, 85). I found that PD-1 engagement by its natural ligand, PD-L1, preferentially blocks LG polarization via specifically impairing the polarization of the central integrin signaling molecule of lymphocytes, ILK, at the NK cell IS. This study uncovers a novel, common master signaling molecule used by PD-1 inhibitory receptor

in human NK cells, which should shed lights on harnessing the power of NK cells by targeting a downstream PD-1 signaling molecule for disease treatment in the future.

Chapter 3

RIP3 dependent necroptosis is involved in acidosis induced cell death *via*

MLKL & AIF

3.1 Background

3.1.1 Ischemic stroke

Stroke is the 5th leading cause of death in the US, with one person dying every 4 minutes as a result of stroke. Strokes occur to approximately 800,000 people each year in the US alone, which is equivalent to about one every 40 seconds (86). However, to date, no effective treatment is available for this disease. A stroke often damages brain because it causes a sudden interruption of the blood supply to the brain. The brain damage leads to long lasting neurological deficits in stroke patients, severely impairing the patients' quality of life.

There are two types of stroke, hemorrhagic and ischemic. Between the two, hemorrhagic stroke is less common and is caused by bleeding into the brain tissue when a blood vessel bursts. Blood spills into or around the brain and creates swelling and pressure, damaging cells in the brain. Ischemic stroke accounts for about 87 percent of all stroke cases. It occurs when a blood vessel carrying blood to the brain is blocked by a blood clot. Currently, the only FDA approved drug to treat ischemic stroke is the thrombolytic agent tissue plasminogen activator (tPA), which is supposed to re-open the clotted vessels. However, this approach has very limited success due to the short therapeutic time window of 3 to 4.5 hours of the first symptoms and side effect of intracranial hemorrhage (87). For people with blood clots in larger arteries,

tpA often does not dissolve them completely.

Several key players in ischemic cell death have been identified, including excitotoxicity, oxidative and nitrosative stress, and inflammation; however, numerous clinical trials have failed to show efficacy of drugs that modulate these mechanisms in patients, despite promising preclinical data (88). Consequently, there is a pressing need for identifying new ways to treat patients with ischemic stroke (86).

3.1.2 Acidosis and acidotoxicity

Acidosis is an increased acidity in the blood and other body tissues. It occurs commonly under pathological conditions when the body homeostasis is disrupted due to inflammation, hypoxia, cancer and other illnesses.

Acidosis is a common feature in cancer. Due to the higher metabolic activity and limitations in blood flow (hypoxia) in tumors, the microenvironment around them tends to be more acidic, reaching pH values of 6.2-6.8 (89, 90). However, hypoxia and oncogene activation also allow cells to adapt to the potentially toxic effects of an excess in acidosis. Hypoxia does so by inducing the activity of a transcription factor the hypoxia-inducible factor-1 (HIF-1), which in turn enhances the expression of a number of intracellular pH regulating systems that cope with acidosis (91). Thus, cancer cells adapt quite well and even thrive in acidity.

On the other hand, acidosis is detrimental to neurons. Acidosis is commonly associated with many central nervous system diseases and neurodegenerative diseases such as seizure (92), Alzheimer's disease (AD) (93), Parkinson's disease (PD) (94) and Huntington's disease (HD) (93, 95). Tissue acidosis is also another well-

characterized feature that contributes to brain injury during cerebral ischemia. The normal brain requires complete oxidation of glucose to fulfill its energy requirements. During ischemia, oxygen depletion forces the brain to switch to anaerobic glycolysis. The accumulation of lactic acid as a byproduct of glycolysis and protons produced by ATP hydrolysis cause the extracellular pH to fall in the ischemic brain, typically to 6.5–6.0 during ischemia under normoglycemic conditions, or even below 6.0 during severe ischemia (96-98). It seems that neurons do not have the capability to handle this sudden drop of pH like tumors do. Acidosis often causes neuronal death and thus it was given a special term called “acidotoxicity”. Although the signaling mechanisms of acidotoxicity remains mysterious, early studies have shown that acid-sensing ion channel type 1a (ASIC1a) plays a critical role in acid-induced neuronal cell death and genetic deletion or pharmacological blockade of ASIC1a is protective against brain damage associated with ischemic stroke in rodent models (98).

3.1.3 Acid-sensing ion channel

Acid-sensing ion channels (ASICs) are voltage-insensitive Na^+ channels activated by external protons (H^+). These channels belong to the epithelial sodium channels/ degenerin (ENaC/Deg) ion channel superfamily. They were first cloned and shown to be widely distributed in the nervous system by Michel Lazdunski group in 1997 (99). In mammals, there are six distinct ASIC isoforms (ASIC1a, ASIC1b, ASIC2a, ASIC2b, ASIC3, and ASIC4) encoded by four different genes (ACCN1–4). All ASICs except ASIC1b are expressed in the central nervous system and all of them are present in the peripheral nervous system. ASICs are formed by combinations of ASIC

subunits in homotrimeric or heterotrimeric complexes. Recently, ASIC5 was reported as a new member of the ASIC family. However, ASIC5 is very divergent from other family members. It forms an ion channel that is insensitive to H⁺ but is sensitive to bile acids. Therefore, it is also named as bile acid-sensitive ion channel (BASIC) (100).

ASICs have been extensively studied and implicated to play important roles in many physiological functions and pathological conditions (101). These include, for examples, learning and memory (102), fear conditioning (103), pain (104), seizure (105), PD (106), HD (107) and so on. Therefore, targeting ASICs may provide novel and effective therapeutic interventions for a number of diseases.

Among the ASIC isoforms, ASIC1a is predominantly expressed in brain neurons and critically involved in acidosis-induced neuronal cell death both *in vitro* and *in vivo* (98, 108). Either gene ablation of ASIC1a or administration of an ASIC1a inhibitor, psalmotoxin 1 (PcTX1), even at up to 5 hrs after the onset of brain ischemia and during reperfusion, protected against the brain damage in the mouse model of ischemic stroke (98, 108). These suggest that ASIC1a is involved in delayed ischemic brain injury and a plausible therapeutic target for mitigating ischemic brain injury. However, PcTX1 is unsuitable to stroke therapy due to low blood-brain barrier permeability and poor stability. The potential on-target side effect on the normal physiological function of ASIC1a also cannot be ignored. Thus, elucidating the downstream mechanism(s) of ASIC1a-mediated neuronal death will help identify new strategies to target this pathway.

Much of the previous work on ASICs and neurotoxicity/acidotoxicity focused on

ASIC1a homotrimeric channels since they are able to conduct Ca^{2+} and induce Ca^{2+} -mediated toxicity (98, 109). Importantly, disrupting the gene encoding ASIC1a in mice eliminated most of the current evoked by extracellular acid in CNS neurons, suggesting that ASIC1a is a critical channel subunit (98, 102). However, the Ca^{2+} permeability of ASIC1a channels is relatively small comparing to other Ca^{2+} -permeable channels, and the increased influx of Ca^{2+} occurs only for seconds in response to acidity.

Recently, my colleagues and I showed that extracellular protons trigger a novel form of neuronal death, necroptosis, via ASIC1a, independent of the channel's ionic conducting function (110). We identified receptor-interacting serine/threonine-protein kinase 1 (RIP1) as a critical component of this form of neuronal necroptosis. Following acid stimulation of primary cultured neurons *in vitro* and brain ischemia in a mouse stroke model *in vivo*, RIP1 became physically associated with ASIC1a and then phosphorylated. Inhibiting RIP1 with its inhibitor, Nec1, protected neurons from acidosis-induced neuronal death (111). However, the downstream changes associated with ASIC1a-mediated RIP1 phosphorylation during acidosis remain to be illustrated.

3.1.4 Necroptosis and Parthanatos

Necroptosis is a form of programmed necrosis, which was dubbed by Junying Yuan's group in 2005 (111). Necrosis has been considered as an uncontrollable accidental cell death for a long time. However, it is now clear that necrosis can also occur in a regulated manner. Differently from apoptosis, the morphological characteristics of necrosis /necroptosis include swelling of organelles, plasma

membrane rupture and subsequent loss of intracellular contents.

The term “necroptosis” was firstly introduced to indicate a tumor necrosis factor receptor 1 (TNFR1) ligation induced regulated necrosis and it can be inhibited by the RIP1 inhibitor necrostatin-1 (Nec1) (111). In fact, before the nomenclature was proposed, a number of studies had shown that caspase inhibition did not block death receptor (DR) agonist-induced cell death but rather led it to necrosis (112-114). After its naming, our understating of molecular mechanisms underlying necroptosis has progressed significantly. It has been well established that conventional necroptotic pathway involves the formation of necrosomes containing RIP1 and its downstream effectors RIP3 and MLKL. Upon phosphorylation by RIP3, MLKL plays a critical role in necroptosis. The phosphorylated MLKL forms oligomers that translocate to cellular membranes (including the plasma membrane) and results in the loss of barrier function (115, 116).

Parthanatos, coined in a review article in 2009 after the personification of death in Greek mythology Thanatos, is a new class of cell death (117). The NCCD classifies it to be one form of RCD other than necroptosis (1). In parthanatos, oxidative damage to DNA results in activation of poly(ADP-ribose) polymerase (PARP) and generation of poly(ADP-ribose) polymers (PAR polymers) that trigger release of mitochondrial apoptosis-inducing factor (AIF) and its translocation to the nucleus (117). Recently, a study showed that parthanatos is one of the mechanisms by which ischemia-associated tissue acidosis augments cell death. The authors showed that acidosis augmented the formation of PAR polymers, the nuclear translocation of AIF, and

neuronal cell death (118).

Both necroptosis and parthanatos play critical roles in many pathophysiological processes including ischemic injury (111, 119). Although we have shown that acidosis triggers necroptosis *via* ASIC1a and RIP1 (110), the downstream signaling steps of acid-induced necroptosis have yet to be elucidated. It is reasonable to expect that RIP3 and/or MLKL is also required for acidosis induced cell death. We also hypothesize that acidosis induced cell death may share some common features with parthanatos. Both of these possibilities were tested in this study. Elucidating the mechanism(s) underlying ASIC1a-mediated neuronal damage will significantly impact our knowledge on neuronal acidotoxicity and help devise new strategies to combat neurological damage caused by ischemic stroke.

In this study, I investigated mechanisms underlying ASIC1a-mediated neuronal damage. I show that RIP3 and MLKL, known to be downstream of RIP1 in necroptosis, are also required for acidosis-induced cell death, in which serum starvation is a critical contributing factor. Although acidosis/starvation-induced cell death is different from parthanatos, AIF translocation is also involved as a downstream event of RIP3 activation. The AIF nuclear translocation due to acidosis/ starvation is facilitated by mitochondrial permeability transition pore (MPTP) and reactive oxygen species (ROS). Inhibiting RIP3 reduced both acid-induced death of mouse cortical neurons *in vitro* and brain infarction in mice elicited by MCAO *in vivo* by the FDA approved anti-cancer drug Dabrafenib.

3.2 Materials and methods

3.2.1 Cell lines and mouse cortical neuron culture

Neuro-2a (N2a), Human Embryonic Kidney 293 (HEK293) and mouse embryonic fibroblast cells were maintained in DMEM (high glucose) with 10% FBS, 100 units/ml penicillin and 100 µg/ml streptomycin at 37°C, 5% CO₂. For experiments where transient expression was used, cells were transfected using Lipofectamine 2000 and used for experiments after 16-20 hours.

For primary culture of mouse cortical neurons, brains from postnatal day 1 wild type C57BL/6 mice were removed rapidly and placed in ice-cold calcium, magnesium free Hank's Balanced Salt Solution (HBSS). Tissues were dissected and incubated with 0.05% trypsin-EDTA for 30 min at 37°C. HBSS with 10% FBS was used to terminate the digestion process and cells were triturated with a 10-ml pipette. Cells were filtered through a 70 micron strainer, resuspended in the culture medium (see below), and plated in poly-D-lysine-coated 10-cm culture dishes or 96-well plates (1 × 10⁷ cells per dish, 5 × 10⁴ cells per well). Neurons were cultured in Neurobasal medium supplemented with B27, 2 mM L-glutamate (ThermoFisher Scientific, USA) and maintained at 37°C 5% CO₂ in an incubator. The medium was half changed twice a week and the neurons used for assay 14–16 days after plating. Glial growth was suppressed by the addition of 5-fluoro-2-deoxyuridine (20 µg/ml; Sigma–Aldrich, USA) and uridine (20 µg/ml; Sigma–Aldrich, USA).

3.2.2 Cell death assay

Acid and starvation induced cell death was achieved as previously described

(110). Briefly, cells were washed once within 5 minutes at room temperature with the treatment extracellular solution (ECS, contains 140 mM NaCl, 2 mM CaCl₂, 5 mM KCl, 1 mM MgCl₂, 10 mM Glucose, 10 mM HEPES), of which the pH was either adjusted to 7.4 or 6.0. Then, they were incubated at 37 °C for 1 hr in the same pH 7.4 or pH 6.0 ECS. At the end of the treatment, the solution was replaced with the normal pH culture medium and the culture resumed at 37 °C. Primary cultured neurons were recovered for 24 hr and N2a cells were recovered for 7 hr due to their ability of fast proliferation. For treatment where inhibitors were used, the neurons were pre-incubated with the drug for 30 minutes in the medium and co-incubated with the pH 7.4 or pH 6.0 ECS for 1 hr. For inhibitor treatment of N2a cells, the drug was applied together with the ECS for 1 hr and present in the culture medium throughout the 7-hr recovery time. The sources and concentrations of all pharmacological reagents used are listed in Table 1.

Cell death was assessed using multiple methods: Cell Titer Blue (CTB), lactate dehydrogenase (LDH) measurement and SYTOXBLUE staining assay. For CTB assay, cells were cultured in the wells of 96-well plates and acid-treated as described above. Then, 20 µl CTB solution (Promega, USA) was added to each well and the plates were incubated for 4 hrs at 37 °C. The fluorescence intensities (excitation 560 nm, emission 590 nm) were measured by the FlexStation Microplate Reader. For LDH assay, the LDH release was measured in the culture medium using the LDH assay kit (Takara Bio, USA). Briefly, 100 µl of the culture medium was transferred from the culture wells to wells of a 96-well plate and mixed with 100 µl of the reaction solution provided by the kit. Optical density was measured at 492 nm 45 min later, using a microplate reader

(Spectra Max Plus, Molecular Devices). Background absorbance at 620 nm was subtracted. For SYTOXBLUE staining, cells were stained with 0.5 μ M SYTOXBLUE (Invitrogene, USA) for 10 minutes in an incubator and then examined by fluorescence microscopy (Leica).

Table 1. Reagents used for cell death assay

Name	Description	Concentration	Company
PcTX1	AISC1 blocker	50 nM	Millipore
Nec1	RIP1 inhibitor	40 μ M	Cayman Chemical
GSK'872	RIP3 inhibitor	3 μ M	APExBIO
Dabrafenib	RIP3 inhibitor	10 μ M	Cayman Chemical
TNF α	Death receptor ligand	30 ng/ml	Millipore
Smac mimetic	IAP antagonist	100 nM	TOCRIS
z-VAD	Caspase inhibitor	20 nM	APExBIO
DIDS	VDAC inhibitor	500 μ M	ANASPEC
TRO19622	VDAC inhibitor	20 μ M	TOCRIS
NAC	antioxidant	6 mM	Oakwood chemical
TEMPOL	antioxidant	500 μ M	Enzo
Trolox	antioxidant	100 μ M	ACROS
ALLN	Calpain inhibitor	10 μ M	APExBIO
DPQ	PARP inhibitor	30 μ M	Cayman Chemical

3.2.3 Knocking down of mouse MLKL

Two plasmids that contain shRNA for mouse MLKL were purchased from Sigma. Their targeting sequence are: “CCGGAGATCCAGTTCAACGATATATCTCGA GATATATCG-TTGAAGTGGATCTTTTTTG” and “CCGGTCCCAACATCTTGCGTATA TTCTCGAGA-ATATACGCAAGATGTTGGGATTTTTG”. A negative control plasmid was kindly provided by Dr. Guangwei Du (University of Texas Health Science Center at Houston). Assays were performed 2 days after transfection and the efficiency of knocking down was assessed by Western blotting.

3.2.4 Patch clamp electrophysiology

Acid-evoked currents were recorded using whole-cell patch-clamp recording techniques at room temperature (22–25°C). For the voltage-clamp recordings, the membrane voltage was held at –60 mV. The standard external solution (SS) contained: 150 mM NaCl, 5 mM KCl, 1 mM MgCl₂, 2 mM CaCl₂, and 10 mM glucose, buffered to various pH values with 10 mM HEPES. The patch pipette solution contained: 120 mM KCl, 30 mM NaCl, 1 mM MgCl₂, 0.5 mM CaCl₂, 5 mM EGTA, 4 mM Mg-ATP, and 10 mM HEPES, pH 7.4. The osmolarity of all solutions was kept at 300–330 mOsm/l. Voltage commands and current recordings were controlled by an EPC10 amplifier with the use of the PatchMaster program. Currents were recorded continuously at 10 kHz.

3.2.5 Co-immunoprecipitation

N2a cells under different treatment were collected and re-suspended in a lysis

buffer containing 20 mM Tris-Cl, pH 7.4, 150 mM NaCl, 1% Triton X-100, 1 mM EDTA, 3 mM NaF, 1 mM β -glycerophosphate, 1 mM sodium orthovanadate, 2 mM N-ethylmaleimide, 10% glycerol, protease inhibitors (Roche, Switzerland) and phosphatase inhibitors (Sigma, USA). The re-suspended lysates were vortexed, incubated on ice for 30 min, and centrifuged at 13000Xg for 15 min at 4°C. The supernatant was incubated with 2 μ g primary antibody overnight at 4°C. The primary antibodies used were mouse monoclonal mCherry antibody (Biolegend) or rabbit polyclonal MLKL antibody. Protein A sepharose beads (Roche) were added to the samples and incubated for 2 hrs at 4°C in the following day. Beads were then washed 5 times with the lysis buffer before elution with 2X SDS sample buffer containing 10% β -mercaptoethanol at 95 °C for 5 min. The eluted proteins were subject to SDS-PAGE and Western blotting.

3.2.6 Immunoblotting (Western blotting)

Protein samples were separated by SDS-PAGE and transferred to polyvinylidene fluoride (PVDF, Thermo Scientific) or nitrocellulose membrane (LI-COR Inc., USA). The membrane was blocked with a blocking buffer (5% milk/0.1% Tween-20 in PBS) for 1 hr at room temperature and then incubated at 4°C overnight with the primary antibody. The primary antibodies were used at the following dilutions: rabbit anti-RIP1 (1:500, BD), rabbit anti-RIP3 (1:500, Cell Signaling Technology, CST), rabbit anti-MLKL (1:500, CST), rabbit anti-pRIP3 (1:500, CST), rabbit anti-pMLKL (1:500, Abcam), mouse anti-mCherry (1:1000, Biolegend), rabbit anti-LC3 (1:1000, Sigma),

rabbit anti-IkBa (1:1000, CST), rabbit anti-AIF (1:1000, CST), chicken anti-ASIC1a (1:1000, Santa Cruz) and mouse anti-Actin (1:3000, Santa Cruz. After washing 3 times with a washing buffer (0.1% Tween-20 in PBS), the membrane was incubated with HRP-conjugated secondary antibodies (1:10000, Roche) or IRDye® secondary antibodies (1:10000, LI-COR Inc.) for 1 hr at the room temperature. After extensive washes with the washing buffer, the blots were visualized by exposure to ECL reagent (Thermo Scientific) when HRP-conjugated secondary antibodies were used or with the use of Odyssey® CLx imaging system (LI-COR Inc.) when IRDye® secondary antibodies were used.

3.2.7 Immunocytochemistry

N2a cells were grown on poly-L-ornithine coated coverslips and subject to different treatments as described. The samples were washed once with PBS and cells fixed with 4% paraformaldehyde in PBS for 10 min. The fixed cells were washed 3 times with PBS and permeabilized with PBS containing 0.1% Triton X-100 and 5% bovine serum albumin (BSA) for 1 hr at 37°C before incubation with the primary AIF antibody (1:300, CST) at 4°C overnight. The cells were washed and probed with the fluorophore-conjugated secondary antibody (Invitrogen, USA) at room temperature for 1.5 hours. Then, the cells were incubated with DAPI (300 nM) solution for 15 min before being mounted by the ProLong Gold antifade reagent (Life Technologies, USA). Slides were examined by fluorescence microscopy (Olympus) and images were analyzed and processed by ImageJ software.

3.2.8 Focal ischemia

The surgery was done by our collaborators in China and the experimental protocols (ethics protocol number: 2014022) were approved by the Animal Care and Use Committee of Shanghai Jiao Tong University School of Medicine, Shanghai, China. A transient focal ischemia model was prepared as described previously (110, 120) via suture occlusion of the middle cerebral artery (MCAO) in male wild type and *ASIC1a*^{-/-} C57BL/6 mice (~25 g). Briefly, animals were anesthetized using 10% chloral hydrate with intubation and ventilation. Rectal and temporalis muscle temperature was maintained at $37 \pm 0.5^{\circ}\text{C}$ with a thermostatically controlled heating pad and lamp. A suture occlusion was made to the middle cerebral artery while cerebral blood flow (CBF) was monitored by transcranial laser Doppler. Animals whose blood flow did not reduce below 20% were excluded. The suture was removed 1 hr after MCAO to allow reperfusion and the mice were euthanized 24 hrs later. Brains were removed, sectioned coronally at 1 mm intervals, and stained with the vital dye 2,3,5-triphenyltetrazolium hydrochloride (TTC).

Intracerebroventricular injection was performed by stereotaxic technique using a microsyringe pump as described previously (120). For each animal, 5 μl of artificial cerebrospinal fluid (aCSF), or 5 μl aCSF containing 2.5 μg Dabrafenib (Cayman Chemical Company, USA) was injected 30 min after reperfusion.

3.2.9 Statistical analysis

Statistical comparisons were performed by Prism software (GraphPad Software, Inc.) using unpaired or paired Student's *t* test where values of $p < 0.05$ are considered significant.

3.3 Results

3.3.1 RIP3 is involved in acidosis-induced neuronal cell death

We have previously demonstrated that acidosis-induced neuronal cell death is ASIC1 and RIP1 dependent. Since RIP3 is phosphorylated by RIP1 kinase and represents another critical kinase responsible for mediating necroptosis, I examined the role of RIP3 in acidosis-induced neuronal cell death. I first examined the phosphorylation of RIP3 in primary cultured mouse cortical neurons treated with either a pH 7.4 extracellular solution (ECS) or a pH 6.0 ECS for 1 hr, followed by recovery in the normal medium for another hr. Using a phospho-RIP3 (p-RIP3) antibody, I detected an increase in the p-RIP3 level in the pH 6.0-treated samples (**Figure 24A**). Because the antibody for total RIP3 did not work well for mouse cortical neuron samples, I used actin as the loading control for this experiment.

To test if RIP3 activity was required for pH 6.0-induced neuronal death, I used GSK'872 and dabrafenib, two recently reported RIP3 inhibitors (121). For this, the neurons were treated with pH 7.4 and pH 6.0 ECs for 1 hr, which was then followed by recovery in the normal culture medium for 24 hrs before cell viability was measured using the CTB assay. Under these conditions, typically about 60-70% neurons die as

a result of the pH 6.0 treatment. To validate the inhibitors, I also treated HT29 cells, a human colorectal adenocarcinoma cell line frequently used to study necroptosis (122), with a mixture of TNF α , smac mimetic, and Z-VAD (TSZ) as an established *in vitro* model of necroptotic death that requires RIP3 activity. Indeed, both GSK'872 and dabrafenib blocked the death of HT29 cells triggered by the treatment with TSZ for 24 hrs, and the RIP1 inhibitor Nec-1 exerted protection (**Figure 24B**). Similarly, GSK'872 and dabrafenib (added at 30 min prior to the acid treatment and not included during the recovery period) also protected the cultured cortical neurons from acidosis-induced death to a similar degree as Nec-1 and the ASIC1a inhibitor, PcTX1 (**Figure 24C**). These results demonstrate that RIP3 is involved in the acidosis-induced neuronal death.

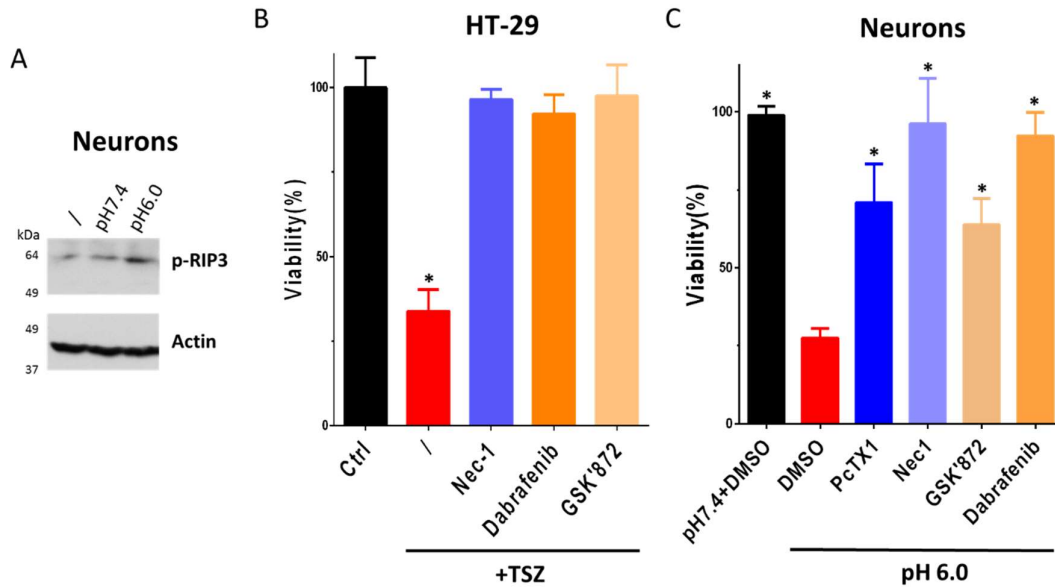


Figure 24. RIP3 is involved in acidosis-induced neuronal cell death. (A) Western blot analysis of phospho-RIP3 levels in lysates from mouse cortical neurons untreated (/) or treated pH 7.4 or pH 6.0 ECS for 1 hr then recovered in the normal medium for another hr. Actin was used as loading control. (B) HT29 cells were treated with TSZ (TNF α : 30 ng/ml, Smac mimetic: 100nM, z-VAD: 20nM), or TSZ with Nec-1 (40 μ M), dabrafenib (10 μ M), or GSK'872 (3 μ M) for 24 hrs. The viability of cells was determined by the Cell-Titer Blue (CTB) assay. (C) Cultured mouse cortical neurons were pretreated with DMSO, PcTX1 (50 nM), Nec-1 (40 μ M), GSK'872 (3 μ M), or dabrafenib (10 μ M) for 30 min and then incubated with pH 7.4 or pH 6.0 ECS for 1 hr. Neurons were recovered for 24 hrs in normal medium before cell viability was performed using the CTB assay. Results are representative of three independent experiments. Error bars represent SDs. *, $P < 0.05$ vs. untreated (B) or pH 6.0 with DMSO (C).

3.3.2 Re-introduction of RIP3 increases cell death in response to acidosis

The failure of the commercial antibody to detect total RIP3 proteins in primary cortical neurons prompted me to search for suitable cell lines to study acidosis-induced cell death. Notably, many cell lines are resistant to acidosis-induced death. It turns out that these cells either lack ASIC1a, for example, HT29, COS7, Chinese hamster ovary (CHO) cells; or they do not express RIP3, such as N2a and HEK293 (**Table 2**). Previous studies have shown that exogenously expressing ASIC1a in COS7 and CHO cells can recapture the acidosis-induced cell death (98, 123). However, it was not known whether reintroduction of RIP3 in the RIP3-negative cells would rescue the acid sensitivity. More interestingly, RIP3 expression has been shown to be lost in many cancers and this may be responsible for their resistance to death in the acidic tumor microenvironment (124).

	Neuron	N2a	HEK293	HT29	COS-7/CHO
ASIC1a	+	+	+	-	-
RIP3	+	-	-	+	+
CAN be killed by pH6.0 ?	✓	✗	✗	✗	✗

Table 2. Different acid sensitivity of various cells. The expression of ASIC1a and RIP3 in different cells is indicated by “+” (*positive*) and “-” (*negative*). Their sensitivity to acid-induced death is indicated by the ✓ and ✗ signs.

To test whether heterologous expression of RIP3 can recapture acidosis-induced cell death, I first tried HEK293 cells. GFP-tagged human RIP3 (hRIP3-GFP) or mCherry-tagged mouse RIP3 (mRIP3-mCherry) were expressed in HEK293 cells by transient transfection and the expression was confirmed by Western blotting. GFP tag only was used as a negative control (**Figure 25**). Treatment with TSZ killed cells that expressed hRIP3 but not those that expressed GFP or mRIP3. Similarly, cells that expressed hRIP3 also became sensitive to 1 h treatment with the pH 6.0 ECS (with 24 hrs of recovery in the normal medium) as compared to pH 7.4 ECS. By contrast, several attempts by introducing mRIP3 to the HEK293 cells failed to confer the sensitivity to pH 6.0 ECS (**Figure 26, 27**). This is consistent with a previous report that there is species specificity for the RIP3-MLKL interaction, where human RIP3 does not interact with mouse MLKL and mouse RIP3 cannot bind to human MLKL (125). As such, the mouse RIP3 expressed in the human cells is not expected to form necrosomes for necroptotic cell killing.

The results in HEK293 cells indicate that RIP3 may play a pivotal role in both TSZ- and acidosis-induced necroptosis. However, in both CTB (**Figure 26**) and LDH (**Figure 27**) assays, the difference between pH 7.4- and pH 6.0-treated hRIP3-expressing cells was moderate. Importantly, the treatment with pH 7.4 ECS already triggered marked cell loss as compared to the control (in normal culture medium, untreated). This suggests that HEK293 cells may be very sensitive to starvation, which can compromise our ability to detect acid-induced RIP3-dependent necroptosis.

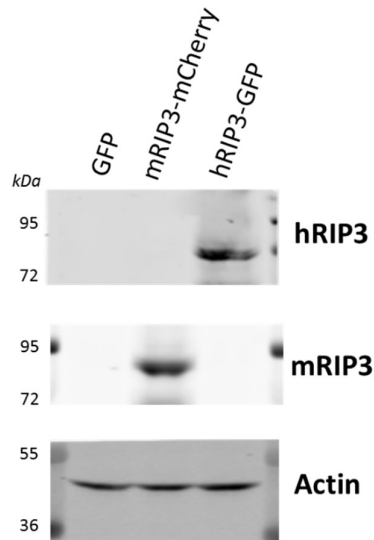


Figure 25. Verification of RIP3 expression in HEK293 cells. After transfection with the corresponding plasmids, the expression of GFP-tagged human RIP3 (hRIP3, upper) or mCherry-tagged mouse RIP3 (mRIP3, middle) was assessed in cell lysates by Western blotting using hRIP3 and mRIP3 antibodies, respectively. Actin was used as the loading control.

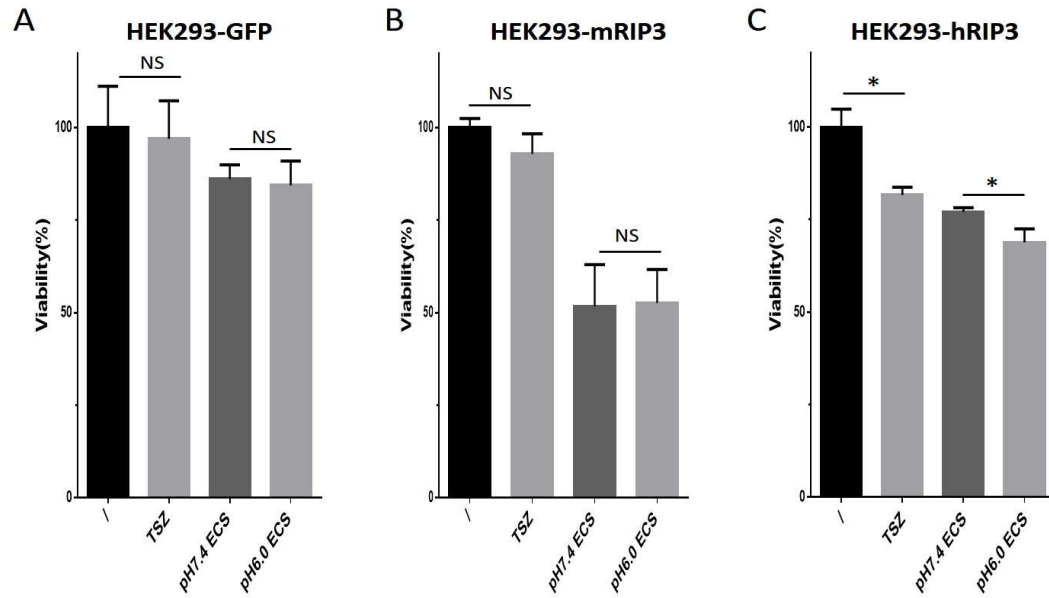


Figure 26. hRIP3 expression confers TSZ-induced cell death and differential responses to pH 7.4 and pH 6.0 ECS, as determined by CTB assay. The viability of HEK293 cells that expressed GFP (**A**), mouse RIP3 (**B**) or human RIP3 (**C**) and were treated with normal culture medium (/), TSZ (24 hrs), or pH 7.4 or pH 6.0 ECS (1 hr treatment plus 24 hr recovery in normal medium) was assessed by CTB assay. *Error bars represent SDs. NS, Not significant. *, $P < 0.05$.*

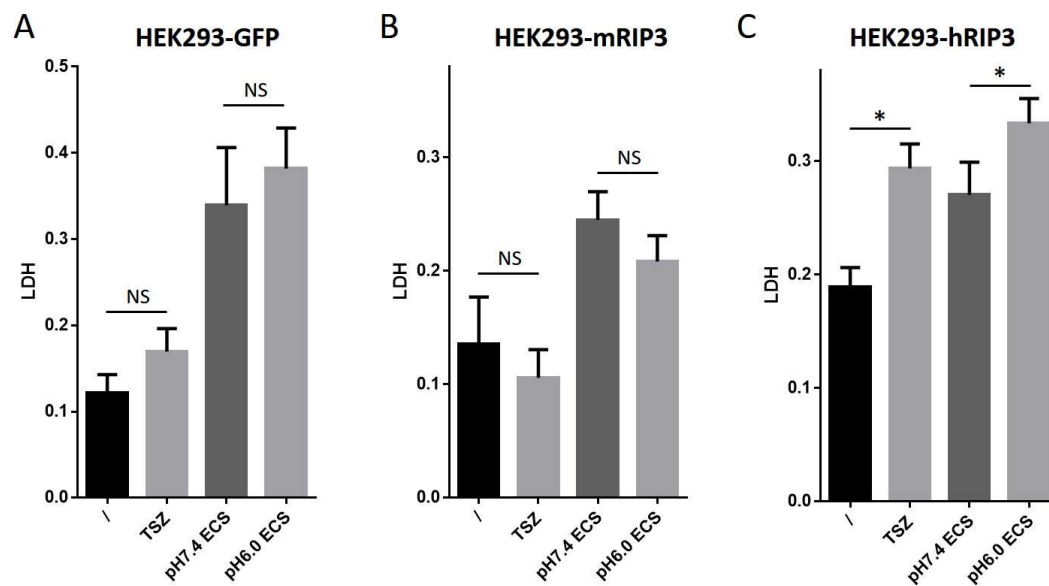


Figure 27. hRIP3 expression confers TSZ-induced cell death and differential responses to pH 7.4 and pH 6.0 ECS, as determined by LDH assay. LDH release from HEK293 cells that expressed GFP (**A**), mouse RIP3 (**B**) or human RIP3 (**C**) and were treated with normal culture medium (I), TSZ (24 hrs), or pH 7.4 or pH 6.0 ECS (1 hr treatment plus 24 hr recovery in normal medium) was assessed by LDH assay. *Error bars represent SDs. NS, Not significant.*

**, $P < 0.05$.*

N2a is a fast-growing mouse neuroblastoma cell line, which had been used for the study of acidosis-induced cell death before. However, the percentage of death reported was very low (around 15%) under 1 hr pH 6.1 treatment (126). Indeed I did not detect any obvious cell death in wild type N2a cells after the treatment with pH 6.0 ECS (**Figure 28A**). Since RIP1, RIP3 and MLKL are thought to be important necroptosis effector molecules (122) and ASIC1 is required for the acid-induced death (98), I checked the expression of ASIC1, RIP1, RIP3 and MLKL in N2a cells by Western blotting. While ASIC1a, RIP1 and MLKL were detected in N2a cells, RIP3 was not (**Figure 28B**). As a control, RIP3 was detected in mouse embryonic fibroblasts (**Figure 28B**). Interestingly, the mouse embryonic fibroblast cells were insensitive to acidosis-induced death (data not shown); however, this may be due to the fact that they do not express ASIC1 (**Figure 28B**). Using whole-cell patch clamp recordings, we were able to detect ASIC-like inward current evoked by the pH 6.0 ECS at the -60mV holding potential in N2a cells (**Figure 28C**). Therefore, N2a cells express ASIC1 but not RIP3, explaining their resistance to acid-induced death.

I then transfected the N2a cells with mCherry-tagged mouse RIP3 (mRIP3-mCherry) to see whether reintroduction of RIP3 could recapture acidosis-induced death in these cells (**Figure 28D**). Comparing to mCherry, the expression of mRIP3-mCherry significantly increased the percentage of dead cells in response to 1 hr pH 6.0 treatment based on the SYTOXBLUE staining (**Figure 28E, F**), which specifically labels dead cells. In N2a cells that were untransfected or transfected with mCherry, the

treatment with pH 7.4 ECS did not trigger any obvious cell death and their response to the pH 6.0 ECS was quite moderate (less than 3%). However, following the expression of mRIP3-mCherry, the percentage of cell death went up to around 10% even in cells exposed to pH 7.4 ECS and this value was further increased to around 40% with the treatment of pH 6.0 ECS.

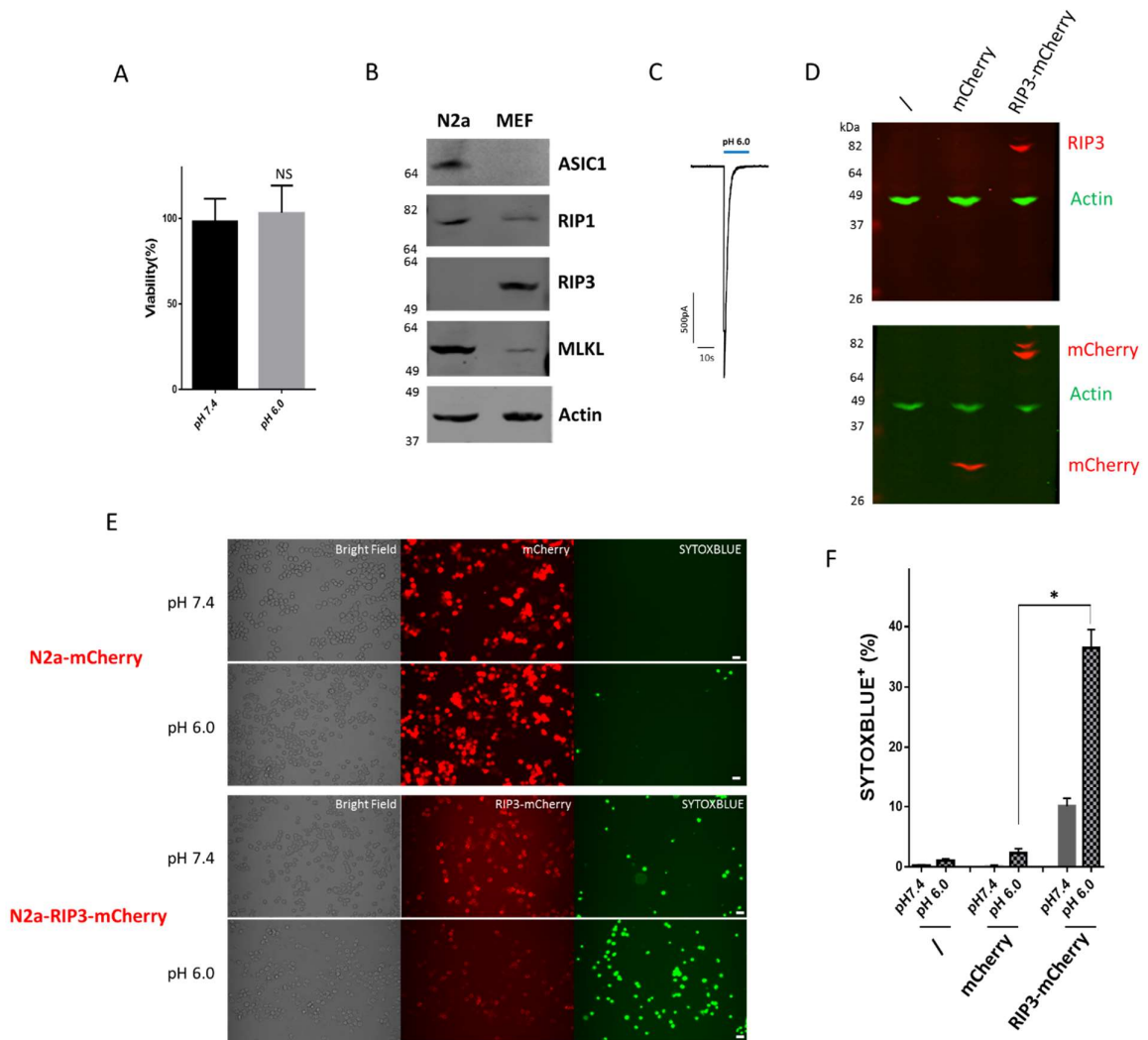


Figure 28. Re-introduction of RIP3 increases acidosis-induced death of mouse neuroblastoma N2a cells. (A) N2a cells were treated with pH 7.4 or pH 6.0 ECS for 1 hr and then recovered in the normal culture medium for 24 hrs. The viability of cells in each group was determined by CTB assay. (B) Protein expression levels of ASIC1, RIP1, RIP3, MLKL, and actin in N2a and MEF cells were tested by Western blotting. (C) ASIC-like acid-induced current recorded at -60 mV from a N2a cell. Representative trace of n=6 cells. (D) The expression of mCherry, and RIP3-mCherry after transfection in N2a cells was confirmed by Western blotting using mCherry (*lower*) and mRIP3 (*upper*) antibodies. (E) N2a cells

transfected with mCherry or mouse RIP3-mCherry were treated with pH 7.4 or pH 6.0 ECS for 1 hr and then recovered in the normal medium for 7 hr. Cells were stained with SYTOXBLUE to reveal dead cells and images were taken by fluorescence microscope. Scale bar: 30 μ m. **(F)** Quantification of percentages of SYTOXBLUE-positive cells as in (E). *Error bars represent SDs. NS, Not significant. *, $P < 0.05$.*

3.3.3 MLKL is involved in acidosis-induced cell death in N2a-RIP3 cells

MLKL is another important component of necrosomes. I examined the phosphorylation of MLKL during and after acid stimulation of N2a cells that expressed mRIP3. Consistent with the idea that MLKL phosphorylation by RIP3 kinase is critically involved in necroptosis, increased levels of phospho-MLKL were detected during the first hr of the pH 6.0 ECS treatment but the increase subsided 1 hr of returning to the normal medium. The total MLKL levels remained unchanged during the time period **(Figure 29 A, B)**. Furthermore, it is well-established that RIP3 and MLKL co-exist in the same protein complex, i.e. necrosomes, during necroptosis (125). To test if this is also the case for acidosis-induced necroptosis, I performed co-IP to check if RIP3 became physically associated with MLKL in response to acid treatment. I found that in the pH 6.0 ECS treated samples, the amount of RIP3 that co-IPed with MLKL was markedly higher than that incubated with pH 7.4 ECS **(Figure 29C)**. Reciprocally, the amount of MLKL that co-IPed with mCherry (for RIP3) was also more in pH 6.0 treated than in pH 7.4 treated samples **(Figure 29C)**. These data indicate that the association between RIP3 and MLKL was increased in response to the acid treatment, consistent

with that happened in the classical necroptosis triggered by $\text{TNF}\alpha$. The activated MLKL could be responsible for the demise of cells exposed to the acidic environment.

Next, I tested the effect of knocking down MLKL expression on the acidosis-induced death of N2a cells that expressed RIP3. Two shRNA constructs targeting mouse MLKL and a control shRNA construct were transfected together with mRIP3 in N2a cells. At 48 hrs after transfection, MLKL protein levels in the MLKL shRNA groups decreased to 29% and 38% of the control shRNA group (**Figure 30A**). After treatment with pH 6.0 ECS for 1 hr, followed by 7 hr recovery in normal medium, cell viability was assessed by SYTOXBLUE staining. Both MLKL shRNA resulted in protection of the N2a cells from the acidosis-induced death, as shown by the reduced percentage of SYTOXBLUE-positive cells (**Figure 30B**).

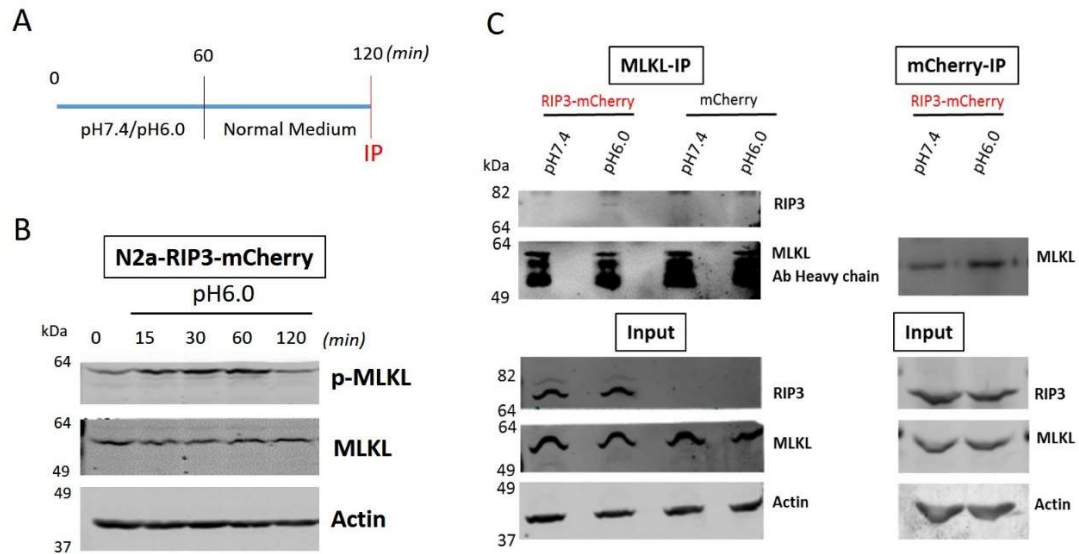


Figure 29. MLKL is involved in acidosis-induced cell death. (A) Schematics of treatment conditions. N2a cells expressing RIP3 were treated with pH 7.4 or pH 6.0 ECS for 1 hr and then recovered in the normal culture medium for another hr. (B) Cells were collected at different time points as indicated and assessed by Western blotting for phospho MLKL (p-MLKL), total MLKL and Actin antibodies. (C) Cells collected at 120 min were subjected to IP by MLKL antibody (MLKL-IP) or mCherry antibody (mCherry-IP) and then tested for the presence of RIP3 and MLKL, respectively, by Western blotting using the corresponding antibodies.

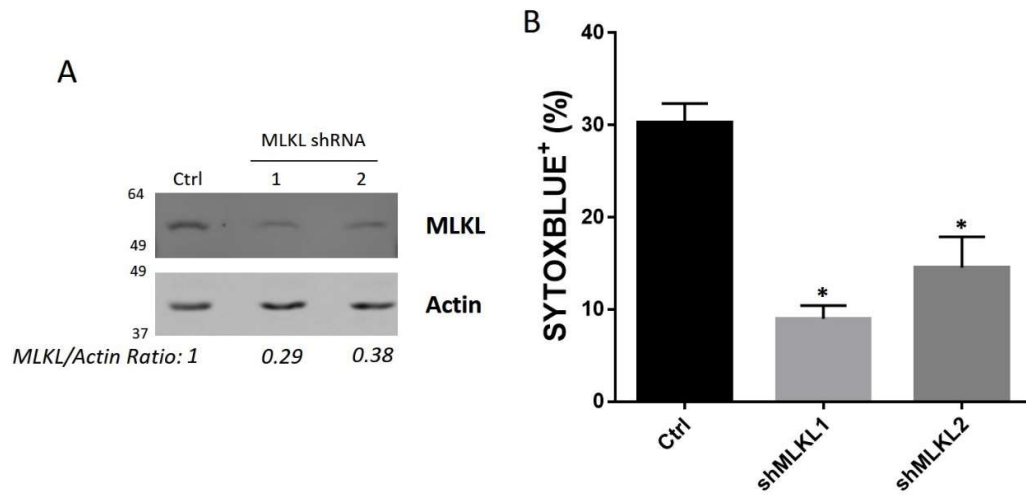


Figure 30. MLKL knocking down suppresses acidosis-induced cell death. N2a cells were transfected with mRIP3-mCherry in combination with either a control shRNA or either of the two MLKL shRNAs and used after 48 hrs. (A) The expression of MLKL was assessed by Western blotting. The intensity ratios of MLKL to actin are shown at the bottom. (B) Cells were treated with pH 7.4 or pH 6.0 ECS for 1 hr and then recovered in the normal culture medium for 7 hrs, followed by SYTOXBLUE staining. The number of SYTOXBLUE-positive cells was counted and the percentage to total calculated. *Error bars represent SDs. *, $P < 0.05$.* Results are representatives of two independent experiments.

3.3.4 pH 6.0 ECS down regulates RIP1 and I κ B α in N2a cells independently of RIP3

Besides RIP3 and MLKL, the conventional DR signaling also includes RIP1 regulation of NF κ B pathway (127). To examine if acidosis-induced RIP1 activation also affects NF κ B function, I measured the levels of I κ B α , whose decrease indicates NF κ B activation, in N2a cells over the time course of 1 hr pH 6.0 ECS treatment and 3 hr recovery. For comparison, I also measured total RIP1 levels in the same cell lysates. Interestingly, both RIP1 and I κ B α were down regulated after the 1 hr treatment of pH 6.0 ECS (**Figure 31B, 32A**), with the decrease of I κ B α occurring slightly earlier than that of RIP1. These changes could be independent, but they could also implicate that NF κ B activation by the acid treatment turned on some genes that cause RIP1 to decrease. Nonetheless, RIP3 appears to be dispensable for the changes found in RIP1 and I κ B α since the decreases occurred in wild type N2a cells that do not express RIP3. The expression of mCherry or RIP3-mCherry in N2a cells did not alter the effect of pH 6.0 ECS on decreasing I κ B α (**Figure 32B**).

Interestingly, it has been reported that ASIC1 expression is important for acidosis-induced ERK-mediated NF κ B activation in tumors, and this pathway is upregulated in some cancers to promote cell invasion and metastasis (128). I also found ASIC1 to be critical for the acidosis-induced NF κ B activation. In HEK293 cells, which express ASIC1 but not RIP3, acidosis decreased I κ B α levels similarly as in N2a cells. In HT29 cells, which do not endogenously express ASIC1, the pH 6.0 ECS failed to induce any change of I κ B α . However, when I introduced ASIC1 into the HT29 cells,

the I κ B α level dropped in response to the pH 6.0 ECS treatment (**Figure 32 C, D**).

Collectively, the above data suggest that the acid-induced activation of NF κ B is dependent on ASIC1 but not RIP3, implicating a functional coupling between ASIC1 and RIP1 in the absence of RIP3.

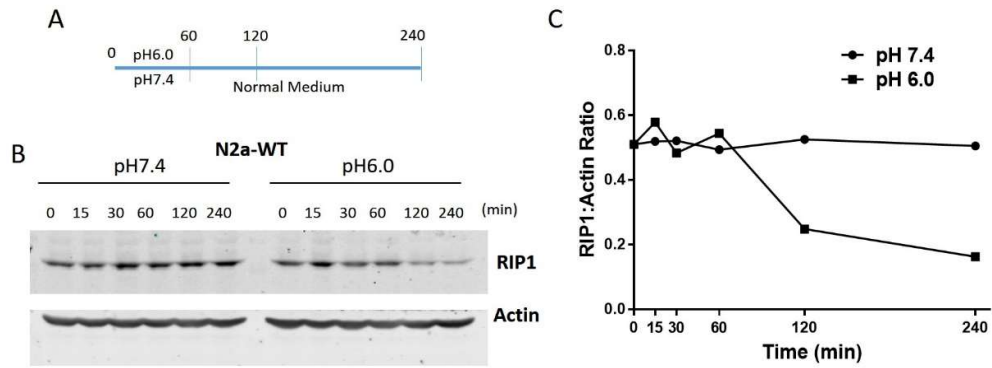


Figure 31. Acidosis down regulates RIP1 independently of RIP3. (A) Schematics of experimental protocol used. Wild type N2a cells were treated with pH 7.4 or pH 6.0 ECS for 1 hr and then recovered in the normal culture medium for another 3 hrs as indicated. (B) Cell lysates from different time points as indicated were subjected to Western blot analysis to measure RIP1 levels. Actin was used as the loading control. (C) RIP1/actin ratios over the time course of pH 7.4 or 6.0 ECS treatment and recovery in the normal medium for experiment shown in (B). Results are representatives of three independent experiments.

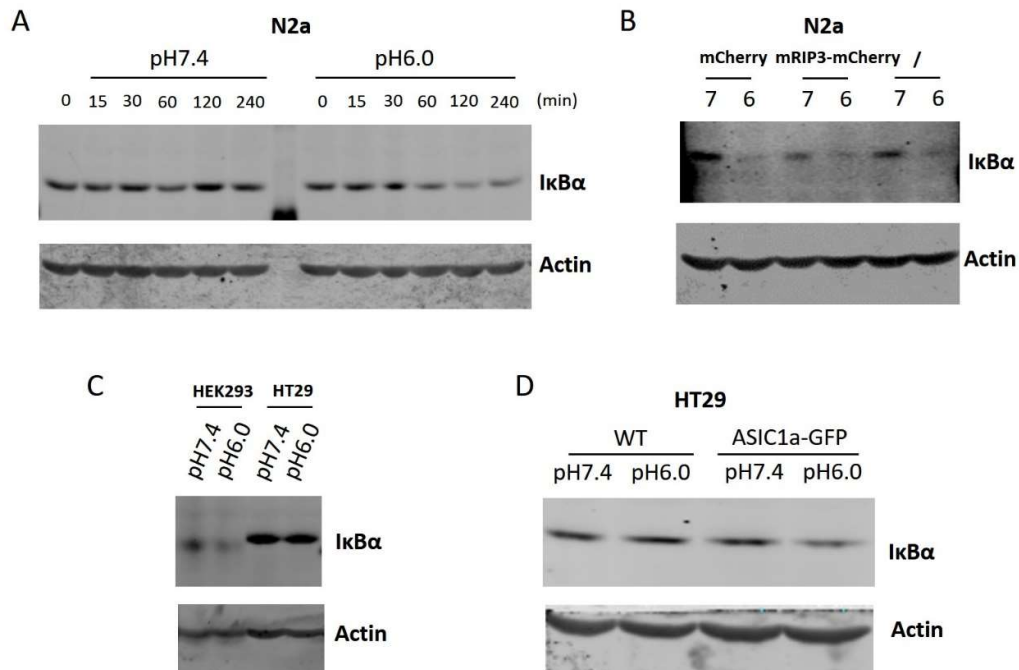


Figure 32. Acidosis down regulates IκBα in an ASIC1-dependent manner but independently of RIP3. (A) The same cell lysates as that used in Figure 29 were subjected to Western blot analysis to measure IκBα levels. Actin was used as the loading control. **(B)** Wild type N2a cells or N2a cells expressing mCherry or RIP3-mCherry were treated as in (A). Cell lysates from the 120-min time point were assessed by Western blotting for IκBα and actin, showing no effect of mCherry or RIP3-mCherry. **(C)** HEK293 and HT29 cells were treated as in (A) but only lysates from the 120-min time point were analyzed by Western blotting for IκBα and actin. Note the decrease in IκBα in pH 6.0-treated HEK293 cells but no change in HT29 cells. **(D)** HT29 cells were transfected with ASIC1a-GFP and then subjected to the treatment with pH 7.4 or pH 6.0 ECS as in (A). Only lysates from the 120-min time point were analyzed by Western blotting for IκBα and actin. The expression of ASIC1a rescued the acidosis-induced IκBα decrease in HT29 cells. Results (A) and (B) are representatives of three independent experiments. Results (C) and (D) are representatives of two independent experiments.

3.3.5 Starvation plays a critical role in acidosis-induced cell death

Acidosis by itself can cause cell death in cultured neurons, but the pH of the medium must be very low (pH<6.2 for ~ 4 hr) or the treatment needs to be prolonged (pH<6.6 for >6 hr) (129). The routine protocol for in vitro acidosis assay, adapted from the literature that examined ASIC1a-dependent acidotoxic neuronal death (98, 123), consists of incubating cells in a pH 6.0 ECS for 1 hr, followed by replacing the treatment solution with the normal culture medium for about 24 hrs. The ECS contains no serum, growth factors or any amino acid, and therefore is typical of starvation treatment routinely used to induce autophagy (130). Indeed, I found the LC3-II and phosphor-p70S6K levels to be decreased in neurons treated for 1 hr in both pH 7.4 and pH 6.0 ECS (**Figure 33**), indicating that the ECS treatment induced autophagy in our system.

To learn if the ECS treatment is necessary for the acid-induced neuronal death, I used culture media with different pH instead of ECS to treat the neurons for 1 h and then allowed the cells to recover in the normal (pH 7.4) culture medium for 24 hrs. Surprisingly, there was no detectable neuronal demise in samples that had been exposed to media with acidic pH (**Figure 34A**). To determine which component(s) of the culture medium protected cells from the acid-induced death, I supplemented the pH 6.0 ECS with 10% FBS or omitted FBS from the DMEM culture medium. The addition of FBS into the pH 6.0 ECS fully abolished the acidosis-induced cell death in N2a cells that expressed RIP3. The serum-free pH 6.0 DMEM, which contains amino acids but not growth factors and other components of the FBS, on the other hand,

moderately supported the acid-induced death, but not as severely as pH 6.0 ECS (**Figure 34B**). These findings suggest that both amino acid starvation and serum contribute to acidosis-induced cell death, with the latter being more pronounced. To examine if starvation is only involved in acidotoxic death or if it is also required for other acidosis-induced and ASIC1a-dependent cellular processes, I also measured the effect of pH 6.0 culture medium (with 10% FBS) on the levels of RIP1 and I κ B α over a period of 0.5 to 4 hrs, with the first hr being pH 6.0 treated and the remaining 3 hrs for recovery in the normal culture medium. Different from the pH 6.0 ECS treatment, RIP1 and I κ B α levels did not change markedly following the treatment of pH 6.0 medium (**Figure 33**), suggesting that similar to acidosis-induced death, starvation is also a cofactor for the acid-induced degradation of RIP1 and I κ B α .

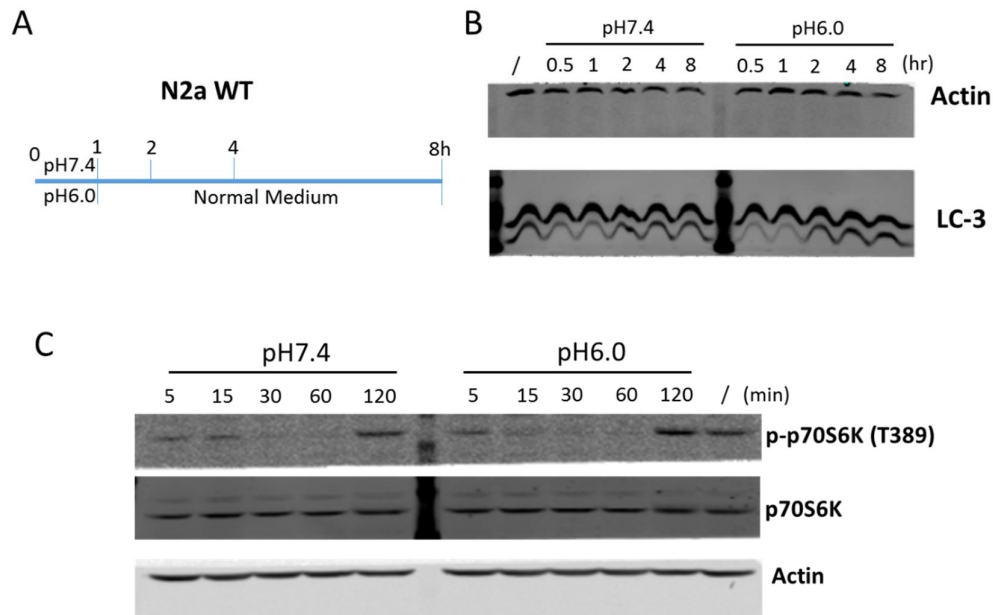


Figure 33. Treatment with ECS triggers a decrease in LC3-II levels in WT N2a cells independent of pH. WT N2a cells were treated with pH 7.4 or pH 6.0 ECS for 1 hr and then recovered in the normal culture medium for another 7 hrs as indicated in **(A)**. Cell lysates from different time points as indicated were subjected to western blot analysis for LC3 **(B)** and phosphor-p70S6K and total p70S6K **(C)** levels, actin was used as a loading control. Results are representatives of three independent experiments.

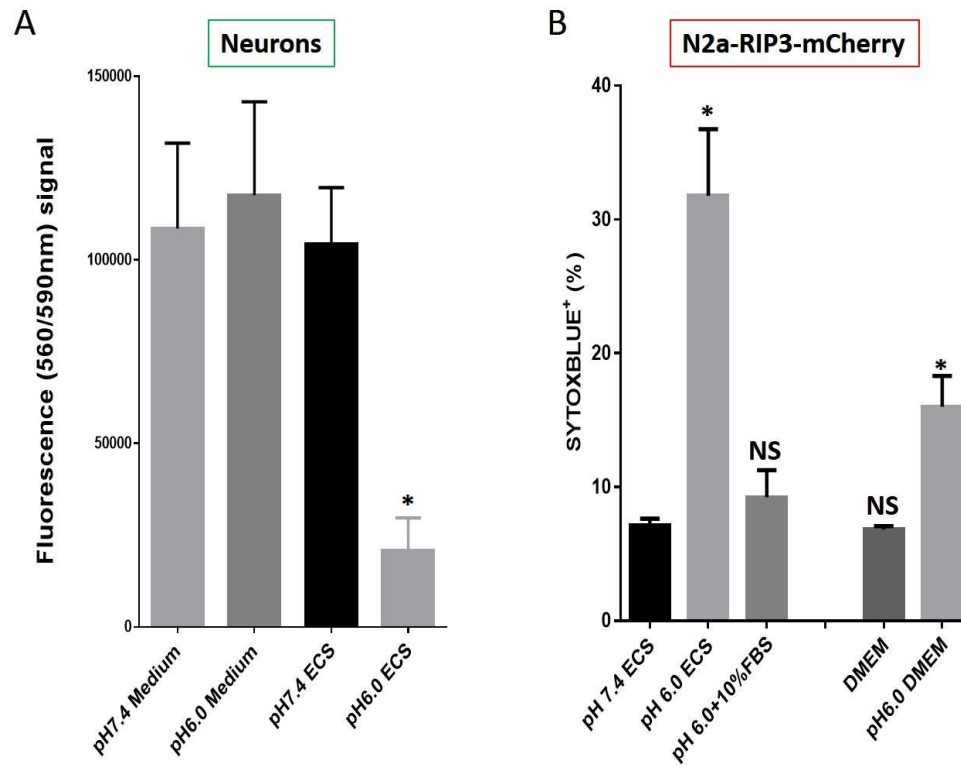


Figure 34. Starvation is required for acidosis induced cell death. (A) Primary neurons were treated for 1 hr with medium or ECS of pH 7.4 or pH 6.0 and then recovered in the normal culture medium for 24 hrs before cell viability was assessed by CTB assay. **(B)** N2a cells expressing RIP3-mCherry were incubated with indicated solutions for 1 hr and recovered in the normal culture medium for 7 hrs. Cells were then stained with SYTOXBLUE and quantified as percentage of SYTOXBLUE positive cells. *Error bars represent SDs. NS, Not significant. *, $P < 0.05$.* Results are representatives of three independent experiments.

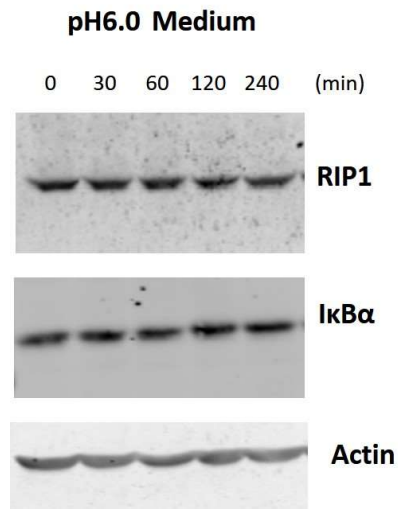


Figure 35. The lack of effect of pH 6.0 medium on RIP1 and IκBα levels in the absence of starvation. WT N2a cells were treated with pH 6.0 medium for 1 hr and then recovered in the normal culture medium for 3 hrs. Cell lysates from different time points as indicated were subjected to western blot analysis to measure the RIP1 and IκBα protein levels. Actin was used as a loading control.

3.3.6 Acidosis induces AIF nuclear translocation

In a recent study, it was shown that parthanatos is one of the mechanisms by which tissue acidosis associated with ischemia augments the formation of PAR polymers, the nuclear translocation of AIF, and neuronal cell death (118). In a separate study it was shown that serum deprivation induces autophagy and predominantly an AIF-dependent apoptosis in cultured hippocampal neuronal cell line HT22, where the nuclear translocation of AIF was also observed (130). These findings prompted us to consider the possibility that AIF nuclear translocation may be involved in our experimental setting, in which both acidosis and starvation occurred during the 1 hr treatment of pH 6.0 ECS. Therefore, I examined the localization of AIF in N2a cells by immunofluorescence staining at 7 hrs after challenging the cells with ECS of different pH for 1 hr. In control cells that expressed mCherry, AIF was localized predominantly in the cytosol and in the perinuclear region of the cytoplasm. In N2a cells expressing RIP3-mCherry treated with pH 6.0 ECS for 1 hr, however, there was an increased co-localization of AIF with DAPI (**Figure 36A**). Quantification of cells showing nuclear staining of AIF revealed a statistically significant augmentation of AIF nuclear translocation in N2a cells expressing RIP3-mCherry that were treated with pH 6.0 ECS as compared to that with pH 7.4 ECS, but not in cells expressing mCherry (**Figure 36B**). Interestingly, I also observed a nuclear translocation of RIP3-mCherry in response to pH 6.0 ECS, consistent with the study showing a physical interaction between AIF and RIP3 (131). The nuclear translocation of RIP3 could also be caused by the rupture of nuclear membrane or nuclear pore, which would allow RIP3-mCherry

to be diffused into the nucleus.

On the other hand, I did not find any upregulation of AIF protein expression as reported for HT22 cells that were serum deprived and underwent AIF-dependent apoptosis (130) (**Figure 36C**). Importantly, I also did not detect any accumulation of PAR following the treatment N2a cells expressing RIP3-mCherry with pH 6.0 ECS, suggesting that the 1 hr treatment of acidosis and starvation triggered AIF release independent of nuclear damage or at least independent of PAR production.

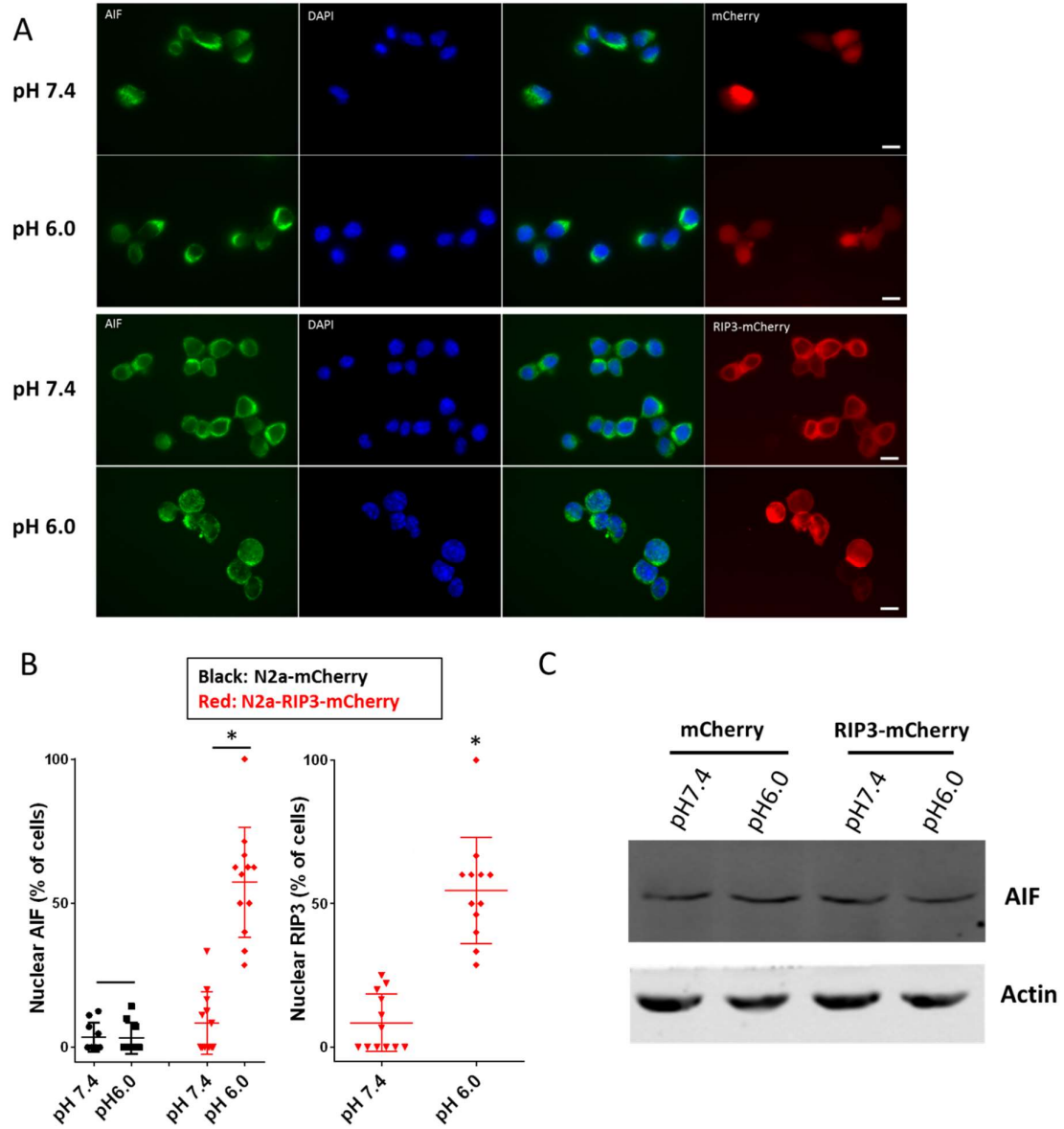


Figure 36. Acidosis induces AIF and RIP3 nuclear translocation. N2a cells expressing mCherry or RIP3-mCherry were treated with pH 7.4 or pH 6.0 ECS for 1 hr and recovered in the normal culture medium for 7 hrs. Cells were fixed and stained with anti-AIF (*green*) and DAPI (*blue, for nuclei staining*). Representative images taken from fluorescent microscope are shown in (A). Scale bar: 15 μ m. The percentage of cells with nuclear staining of AIF or RIP3 was quantified in (B). (C) Western blot analysis of AIF protein from cell lysates collected at the same time points as above.

3.3.7 ROS and MPTP are involved in AIF nuclear translocation in response to acidosis/ starvation

In order to be translocated to the nucleus, AIF must be released from mitochondria first. Previously, it has been showed that mitochondrial permeability transition pore (MPTP), reactive oxygen species (ROS), calpain as well as PARP contribute to the AIF release from mitochondria. To explore the molecular mechanism(s) underlying acid and starvation induced AIF translocation, I tested whether or not disrupting the above pathways could protect cells from death induced by the pH 6.0 ECS. I used inhibitors for voltage-dependent anion channels (VDAC, an essential component of MPTP), DIDS (500 μ M) and TRO19622 (20 μ M); antioxidants: NAC (6 mM), TEMPOL (500 μ M), and Trolox (100 μ M); a calpain inhibitor: ALLN (10 μ M); and a PARP inhibitor: DPQ (30 μ M). Interestingly, the pH 6.0 ECS-induced death of RIP3-expressing N2a cells was suppressed by VDAC inhibitors and antioxidants but not by inhibiting calpain or PARP (**Figure 37**), suggesting that MPTP and ROS are involved in the acidosis/starvation-induced cell death, which may occur independently of calpain-mediated cleavage and PARP activation .

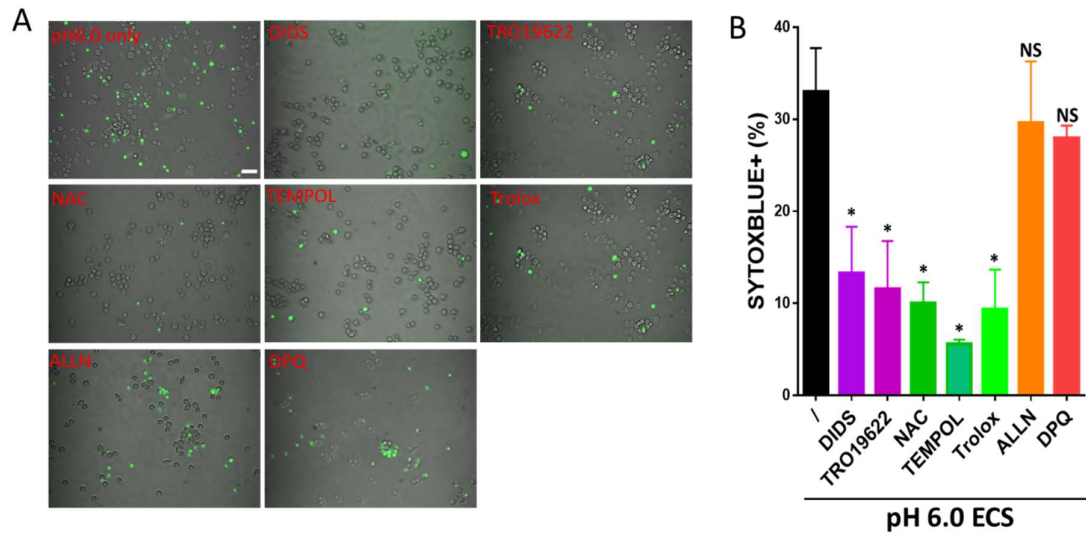


Figure 37. VDAC inhibitors and antioxidants attenuated acidosis induced cell death. (A)

Live-cell fluorescent images of SYTOXBLUE staining (green) of N2a cells expressing RIP3-mCherry treated with pH 6.0 ECS in the absence (pH 6.0 only) and the presence of indicated drugs, VDAC inhibitors: DIDS (500 μ M), TRO19622 (20 μ M); antioxidants: NAC (6 mM), TEMPOL (500 μ M), Trolox (100 μ M); calpain inhibitor: ALLN (10 μ M); Poly(ADP-ribose) polymerase (PARP) inhibitor: DPQ (30 μ M). For each condition, the fluorescence image was merged with bright field image to show the overall cell distribution and morphology. (B) Quantification for (A) showing the percentage of SYTOXBLUE-positive cells among the total cells under each condition. *Error bars represent SDs. NS, Not significant. *, $P < 0.05$.* Results are representatives of three independent experiments.

3.3.8 RIP3 inhibitor dabrafenib attenuated ischemic brain damage *in vivo*

The above *in vitro* data demonstrate that RIP3 and its downstream signaling molecules including MLKL and AIF contribute to acidosis and starvation induced cell death through ASIC1a and RIP1. Given that acidotoxicity is an important contributor of brain damage associated with ischemic stroke, it is anticipated that targeting one or more of the key contributors of the acidosis-induced necroptotic pathway will protect neurons from injury during or following ischemic stroke. Among the key contributors to acidosis-induced death, blocking ASIC1a with PcTX1, inhibiting RIP1 with Nec1, disrupting VDAC with its inhibitors, and using antioxidants to sequester ROS have all been shown to be neuroprotective in the stroke models (98, 111, 132, 133). However, whether or not inhibiting RIP3 with its antagonists, e.g. dabrafenib, an FDA approved drug, would also be neuroprotective was not known. Therefore, we examined the possible protection effect of dabrafenib for the first time in the mouse model of cerebral ischemia, in which ischemia was induced by MCAO. Dabrafenib 2.5 µg (0.5 µg/µl x 5 µl), was intracerebroventricularly (i.c.v.) injected 30 min after 1-hr MCAO. Comparing to mice injected with vehicle or nothing, Dabrafenib significantly decreased the infarct volumes as assessed by TTC staining (**Figure 38**). Similar decrease was also achieved by ASIC1a gene knockout. Thus, our *in vivo* data indicate that inhibiting RIP3 by dabrafenib may be of therapeutic value for neuroprotection in ischemic stroke, just like that previously shown for antioxidants, and RIP1 and VDAC inhibitors.

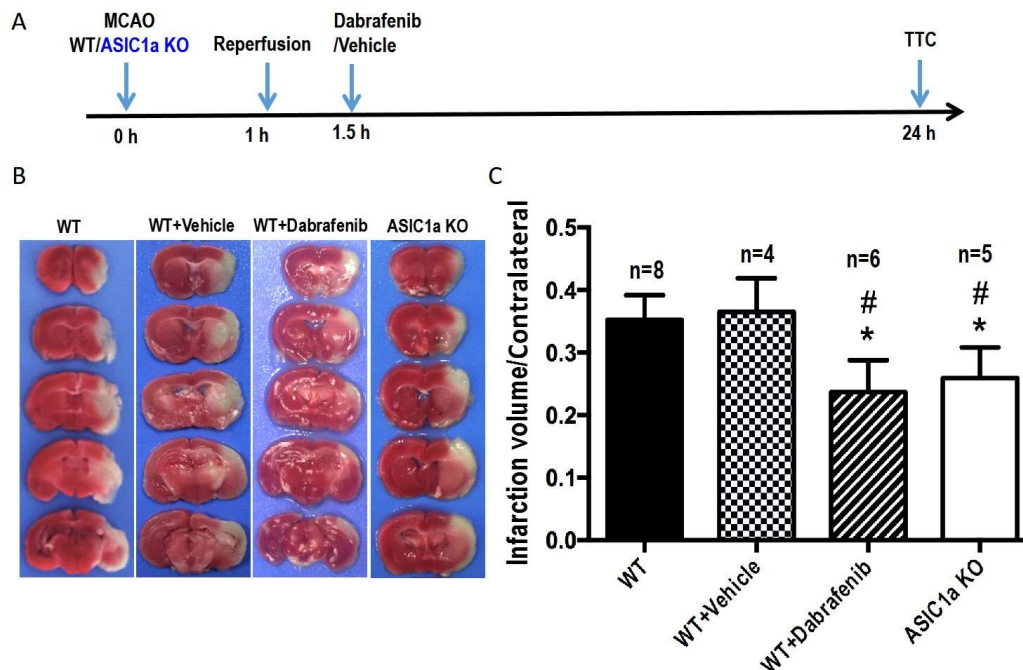


Figure 38. Neuroprotection by RIP3 inhibitor dabrafenib and ASIC1a gene knock out. (A)

Scheme of middle cerebral artery occlusion (MCAO) treatment and assay protocol. Mouse brain slices after 1 hr of MCAO treatment followed by 24 hr reperfusion were collected for TTC staining. Dabrafenib, 2.5 μg (0.5 $\mu\text{g}/\mu\text{l}$ x 5 μl), was intracerebroventricularly (*i.c.v.*) injected at 30 min after the start of reperfusion. **(B)** TTC-stained brain sections showing infarct areas in the ischemic brains from WT mice, WT mice injected with vehicle or dabrafenib, and ASIC1a KO mice. **(C)** Summary data for B showing the ratio of infarct volumes to contralateral area in each condition. Error bars represent SDs for *n* number of animals tested. * $p < 0.05$, vs. WT; # $p < 0.05$, vs. WT+Vehicle.

3.4 Summary and discussion

Necroptosis has been shown to play an important role in ischemic brain injury. Our recent work showed that an ASIC1a-RIP1 interaction induced by acidosis is important for the activation of necroptosis in brain neurons in response to ischemic stroke (110). In this study, I identified serum starvation as a critical contributing factor for acidosis-induced cell death. I provide evidence that RIP3 is also required for acidosis/starvation induced necroptosis. Inhibiting RIP3 reduced both acid-induced death of cultured mouse cortical neurons *in vitro* and brain infarction in mice subject to MCAO *in vivo*. I showed that there are at least two key downstream molecules of RIP3 that are involved in acidosis/starvation-induced cell death: MLKL and AIF.

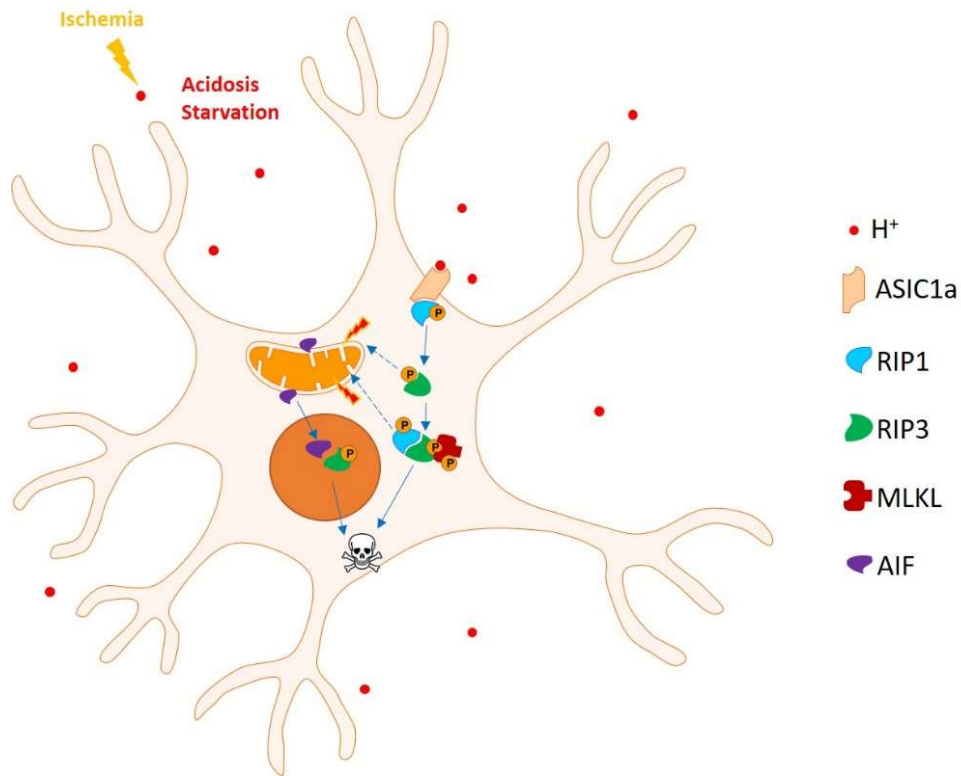


Figure 39. Schematic working model. Under ischemic conditions, the coincident occurrence of acidosis and starvation triggers the interaction of ASIC1a and RIP1, which subsequently causes phosphorylation of RIP3 and MLKL. The formation of RIP1/RIP3/MLKL necrosome induces necroptosis. At the same time, AIF is translocated from mitochondria to the nucleus and contributes to neuronal death.

3.4.1 Starvation is a critical contributing factor for acidosis induced cell death

My data indicate that starvation is crucial for acidosis-induced cell death as in the presence of 10% FBS, the low pH treatment (1 h pH 6.0) with either medium or ECS did not induce cell death. This is consistent with previous findings that only severe or prolonged acidification could kill the neurons (129). I found an increase in autophagy as indicated by the decrease in pS6K levels during the 1-h ECS treatment.

Autophagy has a dual role as an intrinsic cell-death mechanism under some circumstances and as a cell-survival pathway under others. Autophagy is commonly induced by TNFR1-triggered necroptosis. However, it was thought that autophagy is a cellular response to necroptosis, rather than a part of the death execution mechanism *per se* (111). The process of autophagy and its role in acidosis-induced cell death need to be further investigated. Inhibition of autophagy by pharmacologic or genetic interventions should be used to test the contribution of autophagy in acidosis/starvation induced cell death in later experiments.

Under ischemic stroke conditions *in vivo*, there should be a combination of acidosis and starvation since the blood supply to neurons was blocked. Indeed, studies using both ASIC1 blocker (98) and autophagy inhibitor 3-MA (131) have shown protective effect of these drugs in rodent model of ischemic stroke.

3.4.2 RIP3 and MLKL are involved in acidosis/starvation-induced cell death

Classic necroptosis induced by death receptors requires the formation of RIP1/RIP3/MLKL necrosome (134). It is not a surprise that acidosis/starvation-induced cell death also requires RIP3 and MLKL since we have demonstrated that RIP1 can bind to ASIC1a upon acidification and become phosphorylated. Given that caspase 8 inhibition is required for necroptosis and acidosis was reported to reduce neuronal apoptosis(135), the acidosis/starvation conditions would favor necroptosis rather than apoptosis. Our data indicate ASIC1a may represent a new DR to trigger necroptosis under acidosis

Due to the lack of a suitable antibody, changes in the total protein level of endogenous RIP3 could not be tested in the cultured neurons in this study. However, in N2a cells heterologously expressing RIP3, I did not find any change in the expressed RIP3 in response to pH 6.0 ECS, although it was reported that RIP3 levels were upregulated in hippocampal neurons under ischemic insults in one study (136). The time course of the changes (expression, phosphorylation, interaction) of RIP1/RIP3/MLKL warrants further evaluation both *in vitro* and *in vivo* since it may provide time window for therapeutic intervention of ischemic stroke.

Interestingly, some recent studies showed that both RIP1 and RIP3 are involved in autophagy regulation, with RIP1 negatively regulating basal autophagic flux (137) while RIP3 positively regulating autophagy (138). These suggest that there are cross talks between necroptosis and autophagy.

3.4.3 AIF translocation in acidosis/starvation induced cell death

Our results also indicate that AIF nuclear translocation contributes to acidosis/starvation-induced cell death, occurring downstream of RIP3. AIF is a protein essential for life due to its critical role as a mitochondrial oxidoreductase. However, once it has arrived in the nucleus, AIF could organize a DNA-degrading complex to cause caspase-independent chromatinolysis and cell death (139).

AIF is imbedded into the inner mitochondrial membrane. Its release from mitochondria usually requires a proteolytic cleavage. Two major elements take part in the AIF proteolytic process: (i) two families of cysteine proteases: calpains and

cathepsins; (ii) the activation of pro-apoptotic molecules from the Bcl-2 family, such as Bax or Bid, to facilitate the mitochondrial outer membrane permeabilization (139). Caspases can trigger the permeabilization of the outer mitochondrial membrane, thereby triggering the release of cytochrome c and/or AIF in apoptosis (140). There are also caspases-independent AIF release. One example is parthanatos, in which PARP-1 is a key regulator (117).

Although RIP1 plays a critical role in both parthanatos and TNFR1-induced necroptosis, the latter cannot be blocked by inhibition of calpains and PARP-1 or by downregulation of AIF. Inhibiting calpain or PARP-1 also failed to suppress acidosis/starvation-induced cell death, in which AIF translocation was found. However, other features of parthanatos like PAR accumulation is not found in our experiments. These suggest that acidosis/starvation-induced cell death is not parthanatos but necroptosis that requires the participation of AIF. Thus acidosis shares some mechanisms of parthanatos and TNFR-1 mediated necroptosis.

How is AIF released from mitochondria under acidosis/starvation is not clear. Our data demonstrate that VDAC and ROS are two important factors. It is reasonable that VDAC serves as an important component of MPTP, which facilitates the release of AIF. Recently, it was described that VDAC can be cleaved and subsequent bind to Bax; these two molecules form a sufficiently large passage for the release of AIF (141).

Although a previous study showed that AIF was increased in response to serum deprivation to mediate AIF-dependent apoptosis in HT22 neurons (130), I did not find any upregulation in AIF protein expression in our system. Although my preliminary data

suggest that there was no cleavage of AIF in acidosis/starvation-induced cell death, this possibility needs more careful examination in future experiments.

3.4.4 Contribution of mitochondria in acidosis/starvation-induced necroptosis

There are some debates on whether or not mitochondria play an essential role in necroptosis. Contrary to the initial belief, the lethal activity of RIP3 kinase is not influenced by the absence of mitochondrial protein phosphatase phosphoglycerate mutase family member 5 (PGAM5) and dynamin 1 like (DNM1L, best known as dynamin-related protein 1, DRP1) (142).

It has been suggested that enhanced metabolism accompanied by increased ROS production is probably responsible in part for the function of RIP3 in mediating necrosis (143). Although there are some papers showing that antioxidant failed to protect neuronal cell death (98, 111, 123), I found that some antioxidants had protective effect on acidosis/starvation-induced death. Some of these drugs have been previously shown to be neuroprotective against ischemic insults (132, 133). However, further experiments should monitor the mitochondrial status and ROS generation during acidosis/starvation-induced cell death, especially since ASIC1a was reported to localize also in mitochondria (144).

3.4.5 Acidosis/starvation-induced necroptosis and stress adaption

Cells subjected to perturbations of homeostasis almost invariably mount a tightly coordinated response aimed at (i) the removal of the initiating stimulus (when

possible), (ii) the repair of molecular and/or organelle damage, and (iii) eventually, the re-establishment of physiological conditions. When these objectives cannot be attained, cells generally undergo RCD as a means to preserve the homeostasis of the whole organism (1). In our system of acidosis/starvation, we also found mobilization of some RCD inhibitory signals such as NF κ B activation and autophagy. The activation of NF κ B and autophagy is usually considered as pro-survival, implicating that cells may also try to fight back to the perturbations of intracellular homeostasis caused by the pH 6.0 ECS as a way of stress adaptation. The death, however, happened drastically to most of the cells after the withdrawal of pH 6.0 ECS and during the re-supply of normal medium. Indeed, during the ischemia/reperfusion process in an injured brain, it is the later reperfusion phase when necroptosis occurred. During this reperfusion phase, both RCD-inhibitory and RCD-promoting signals may coexist and counteract with each other. Thus, it is highly possible that these signals can be modified to change the final outcome of the RCD, especially with the better understanding of the key components and their interactions.

Here, I defined some of the signaling pathways of the ASIC1a-RIP1 triggered necroptosis. Elucidating the signaling pathway can also help identify better points of intervention for therapeutic targeting. For example, inhibiting RIP3 rather than others may have its own benefits. First, the crucial physiological function mediated by ASIC1a and RIP1 will be maintained, particularly the decreased I κ B α indicating activation of NF κ B in response to acidic and starvation stress may be beneficial for cell survival via turning on gene expression to fight with the stress; Second, RIP3 may have multiple

downstream targets that contribute to cell death, such as VDAC, ROS, and MLKL.

Perturbation of them singly may not be sufficient to fully block the cell death triggered by the stress.

Chapter 4

Discussion

In this thesis, I showed clear evidence and some of the molecular mechanisms for PD-1 inhibition of RCD triggered by NK cells in the immune system and RIP3-mediated RCD in neurons in the nervous system. Both will shed lights on a better understanding of RCD and ways to interrupt of signal steps to either block PD-1 to promote NK cytotoxicity or inhibit RIP3 to protect neurons from dying. These studies also have broader perspectives because the molecules I have studied have multiple functions in different systems. PD-1 is not restricted to the immune system; it also plays important roles in the nervous system. RIP3 is not only involved in the nervous system; it also contributes importantly to immune response.

PD-1 and PD-L1 are functional in the nervous system and they are changeable under certain conditions. PD-L1 is constitutively expressed in nonlymphoid organs, such as heart, lung, pancreas and brain, and has been implicated in the maintenance of peripheral tolerance involving these tissues (145). The levels of PD-1/PD-L1 in primary human macrophages, brain endothelial cells (hBECs), microglia, and neurons were reported to be increased after exposure to methamphetamine (METH). The moderate levels of endogenous PD-1/PD-L1 in astrocytes were diminished by METH exposure, suggesting that a PD-1/PD-L1 interplay in these cell types could orchestrate the intercellular interactive communication for neuronal death or protection in the brain environment (146). PD-1 is expressed in large retinal ganglion cells (RGC) and is upregulated after optic nerve crush. PD-1 positive large RGCs do not express cleaved

caspase-3 after optic nerve injury (147). PD-1 mediates signaling pathway in developmental programmed cell death (PCD) during postnatal RGC maturation (148).

In contrast to PD-1 signaling, which is indubitable an immune suppresser. There are some controversial reports about RIP1/RIP3-mediated necroptosis in cancer. RIP3 and MLKL are reported to participate in chemotherapy-induced tumor immunogenic cell death (ICD). The failure to induce necroptosis is coupled to a lack of immune infiltration of the tumors post-chemotherapy, as well as to the failure of tumor growth reduction (149). RIP3-deficient mice are more susceptible to infection by a number of pathogenic viruses (150, 151), supporting the idea that necroptosis can restrain viral infection. However, it is reported that the necrosome promotes pancreatic oncogenesis *via* immune suppression(152).

Thus, expanding our understanding on molecular signaling in RCD in one system would help to understand its function in other systems and different pathological conditions. There are usually multiple contributors to cell death under any given pathophysiological situation.

However, there are still many unanswered questions about the detailed molecular mechanisms of RCD. For examples, how does PD-1 affect the ILK polarization, how does calcium affect the LG polarization, whether PD-1 affects the distribution of LFA 1 and activating receptors? And with respect to necroptosis, what is the time course of changes (expression, phosphorylation, interaction) of RIP1, RIP3 and MLKL in acidosis-induced cell death and ischemic brain, how does AIF get released from mitochondria, does mitochondria damage contribute to the acidosis

induced necroptosis, does ASIC1a translocate to in mitochondria in response to acidosis and then play a role in this process, how does ASIC1a and many other DRs contribute to brain injury in ischemia? Addressing these questions would help provide more complete elucidation of signaling pathways associated with PD-1 in NK cells and that associated with ASIC1 and RIP3 in neurons and offer new clues towards development of novel therapeutic strategies for cancer and neuroprotection in ischemic stroke.

References

1. Galluzzi, L., J. M. Bravo-San Pedro, I. Vitale, S. A. Aaronson, J. M. Abrams, D. Adam, E. S. Alnemri, L. Altucci, D. Andrews, M. Annicchiarico-Petruzzelli, E. H. Baehrecke, N. G. Bazan, M. J. Bertrand, K. Bianchi, M. V. Blagosklonny, K. Blomgren, C. Borner, D. E. Bredesen, C. Brenner, M. Campanella, E. Candi, F. Cecconi, F. K. Chan, N. S. Chandel, E. H. Cheng, J. E. Chipuk, J. A. Cidlowski, A. Ciechanover, T. M. Dawson, V. L. Dawson, V. De Laurenzi, R. De Maria, K. M. Debatin, N. Di Daniele, V. M. Dixit, B. D. Dynlacht, W. S. El-Deiry, G. M. Fimia, R. A. Flavell, S. Fulda, C. Garrido, M. L. Gougeon, D. R. Green, H. Gronemeyer, G. Hajnoczky, J. M. Hardwick, M. O. Hengartner, H. Ichijo, B. Joseph, P. J. Jost, T. Kaufmann, O. Kepp, D. J. Klionsky, R. A. Knight, S. Kumar, J. J. Lemasters, B. Levine, A. Linkermann, S. A. Lipton, R. A. Lockshin, C. Lopez-Otin, E. Lugli, F. Madeo, W. Malorni, J. C. Marine, S. J. Martin, J. C. Martinou, J. P. Medema, P. Meier, S. Melino, N. Mizushima, U. Moll, C. Munoz-Pinedo, G. Nunez, A. Oberst, T. Panaretakis, J. M. Penninger, M. E. Peter, M. Piacentini, P. Pinton, J. H. Prehn, H. Puthalakath, G. A. Rabinovich, K. S. Ravichandran, R. Rizzuto, C. M. Rodrigues, D. C. Rubinsztein, T. Rudel, Y. Shi, H. U. Simon, B. R. Stockwell, G. Szabadkai, S. W. Tait, H. L. Tang, N. Tavernarakis, Y. Tsujimoto, T. Vanden Berghe, P. Vandenabeele, A. Villunger, E. F. Wagner, H. Walczak, E. White, W. G. Wood, J. Yuan, Z. Zakeri, B. Zhivotovsky, G. Melino, and G. Kroemer. 2015. Essential versus accessory aspects of cell death: recommendations of the NCCD 2015. *Cell Death Differ* 22: 58-73.
2. Bryceson, Y. T., and E. O. Long. 2008. Line of attack: NK cell specificity and integration of signals. *Curr Opin Immunol* 20: 344-352.
3. Long, E. O., H. S. Kim, D. Liu, M. E. Peterson, and S. Rajagopalan. 2013. Controlling natural killer cell responses: integration of signals for activation and inhibition. *Annu Rev Immunol* 31: 227-

258.

4. Gregoire, C., L. Chasson, C. Luci, E. Tomasello, F. Geissmann, E. Vivier, and T. Walzer. 2007. The trafficking of natural killer cells. *Immunol Rev* 220: 169-182.
5. Childs, R. W., and M. Carlsten. 2015. Therapeutic approaches to enhance natural killer cell cytotoxicity against cancer: the force awakens. *Nat Rev Drug Discov* 14: 487-498.
6. Long, E. O. 1999. Regulation of immune responses through inhibitory receptors. *Annu Rev Immunol* 17: 875-904.
7. Ishida, Y., Y. Agata, K. Shibahara, and T. Honjo. 1992. Induced expression of PD-1, a novel member of the immunoglobulin gene superfamily, upon programmed cell death. *EMBO J* 11: 3887-3895.
8. Francisco, L. M., V. H. Salinas, K. E. Brown, V. K. Vanguri, G. J. Freeman, V. K. Kuchroo, and A. H. Sharpe. 2009. PD-L1 regulates the development, maintenance, and function of induced regulatory T cells. *The Journal of experimental medicine* 206: 3015-3029.
9. Alvarez, I. B., V. Pasquinelli, J. O. Jurado, E. Abbate, R. M. Musella, S. S. de la Barrera, and V. E. Garcia. 2010. Role played by the programmed death-1-programmed death ligand pathway during innate immunity against Mycobacterium tuberculosis. *J Infect Dis* 202: 524-532.
10. Benson, D. M., Jr., C. E. Bakan, A. Mishra, C. C. Hofmeister, Y. Efebera, B. Becknell, R. A. Baiocchi, J. Zhang, J. Yu, M. K. Smith, C. N. Greenfield, P. Porcu, S. M. Devine, R. Rotem-Yehudar, G. Lozanski, J. C. Byrd, and M. A. Caligiuri. 2010. The PD-1/PD-L1 axis modulates the natural killer cell versus multiple myeloma effect: a therapeutic target for CT-011, a novel monoclonal anti-PD-1 antibody. *Blood* 116: 2286-2294.
11. Keir, M. E., M. J. Butte, G. J. Freeman, and A. H. Sharpe. 2008. PD-1 and its ligands in tolerance

and immunity. *Annu Rev Immunol* 26: 677-704.

12. Dong, H., G. Zhu, K. Tamada, and L. Chen. 1999. B7-H1, a third member of the B7 family, co-stimulates T-cell proliferation and interleukin-10 secretion. *Nat Med* 5: 1365-1369.
13. Latchman, Y., C. R. Wood, T. Chernova, D. Chaudhary, M. Borde, I. Chernova, Y. Iwai, A. J. Long, J. A. Brown, R. Nunes, E. A. Greenfield, K. Bourque, V. A. Boussiotis, L. L. Carter, B. M. Carreno, N. Malenkovich, H. Nishimura, T. Okazaki, T. Honjo, A. H. Sharpe, and G. J. Freeman. 2001. PD-L2 is a second ligand for PD-1 and inhibits T cell activation. *Nat Immunol* 2: 261-268.
14. Sheppard, K. A., L. J. Fitz, J. M. Lee, C. Benander, J. A. George, J. Wooters, Y. Qiu, J. M. Jussif, L. L. Carter, C. R. Wood, and D. Chaudhary. 2004. PD-1 inhibits T-cell receptor induced phosphorylation of the ZAP70/CD3zeta signalosome and downstream signaling to PKCtheta. *FEBS Lett* 574: 37-41.
15. Pedoeem, A., I. Azoulay-Alfaguter, M. Strazza, G. J. Silverman, and A. Mor. 2014. Programmed death-1 pathway in cancer and autoimmunity. *Clin Immunol* 153: 145-152.
16. Patsoukis, N., D. Sari, and V. A. Boussiotis. 2012. PD-1 inhibits T cell proliferation by upregulating p27 and p15 and suppressing Cdc25A. *Cell Cycle* 11: 4305-4309.
17. Riley, J. L. 2009. PD-1 signaling in primary T cells. *Immunol Rev* 229: 114-125.
18. Fife, B. T., K. E. Pauken, T. N. Eagar, T. Obu, J. Wu, Q. Tang, M. Azuma, M. F. Krummel, and J. A. Bluestone. 2009. Interactions between PD-1 and PD-L1 promote tolerance by blocking the TCR-induced stop signal. *Nat Immunol* 10: 1185-1192.
19. Wei, F., S. Zhong, Z. Ma, H. Kong, A. Medvec, R. Ahmed, G. J. Freeman, M. Krogsaard, and J. L. Riley. 2013. Strength of PD-1 signaling differentially affects T-cell effector functions. *Proceedings of the National Academy of Sciences of the United States of America* 110: E2480-

2489.

20. Santarpià, M., and N. Karachaliou. 2015. Tumor immune microenvironment characterization and response to anti-PD-1 therapy. *Cancer Biol Med* 12: 74-78.
21. Ma, W., B. M. Gilligan, J. Yuan, and T. Li. 2016. Current status and perspectives in translational biomarker research for PD-1/PD-L1 immune checkpoint blockade therapy. *J Hematol Oncol* 9: 47.
22. Powles, T., J. P. Eder, G. D. Fine, F. S. Braiteh, Y. Loriot, C. Cruz, J. Bellmunt, H. A. Burris, D. P. Petrylak, S. L. Teng, X. Shen, Z. Boyd, P. S. Hegde, D. S. Chen, and N. J. Vogelzang. 2014. MPDL3280A (anti-PD-L1) treatment leads to clinical activity in metastatic bladder cancer. *Nature* 515: 558-562.
23. Tumeu, P. C., C. L. Harview, J. H. Yearley, I. P. Shintaku, E. J. Taylor, L. Robert, B. Chmielowski, M. Spasic, G. Henry, V. Ciobanu, A. N. West, M. Carmona, C. Kivork, E. Seja, G. Cherry, A. J. Gutierrez, T. R. Grogan, C. Mateus, G. Tomasic, J. A. Glaspy, R. O. Emerson, H. Robins, R. H. Pierce, D. A. Elashoff, C. Robert, and A. Ribas. 2014. PD-1 blockade induces responses by inhibiting adaptive immune resistance. *Nature* 515: 568-571.
24. Herbst, R. S., J. C. Soria, M. Kowanetz, G. D. Fine, O. Hamid, M. S. Gordon, J. A. Sosman, D. F. McDermott, J. D. Powderly, S. N. Gettinger, H. E. Kohrt, L. Horn, D. P. Lawrence, S. Rost, M. Leabman, Y. Xiao, A. Mokatrín, H. Koeppen, P. S. Hegde, I. Mellman, D. S. Chen, and F. S. Hodi. 2014. Predictive correlates of response to the anti-PD-L1 antibody MPDL3280A in cancer patients. *Nature* 515: 563-567.
25. El-Far, M., R. Halwani, E. Said, L. Trautmann, M. Doroudchi, L. Janbazian, S. Fonseca, J. van Grevenynghe, B. Yassine-Diab, R. P. Sekaly, and E. K. Haddad. 2008. T-cell exhaustion in HIV

- infection. *Curr HIV/AIDS Rep* 5: 13-19.
26. Kaufmann, D. E., and B. D. Walker. 2008. Programmed death-1 as a factor in immune exhaustion and activation in HIV infection. *Curr Opin HIV AIDS* 3: 362-367.
 27. Nakamoto, N., D. E. Kaplan, J. Coleclough, Y. Li, M. E. Valiga, M. Kaminski, A. Shaked, K. Olthoff, E. Gostick, D. A. Price, G. J. Freeman, E. J. Wherry, and K. M. Chang. 2008. Functional restoration of HCV-specific CD8 T cells by PD-1 blockade is defined by PD-1 expression and compartmentalization. *Gastroenterology* 134: 1927-1937, 1937 e1921-1922.
 28. Fuller, M. J., B. Callendret, B. Zhu, G. J. Freeman, D. L. Hasselschwert, W. Satterfield, A. H. Sharpe, L. B. Dustin, C. M. Rice, A. Grakoui, R. Ahmed, and C. M. Walker. 2013. Immunotherapy of chronic hepatitis C virus infection with antibodies against programmed cell death-1 (PD-1). *Proceedings of the National Academy of Sciences of the United States of America* 110: 15001-15006.
 29. Fisicaro, P., C. Valdatta, M. Massari, E. Loggi, E. Biasini, L. Sacchelli, M. C. Cavallo, E. M. Silini, P. Andreone, G. Missale, and C. Ferrari. 2010. Antiviral intrahepatic T-cell responses can be restored by blocking programmed death-1 pathway in chronic hepatitis B. *Gastroenterology* 138: 682-693, 693 e681-684.
 30. Tzeng, H. T., H. F. Tsai, H. J. Liao, Y. J. Lin, L. Chen, P. J. Chen, and P. N. Hsu. 2012. PD-1 blockage reverses immune dysfunction and hepatitis B viral persistence in a mouse animal model. *PLoS One* 7: e39179.
 31. Giancotti, F. G., and E. Ruoslahti. 1999. Integrin signaling. *Science* 285: 1028-1032.
 32. Springer, T. A., and M. L. Dustin. 2012. Integrin inside-out signaling and the immunological synapse. *Curr Opin Cell Biol* 24: 107-115.

33. Anderson, D. C., and T. A. Springer. 1987. Leukocyte adhesion deficiency: an inherited defect in the Mac-1, LFA-1, and p150,95 glycoproteins. *Annu Rev Med* 38: 175-194.
34. Luo, B. H., C. V. Carman, and T. A. Springer. 2007. Structural basis of integrin regulation and signaling. *Annual review of immunology* 25: 619-647.
35. Shen, B., M. K. Delaney, and X. Du. 2012. Inside-out, outside-in, and inside-outside-in: G protein signaling in integrin-mediated cell adhesion, spreading, and retraction. *Current opinion in cell biology* 24: 600-606.
36. Anikeeva, N., K. Somersalo, T. N. Sims, V. K. Thomas, M. L. Dustin, and Y. Sykulev. 2005. Distinct role of lymphocyte function-associated antigen-1 in mediating effective cytolytic activity by cytotoxic T lymphocytes. *Proc Natl Acad Sci U S A* 102: 6437-6442.
37. Bryceson, Y. T., M. E. March, D. F. Barber, H. G. Ljunggren, and E. O. Long. 2005. Cytolytic granule polarization and degranulation controlled by different receptors in resting NK cells. *J Exp Med* 202: 1001-1012.
38. Zhang, M., M. E. March, W. S. Lane, and E. O. Long. 2014. A signaling network stimulated by beta2 integrin promotes the polarization of lytic granules in cytotoxic cells. *Sci Signal* 7: ra96.
39. Takayama, H., and M. V. Sitkovsky. 1987. Antigen receptor-regulated exocytosis in cytotoxic T lymphocytes. *J Exp Med* 166: 725-743.
40. Leibson, P. J., D. E. Midthun, K. P. Windebank, and R. T. Abraham. 1990. Transmembrane signaling during natural killer cell-mediated cytotoxicity. Regulation by protein kinase C activation. *J Immunol* 145: 1498-1504.
41. Cahalan, M. D. 2009. STIMulating store-operated Ca(2+) entry. *Nat Cell Biol* 11: 669-677.
42. Feske, S., Y. Gwack, M. Prakriya, S. Srikanth, S. H. Puppel, B. Tanasa, P. G. Hogan, R. S. Lewis, M.

- Daly, and A. Rao. 2006. A mutation in Orai1 causes immune deficiency by abrogating CRAC channel function. *Nature* 441: 179-185.
43. Picard, C., C. A. McCarl, A. Papolos, S. Khalil, K. Luthy, C. Hivroz, F. LeDeist, F. Rieux-Laucat, G. Rechavi, A. Rao, A. Fischer, and S. Feske. 2009. STIM1 mutation associated with a syndrome of immunodeficiency and autoimmunity. *N Engl J Med* 360: 1971-1980.
 44. Maul-Pavicic, A., S. C. Chiang, A. Rensing-Ehl, B. Jessen, C. Fauriat, S. M. Wood, S. Sjoqvist, M. Hufnagel, I. Schulze, T. Bass, W. W. Schamel, S. Fuchs, H. Pircher, C. A. McCarl, K. Mikoshiba, K. Schwarz, S. Feske, Y. T. Bryceson, and S. Ehl. 2011. ORAI1-mediated calcium influx is required for human cytotoxic lymphocyte degranulation and target cell lysis. *Proc Natl Acad Sci U S A* 108: 3324-3329.
 45. Alpert, M. D., J. D. Harvey, W. A. Lauer, R. K. Reeves, M. Piatak, Jr., A. Carville, K. G. Mansfield, J. D. Lifson, W. Li, R. C. Desrosiers, R. P. Johnson, and D. T. Evans. 2012. ADCC develops over time during persistent infection with live-attenuated SIV and is associated with complete protection against SIV(mac)251 challenge. *PLoS pathogens* 8: e1002890.
 46. Jang, J. H., Y. Huang, P. Zheng, M. C. Jo, G. Bertolet, M. X. Zhu, L. Qin, and D. Liu. 2015. Imaging of Cell-Cell Communication in a Vertical Orientation Reveals High-Resolution Structure of Immunological Synapse and Novel PD-1 Dynamics. *J Immunol* 195: 1320-1330.
 47. Grier, J. T., L. R. Forbes, L. Monaco-Shawver, J. Oshinsky, T. P. Atkinson, C. Moody, R. Pandey, K. S. Campbell, and J. S. Orange. 2012. Human immunodeficiency-causing mutation defines CD16 in spontaneous NK cell cytotoxicity. *The Journal of clinical investigation* 122: 3769-3780.
 48. Barber, D. F., M. Faure, and E. O. Long. 2004. LFA-1 contributes an early signal for NK cell cytotoxicity. *J Immunol* 173: 3653-3659.

49. Liu, D., M. E. Peterson, and E. O. Long. 2012. The adaptor protein crk controls activation and inhibition of natural killer cells. *Immunity* 36: 600-611.
50. Song, H., J. Kim, D. Cosman, and I. Choi. 2006. Soluble ULBP suppresses natural killer cell activity via down-regulating NKG2D expression. *Cellular immunology* 239: 22-30.
51. Alpert, M. D., L. N. Heyer, D. E. Williams, J. D. Harvey, T. Greenough, M. Allhorn, and D. T. Evans. 2012. A novel assay for antibody-dependent cell-mediated cytotoxicity against HIV-1- or SIV-infected cells reveals incomplete overlap with antibodies measured by neutralization and binding assays. *Journal of virology* 86: 12039-12052.
52. Pentcheva-Hoang, T., L. Chen, D. M. Pardoll, and J. P. Allison. 2007. Programmed death-1 concentration at the immunological synapse is determined by ligand affinity and availability. *Proceedings of the National Academy of Sciences of the United States of America* 104: 17765-17770.
53. Orange, J. S. 2008. Formation and function of the lytic NK-cell immunological synapse. *Nat Rev Immunol* 8: 713-725.
54. Bromley, S. K., W. R. Burack, K. G. Johnson, K. Somersalo, T. N. Sims, C. Sumen, M. M. Davis, A. S. Shaw, P. M. Allen, and M. L. Dustin. 2001. The immunological synapse. *Annu Rev Immunol* 19: 375-396.
55. Liu, D., Y. T. Bryceson, T. Meckel, G. Vasiliver-Shamis, M. L. Dustin, and E. O. Long. 2009. Integrin-dependent organization and bidirectional vesicular traffic at cytotoxic immune synapses. *Immunity* 31: 99-109.
56. Yokosuka, T., M. Takamatsu, W. Kobayashi-Imanishi, A. Hashimoto-Tane, M. Azuma, and T. Saito. 2012. Programmed cell death 1 forms negative costimulatory microclusters that directly inhibit

- T cell receptor signaling by recruiting phosphatase SHP2. *The Journal of experimental medicine* 209: 1201-1217.
57. Mace, E. M., P. Dongre, H. T. Hsu, P. Sinha, A. M. James, S. S. Mann, L. R. Forbes, L. B. Watkin, and J. S. Orange. 2014. Cell biological steps and checkpoints in accessing NK cell cytotoxicity. *Immunol Cell Biol* 92: 245-255.
 58. Kamphorst, A. O., and R. Ahmed. 2013. Manipulating the PD-1 pathway to improve immunity. *Curr Opin Immunol* 25: 381-388.
 59. Abeyweera, T. P., M. Kaissar, and M. Huse. 2013. Inhibitory receptor signaling destabilizes immunological synapse formation in primary NK cells. *Front Immunol* 4: 410.
 60. Eissmann, P., and D. M. Davis. 2010. Inhibitory and regulatory immune synapses. *Curr Top Microbiol Immunol* 340: 63-79.
 61. Zinselmeyer, B. H., S. Heydari, C. Sacristan, D. Nayak, M. Cammer, J. Herz, X. Cheng, S. J. Davis, M. L. Dustin, and D. B. McGavern. 2013. PD-1 promotes immune exhaustion by inducing antiviral T cell motility paralysis. *The Journal of experimental medicine* 210: 757-774.
 62. Schleinitz, N., M. E. March, and E. O. Long. 2008. Recruitment of activation receptors at inhibitory NK cell immune synapses. *PLoS One* 3: e3278.
 63. Dieckmann, N. M., G. L. Frazer, Y. Asano, J. C. Stinchcombe, and G. M. Griffiths. 2016. The cytotoxic T lymphocyte immune synapse at a glance. *J Cell Sci* 129: 2881-2886.
 64. Dustin, M. L., and J. T. Groves. 2012. Receptor signaling clusters in the immune synapse. *Annu Rev Biophys* 41: 543-556.
 65. Ohaegbulam, K. C., A. Assal, E. Lazar-Molnar, Y. Yao, and X. Zang. 2015. Human cancer immunotherapy with antibodies to the PD-1 and PD-L1 pathway. *Trends Mol Med* 21: 24-33.

66. Kinashi, T. 2012. Overview of integrin signaling in the immune system. *Methods Mol Biol* 757: 261-278.
67. Azoulay-Alfaguter, I., M. Strazza, A. Pedoeem, and A. Mor. 2015. The coreceptor programmed death 1 inhibits T-cell adhesion by regulating Rap1. *J Allergy Clin Immunol* 135: 564-567.
68. Saunders, P. A., V. R. Hendrycks, W. A. Lidinsky, and M. L. Woods. 2005. PD-L2:PD-1 involvement in T cell proliferation, cytokine production, and integrin-mediated adhesion. *Eur J Immunol* 35: 3561-3569.
69. Das, A., and E. O. Long. 2010. Lytic granule polarization, rather than degranulation, is the preferred target of inhibitory receptors in NK cells. *J Immunol* 185: 4698-4704.
70. van Kooyk, Y., P. Weder, K. Heije, R. de Waal Malefijt, and C. G. Figdor. 1993. Role of intracellular Ca²⁺ levels in the regulation of CD11a/CD18 mediated cell adhesion. *Cell Adhes Commun* 1: 21-32.
71. Wacholtz, M. C., S. S. Patel, and P. E. Lipsky. 1989. Leukocyte function-associated antigen 1 is an activation molecule for human T cells. *J Exp Med* 170: 431-448.
72. Sirim, P., L. Zeitlmann, B. Kellersch, C. S. Falk, D. J. Schendel, and W. Kolanus. 2001. Calcium signaling through the beta 2-cytoplasmic domain of LFA-1 requires intracellular elements of the T cell receptor complex. *J Biol Chem* 276: 42945-42956.
73. Bryceson, Y. T., M. E. March, H. G. Ljunggren, and E. O. Long. 2006. Synergy among receptors on resting NK cells for the activation of natural cytotoxicity and cytokine secretion. *Blood* 107: 159-166.
74. Kaufman, D. S., R. A. Schoon, M. J. Robertson, and P. J. Leibson. 1995. Inhibition of selective signaling events in natural killer cells recognizing major histocompatibility complex class I. *Proc*

Natl Acad Sci U S A 92: 6484-6488.

75. Chapon, M., C. Randriamampita, E. Maubec, C. Badoual, S. Fouquet, S. F. Wang, E. Marinho, D. Farhi, M. Garcette, S. Jacobelli, A. Rouquette, A. Carlotti, A. Girod, A. Prevost-Blondel, A. Trautmann, M. F. Avril, and N. Bercovici. 2011. Progressive upregulation of PD-1 in primary and metastatic melanomas associated with blunted TCR signaling in infiltrating T lymphocytes. *J Invest Dermatol* 131: 1300-1307.
76. Ting, A. T., R. A. Schoon, R. T. Abraham, and P. J. Leibson. 1992. Interaction between protein kinase C-dependent and G protein-dependent pathways in the regulation of natural killer cell granule exocytosis. *J Biol Chem* 267: 23957-23962.
77. Lindorfer, M. A., H. B. Jinivizian, P. L. Foley, A. D. Kennedy, M. D. Solga, and R. P. Taylor. 2003. B cell complement receptor 2 transfer reaction. *Journal of immunology* 170: 3671-3678.
78. Mack, M., A. Kleinschmidt, H. Bruhl, C. Klier, P. J. Nelson, J. Cihak, J. Plachy, M. Stangassinger, V. Erfle, and D. Schlondorff. 2000. Transfer of the chemokine receptor CCR5 between cells by membrane-derived microparticles: a mechanism for cellular human immunodeficiency virus 1 infection. *Nature medicine* 6: 769-775.
79. Choudhuri, K., J. Llodra, E. W. Roth, J. Tsai, S. Gordo, K. W. Wucherpfennig, L. C. Kam, D. L. Stokes, and M. L. Dustin. 2014. Polarized release of T-cell-receptor-enriched microvesicles at the immunological synapse. *Nature* 507: 118-123.
80. Jewett, A., and B. Bonavida. 1995. Target-induced anergy of natural killer cytotoxic function is restricted to the NK-target conjugate subset. *Cellular immunology* 160: 91-97.
81. Bhat, R., and C. Watzl. 2007. Serial killing of tumor cells by human natural killer cells--enhancement by therapeutic antibodies. *PloS one* 2: e326.

82. Choi, P. J., and T. J. Mitchison. 2013. Imaging burst kinetics and spatial coordination during serial killing by single natural killer cells. *Proceedings of the National Academy of Sciences of the United States of America* 110: 6488-6493.
83. Ameratunga, M., K. Asadi, X. Lin, M. Walkiewicz, C. Murone, S. Knight, P. Mitchell, P. Boutros, and T. John. 2016. PD-L1 and Tumor Infiltrating Lymphocytes as Prognostic Markers in Resected NSCLC. *PLoS One* 11: e0153954.
84. Beldi-Ferchiou, A., M. Lambert, S. Dogniaux, F. Vely, E. Vivier, D. Olive, S. Dupuy, F. Levasseur, D. Zucman, C. Lebbe, D. Sene, C. Hivroz, and S. Caillat-Zucman. 2016. PD-1 mediates functional exhaustion of activated NK cells in patients with Kaposi sarcoma. *Oncotarget*.
85. Pesce, S., M. Greppi, G. Tabellini, F. Rampinelli, S. Parolini, D. Olive, L. Moretta, A. Moretta, and E. Marcenaro. 2016. Identification of a subset of human natural killer cells expressing high levels of programmed death 1: A phenotypic and functional characterization. *J Allergy Clin Immunol*.
86. Writing Group, M., D. Mozaffarian, E. J. Benjamin, A. S. Go, D. K. Arnett, M. J. Blaha, M. Cushman, S. R. Das, S. de Ferranti, J. P. Despres, H. J. Fullerton, V. J. Howard, M. D. Huffman, C. R. Isasi, M. C. Jimenez, S. E. Judd, B. M. Kissela, J. H. Lichtman, L. D. Lisabeth, S. Liu, R. H. Mackey, D. J. Magid, D. K. McGuire, E. R. Mohler, 3rd, C. S. Moy, P. Muntner, M. E. Mussolino, K. Nasir, R. W. Neumar, G. Nichol, L. Palaniappan, D. K. Pandey, M. J. Reeves, C. J. Rodriguez, W. Rosamond, P. D. Sorlie, J. Stein, A. Towfighi, T. N. Turan, S. S. Virani, D. Woo, R. W. Yeh, M. B. Turner, C. American Heart Association Statistics, and S. Stroke Statistics. 2016. Heart Disease and Stroke Statistics-2016 Update: A Report From the American Heart Association. *Circulation* 133: e38-60.

87. Xiong, Z. G., and T. L. Xu. 2012. The role of ASICs in cerebral ischemia. *Wiley Interdiscip Rev Membr Transp Signal* 1: 655-662.
88. Chamorro, Á., U. Dirnagl, X. Urra, and A. M. Planas. 2016. Neuroprotection in acute stroke: targeting excitotoxicity, oxidative and nitrosative stress, and inflammation. *The Lancet Neurology*.
89. Cardone, R. A., V. Casavola, and S. J. Reshkin. 2005. The role of disturbed pH dynamics and the Na⁺/H⁺ exchanger in metastasis. *Nat Rev Cancer* 5: 786-795.
90. Gillies, R. J., N. Raghunand, G. S. Karczmar, and Z. M. Bhujwala. 2002. MRI of the tumor microenvironment. *J Magn Reson Imaging* 16: 430-450.
91. Chiche, J., M. C. Brahimi-Horn, and J. Pouyssegur. 2010. Tumour hypoxia induces a metabolic shift causing acidosis: a common feature in cancer. *J Cell Mol Med* 14: 771-794.
92. Somjen, G. G. 1984. Acidification of interstitial fluid in hippocampal formation caused by seizures and by spreading depression. *Brain Res* 311: 186-188.
93. Yates, C. M., J. Butterworth, M. C. Tennant, and A. Gordon. 1990. Enzyme activities in relation to pH and lactate in postmortem brain in Alzheimer-type and other dementias. *J Neurochem* 55: 1624-1630.
94. Bowen, B. C., R. E. Block, J. Sanchez-Ramos, P. M. Pattany, D. A. Lampman, J. B. Murdoch, and R. M. Quencer. 1995. Proton MR spectroscopy of the brain in 14 patients with Parkinson disease. *AJNR Am J Neuroradiol* 16: 61-68.
95. Jenkins, B. G., W. J. Koroshetz, M. F. Beal, and B. R. Rosen. 1993. Evidence for impairment of energy metabolism in vivo in Huntington's disease using localized ¹H NMR spectroscopy. *Neurology* 43: 2689-2695.

96. Rehncrona, S. 1985. Brain acidosis. *Ann Emerg Med* 14: 770-776.
97. Siesjo, B. K., K. Katsura, and T. Kristian. 1996. Acidosis-related damage. *Adv Neurol* 71: 209-233; discussion 234-206.
98. Xiong, Z. G., X. M. Zhu, X. P. Chu, M. Minami, J. Hey, W. L. Wei, J. F. MacDonald, J. A. Wemmie, M. P. Price, M. J. Welsh, and R. P. Simon. 2004. Neuroprotection in ischemia: blocking calcium-permeable acid-sensing ion channels. *Cell* 118: 687-698.
99. Waldmann, R., G. Champigny, F. Bassilana, C. Heurteaux, and M. Lazdunski. 1997. A proton-gated cation channel involved in acid-sensing. *Nature* 386: 173-177.
100. Hanukoglu, I. 2017. ASIC and ENaC type sodium channels: conformational states and the structures of the ion selectivity filters. *FEBS J* 284: 525-545.
101. Chu, X. P., and Z. G. Xiong. 2012. Physiological and pathological functions of acid-sensing ion channels in the central nervous system. *Curr Drug Targets* 13: 263-271.
102. Wemmie, J. A., J. Chen, C. C. Askwith, A. M. Hruska-Hageman, M. P. Price, B. C. Nolan, P. G. Yoder, E. Lamani, T. Hoshi, J. H. Freeman, Jr., and M. J. Welsh. 2002. The acid-activated ion channel ASIC contributes to synaptic plasticity, learning, and memory. *Neuron* 34: 463-477.
103. Wemmie, J. A., C. C. Askwith, E. Lamani, M. D. Cassell, J. H. Freeman, Jr., and M. J. Welsh. 2003. Acid-sensing ion channel 1 is localized in brain regions with high synaptic density and contributes to fear conditioning. *J Neurosci* 23: 5496-5502.
104. Duan, B., D. S. Liu, Y. Huang, W. Z. Zeng, X. Wang, H. Yu, M. X. Zhu, Z. Y. Chen, and T. L. Xu. 2012. PI3-kinase/Akt pathway-regulated membrane insertion of acid-sensing ion channel 1a underlies BDNF-induced pain hypersensitivity. *The Journal of neuroscience : the official journal of the Society for Neuroscience* 32: 6351-6363.

105. Biagini, G., K. Babinski, M. Avoli, M. Marcinkiewicz, and P. Seguela. 2001. Regional and subunit-specific downregulation of acid-sensing ion channels in the pilocarpine model of epilepsy. *Neurobiol Dis* 8: 45-58.
106. Arias, R. L., M. L. Sung, D. Vasylyev, M. Y. Zhang, K. Albinson, K. Kubek, N. Kagan, C. Beyer, Q. Lin, J. M. Dwyer, M. M. Zaleska, M. R. Bowlby, J. Dunlop, and M. Monaghan. 2008. Amiloride is neuroprotective in an MPTP model of Parkinson's disease. *Neurobiol Dis* 31: 334-341.
107. Wong, H. K., P. O. Bauer, M. Kurosawa, A. Goswami, C. Washizu, Y. Machida, A. Tosaki, M. Yamada, T. Knopfel, T. Nakamura, and N. Nukina. 2008. Blocking acid-sensing ion channel 1 alleviates Huntington's disease pathology via an ubiquitin-proteasome system-dependent mechanism. *Hum Mol Genet* 17: 3223-3235.
108. Pignataro, G., R. P. Simon, and Z. G. Xiong. 2007. Prolonged activation of ASIC1a and the time window for neuroprotection in cerebral ischaemia. *Brain* 130: 151-158.
109. Yermolaieva, O., A. S. Leonard, M. K. Schnizler, F. M. Abboud, and M. J. Welsh. 2004. Extracellular acidosis increases neuronal cell calcium by activating acid-sensing ion channel 1a. *Proc Natl Acad Sci U S A* 101: 6752-6757.
110. Wang, Y. Z., J. J. Wang, Y. Huang, F. Liu, W. Z. Zeng, Y. Li, Z. G. Xiong, M. X. Zhu, and T. L. Xu. 2015. Tissue acidosis induces neuronal necroptosis via ASIC1a channel independent of its ionic conduction. *Elife* 4: e05682.
111. Degterev, A., Z. Huang, M. Boyce, Y. Li, P. Jagtap, N. Mizushima, G. D. Cuny, T. J. Mitchison, M. A. Moskowitz, and J. Yuan. 2005. Chemical inhibitor of nonapoptotic cell death with therapeutic potential for ischemic brain injury. *Nat Chem Biol* 1: 112-119.
112. Vercammen, D., P. Vandenabeele, R. Beyaert, W. Declercq, and W. Fiers. 1997. Tumour necrosis

- factor-induced necrosis versus anti-Fas-induced apoptosis in L929 cells. *Cytokine* 9: 801-808.
113. Holler, N., R. Zaru, O. Micheau, M. Thome, A. Attinger, S. Valitutti, J. L. Bodmer, P. Schneider, B. Seed, and J. Tschopp. 2000. Fas triggers an alternative, caspase-8-independent cell death pathway using the kinase RIP as effector molecule. *Nat Immunol* 1: 489-495.
 114. Matsumura, H., Y. Shimizu, Y. Ohsawa, A. Kawahara, Y. Uchiyama, and S. Nagata. 2000. Necrotic death pathway in Fas receptor signaling. *J Cell Biol* 151: 1247-1256.
 115. Sun, L., H. Wang, Z. Wang, S. He, S. Chen, D. Liao, L. Wang, J. Yan, W. Liu, X. Lei, and X. Wang. 2012. Mixed lineage kinase domain-like protein mediates necrosis signaling downstream of RIP3 kinase. *Cell* 148: 213-227.
 116. Cai, Z., S. Jitkaew, J. Zhao, H. C. Chiang, S. Choksi, J. Liu, Y. Ward, L. G. Wu, and Z. G. Liu. 2014. Plasma membrane translocation of trimerized MLKL protein is required for TNF-induced necroptosis. *Nat Cell Biol* 16: 55-65.
 117. David, K. K., S. A. Andrabhi, T. M. Dawson, and V. L. Dawson. 2009. Parthanatos, a messenger of death. *Front Biosci (Landmark Ed)* 14: 1116-1128.
 118. Zhang, J., X. Li, H. Kwansa, Y. T. Kim, L. Yi, G. Hong, S. A. Andrabhi, V. L. Dawson, T. M. Dawson, R. C. Koehler, and Z. J. Yang. 2016. Augmentation of poly(ADP-ribose) polymerase-dependent neuronal cell death by acidosis. *J Cereb Blood Flow Metab*: 271678X16658491.
 119. Zhao, H., J. Ning, A. Lemaire, F. S. Koumpa, J. J. Sun, A. Fung, J. Gu, B. Yi, K. Lu, and D. Ma. 2015. Necroptosis and parthanatos are involved in remote lung injury after receiving ischemic renal allografts in rats. *Kidney Int* 87: 738-748.
 120. Duan, B., Y. Z. Wang, T. Yang, X. P. Chu, Y. Yu, Y. Huang, H. Cao, J. Hansen, R. P. Simon, M. X. Zhu, Z. G. Xiong, and T. L. Xu. 2011. Extracellular spermine exacerbates ischemic neuronal injury

- through sensitization of ASIC1a channels to extracellular acidosis. *The Journal of neuroscience : the official journal of the Society for Neuroscience* 31: 2101-2112.
121. Li, J. X., J. M. Feng, Y. Wang, X. H. Li, X. X. Chen, Y. Su, Y. Y. Shen, Y. Chen, B. Xiong, C. H. Yang, J. Ding, and Z. H. Miao. 2014. The B-Raf(V600E) inhibitor dabrafenib selectively inhibits RIP3 and alleviates acetaminophen-induced liver injury. *Cell Death Dis* 5: e1278.
 122. Zhao, J., S. Jitkaew, Z. Cai, S. Choksi, Q. Li, J. Luo, and Z. G. Liu. 2012. Mixed lineage kinase domain-like is a key receptor interacting protein 3 downstream component of TNF-induced necrosis. *Proc Natl Acad Sci U S A* 109: 5322-5327.
 123. Wang, Y. Z., J. J. Wang, Y. Huang, F. Liu, W. Z. Zeng, Y. Li, Z. G. Xiong, M. X. Zhu, and T. L. Xu. 2015. Tissue acidosis induces neuronal necroptosis via ASIC1a channel independent of its ionic conduction. *Elife* 4.
 124. Morgan, M. J., and Y.-S. Kim. 2015. The serine threonine kinase RIP3: lost and found. *BMB Reports* 48: 303-312.
 125. Chen, W., Z. Zhou, L. Li, C. Q. Zhong, X. Zheng, X. Wu, Y. Zhang, H. Ma, D. Huang, W. Li, Z. Xia, and J. Han. 2013. Diverse sequence determinants control human and mouse receptor interacting protein 3 (RIP3) and mixed lineage kinase domain-like (MLKL) interaction in necroptotic signaling. *J Biol Chem* 288: 16247-16261.
 126. Jetli, S. K., S. M. Swain, S. Majumder, S. Chatterjee, V. Poornima, and A. K. Bera. 2010. Evaluation of the role of nitric oxide in acid sensing ion channel mediated cell death. *Nitric Oxide* 22: 213-219.
 127. Wajant, H., K. Pfizenmaier, and P. Scheurich. 2003. Tumor necrosis factor signaling. *Cell Death Differ* 10: 45-65.

128. Gupta, S. C., R. Singh, M. Asters, J. Liu, X. Zhang, M. R. Pabbidi, K. Watabe, and Y. Y. Mo. 2016. Regulation of breast tumorigenesis through acid sensors. *Oncogene* 35: 4102-4111.
129. Nedergaard, M., S. A. Goldman, S. Desai, and W. A. Pulsinelli. 1991. Acid-induced death in neurons and glia. *J Neurosci* 11: 2489-2497.
130. Steiger-Barraissoul, S., and A. Rami. 2009. Serum deprivation induced autophagy and predominantly an AIF-dependent apoptosis in hippocampal HT22 neurons. *Apoptosis* 14: 1274-1288.
131. Xu, Y., J. Wang, X. Song, L. Qu, R. Wei, F. He, K. Wang, and B. Luo. 2016. RIP3 induces ischemic neuronal DNA degradation and programmed necrosis in rat via AIF. *Sci Rep* 6: 29362.
132. Lipman, T., R. Tabakman, and P. Lazarovici. 2006. Neuroprotective effects of the stable nitroxide compound Tempol on 1-methyl-4-phenylpyridinium ion-induced neurotoxicity in the Nerve Growth Factor-differentiated model of pheochromocytoma PC12 cells. *Eur J Pharmacol* 549: 50-57.
133. Katnik, C., and J. Cuevas. 2014. Non-specific inhibition of ischemia- and acidosis-induced intracellular calcium elevations and membrane currents by alpha-phenyl-N-tert-butyl nitrone, butylated hydroxytoluene and trolox. *Int J Mol Sci* 15: 3596-3611.
134. Pasparakis, M., and P. Vandenabeele. 2015. Necroptosis and its role in inflammation. *Nature* 517: 311-320.
135. Xu, L., A. J. Glassford, A. J. Giaccia, and R. G. Giffard. 1998. Acidosis reduces neuronal apoptosis. *Neuroreport* 9: 875-879.
136. Vieira, M., J. Fernandes, L. Carreto, B. Anuncibay-Soto, M. Santos, J. Han, A. Fernandez-Lopez, C. B. Duarte, A. L. Carvalho, and A. E. Santos. 2014. Ischemic insults induce necroptotic cell

- death in hippocampal neurons through the up-regulation of endogenous RIP3. *Neurobiol Dis* 68: 26-36.
137. Yonekawa, T., G. Gamez, J. Kim, A. C. Tan, J. Thorburn, J. Gump, A. Thorburn, and M. J. Morgan. 2015. RIP1 negatively regulates basal autophagic flux through TFEB to control sensitivity to apoptosis. *EMBO Rep* 16: 700-708.
 138. Harris, K. G., S. A. Morosky, C. G. Drummond, M. Patel, C. Kim, D. B. Stolz, J. M. Bergelson, S. Cherry, and C. B. Coyne. 2015. RIP3 Regulates Autophagy and Promotes Coxsackievirus B3 Infection of Intestinal Epithelial Cells. *Cell Host Microbe* 18: 221-232.
 139. Delavallee, L., L. Cabon, P. Galan-Malo, H. K. Lorenzo, and S. A. Susin. 2011. AIF-mediated caspase-independent necroptosis: a new chance for targeted therapeutics. *IUBMB Life* 63: 221-232.
 140. Cande, C., N. Vahsen, C. Garrido, and G. Kroemer. 2004. Apoptosis-inducing factor (AIF): caspase-independent after all. *Cell Death Differ* 11: 591-595.
 141. Ozaki, T., T. Yamashita, and S. Ishiguro. 2009. Mitochondrial m-calpain plays a role in the release of truncated apoptosis-inducing factor from the mitochondria. *Biochim Biophys Acta* 1793: 1848-1859.
 142. Moujalled, D. M., W. D. Cook, J. M. Murphy, and D. L. Vaux. 2014. Necroptosis induced by RIPK3 requires MLKL but not Drp1. *Cell Death Dis* 5: e1086.
 143. Zhang, D. W., J. Shao, J. Lin, N. Zhang, B. J. Lu, S. C. Lin, M. Q. Dong, and J. Han. 2009. RIP3, an energy metabolism regulator that switches TNF-induced cell death from apoptosis to necrosis. *Science* 325: 332-336.
 144. Wang, Y. Z., W. Z. Zeng, X. Xiao, Y. Huang, X. L. Song, Z. Yu, D. Tang, X. P. Dong, M. X. Zhu, and T.

- L. Xu. 2013. Intracellular ASIC1a regulates mitochondrial permeability transition-dependent neuronal death. *Cell death and differentiation* 20: 1359-1369.
145. Sharpe, A. H., E. J. Wherry, R. Ahmed, and G. J. Freeman. 2007. The function of programmed cell death 1 and its ligands in regulating autoimmunity and infection. *Nat Immunol* 8: 239-245.
146. Mishra, V., H. Schuetz, and J. Haorah. 2015. Differential induction of PD-1/PD-L1 in Neuroimmune cells by drug of abuse. *Int J Physiol Pathophysiol Pharmacol* 7: 87-97.
147. Wang, W., A. Chan, Y. Qin, J. M. Kwong, J. Caprioli, R. Levinson, L. Chen, and L. K. Gordon. 2015. Programmed cell death-1 is expressed in large retinal ganglion cells and is upregulated after optic nerve crush. *Exp Eye Res* 140: 1-9.
148. Chen, L., C. W. Sham, A. M. Chan, L. M. Francisco, Y. Wu, S. Mareninov, A. H. Sharpe, G. J. Freeman, X. J. Yang, J. Braun, and L. K. Gordon. 2009. Role of the immune modulator programmed cell death-1 during development and apoptosis of mouse retinal ganglion cells. *Invest Ophthalmol Vis Sci* 50: 4941-4948.
149. Yang, H., Y. Ma, G. Chen, H. Zhou, T. Yamazaki, C. Klein, F. Pietrocola, E. Vacchelli, S. Souquere, A. Sauvat, L. Zitvogel, O. Kepp, and G. Kroemer. 2016. Contribution of RIP3 and MLKL to immunogenic cell death signaling in cancer chemotherapy. *Oncoimmunology* 5: e1149673.
150. Upton, J. W., W. J. Kaiser, and E. S. Mocarski. 2012. DAI/ZBP1/DLM-1 complexes with RIP3 to mediate virus-induced programmed necrosis that is targeted by murine cytomegalovirus vIRA. *Cell Host Microbe* 11: 290-297.
151. Huang, Z., S. Q. Wu, Y. Liang, X. Zhou, W. Chen, L. Li, J. Wu, Q. Zhuang, C. Chen, J. Li, C. Q. Zhong, W. Xia, R. Zhou, C. Zheng, and J. Han. 2015. RIP1/RIP3 binding to HSV-1 ICP6 initiates necroptosis to restrict virus propagation in mice. *Cell Host Microbe* 17: 229-242.

152. Seifert, L., G. Werba, S. Tiwari, N. N. Giao Ly, S. Alothman, D. Alqunaibit, A. Avanzi, R. Barilla, D. Daley, S. H. Greco, A. Torres-Hernandez, M. Pergamo, A. Ochi, C. P. Zambirinis, M. Pansari, M. Rendon, D. Tipples, M. Hundeyin, V. R. Mani, C. Hajdu, D. Engle, and G. Miller. 2016. The necrosome promotes pancreatic oncogenesis via CXCL1 and Mincle-induced immune suppression. *Nature* 532: 245-249.

Vita

Yu Huang was born in Anqing, Anhui, P.R. China, on January 13, 1985, the son of Yasheng Huang and Xiaohong Wang. After completing his education at NO.1 Middle School, Anqing, Anhui, P.R. China in 2003, he entered Jinan University, Guangzhou, Guangdong, P. R. China. He received the degree of Bachelor of Science with a major in Biological Sciences from Jinan University in June, 2007. He then worked as lab manager in Dr. Tianle Xu's lab at Laboratory of Synaptic Physiology, Institute of Neuroscience, Chinese Academy of Sciences for four years. In August of 2011 he entered The University of Texas MD Anderson Cancer Center UT Health Graduate School of Biomedical Sciences and joined Dr. Michael Xi Zhu's lab in UTHealth.

Permanent address:

168 Wanjiang Road, Building #9, Unit 1, Rm602

Anqing, Anhui, China, 246003